UPPSALA
UNIVERSITET

Digital Comprehensive Summaries of Uppsala Dissertations from the Faculty of Science and Technology 2220

Unravelling Sensitisation and Quenching Pathways in Lanthanide Luminophores

SALAUAT KIRAEV

ACTA
UNIVERSITATIS
UPSALIENSIS
UPPSALA
2022

ISSN 1651-6214
ISBN 978-91-513-1664-2
URN urn:nbn:se:uu:diva-489083

Dissertation presented at Uppsala University to be publicly examined in Sonja Lyttkens, Ångströmlaboratoriet, Lägerhyddsvägen 1, Uppsala, Monday, 30 January 2023 at 09:15 for the degree of Doctor of Philosophy. The examination will be conducted in English. Faculty examiner: Professor Thomas Just Sørensen (Nano-Science Center & Department of Chemistry, University of Copenhagen).

Abstract

Kiraev, S. 2022. Unravelling Sensitisation and Quenching Pathways in Lanthanide Luminophores. *Digital Comprehensive Summaries of Uppsala Dissertations from the Faculty of Science and Technology* 2220. 105 pp. Uppsala: Acta Universitatis Upsaliensis. ISBN 978-91-513-1664-2.

Lanthanide (Ln) ions find use in cellular detection and probing of many analytes, owing to their unique photophysical properties. However, to make the Ln emission efficient, one has to develop a light-harvesting antenna, which is an organic chromophore that absorbs and transfers energy to the Ln. By exciting the Ln complex, photoinduced electron transfer (PeT) from the antenna to the readily reducible Ln might occur. Usually, PeT is quenching Ln emission intensity. Thus, the work herein aims to evaluate and distinguish sensitising and quenching pathways in Ln emission to improve the brightness of Ln luminophores for biological applications.

After presenting an introduction to Ln photophysics and sensitisation in chapter 1, chapter 2 describes our work on Ln octa- and nonacoordinate complexes bearing the same antenna. We demonstrated that the azide and alkyne reactive groups could be attached to the antenna to make Ln complexes bioconjugable. The saturation of the Ln coordination environment resulted in intraligand PeT, which cancelled out the benefits of eliminated quenching from the coordinated water molecule.

To study the effect of photoredox quenching in Eu emission, we focused on tuning reduction potentials for a possible response in luminescence properties in chapter 3. Increasing positive charges of complexes destabilised Eu^{3+} and decreased Ln emission quantum yields. This behaviour was due to PeT quenching of the more readily reducible Eu under similar sensitisation conditions. Fluoride binding boosted Ln emission intensity in the least Eu^{3+}-stabilising ligand field.

In chapter 4, the role of a tertiary amide linker between the antenna and the metal binding site was examined. For poorly emissive coumarin-appended complexes quenching via photoinduced reduction of Eu from the antenna was unlikely, while in carbostyril-sensitised complexes PeT was efficient.

Ln compounds with lower ligand denticity allowed better fluoride detection via the increased effect of PeT quenching and the larger number of water molecules, as shown in chapter 5. However, the presence of cyanide significantly quenched Eu emissions of the same complexes, making it possible to distinguish cyanide from fluoride.

Chapters 6–7 were devoted to the sensitisation of Yb luminescence. The NIR emission intensity increased marginally in the complexes with efficient PeT. The main sensitising effect originated from phonon-assisted energy transfer favourable in our Yb complexes. When picolinate donors stimulated intraligand PeT, detrimental to the ligand fluorescence in Yb compounds, Yb emission was noticeably more intense than in the first series without picolinates.

Keywords: Lanthanide, Luminescence, Sensitisation, Quenching, Energy Transfer, Electron transfer

Salauat Kiraev, Department of Chemistry - Ångström, Synthetic Molecular Chemistry, 523, Uppsala University, SE-751 20 Uppsala, Sweden.

ISSN 1651-6214
ISBN 978-91-513-1664-2
URN urn:nbn:se:uu:diva-489083 (http://urn.kb.se/resolve?urn=urn:nbn:se:uu:diva-489083)

Уҡыу – эҙ менән ҡойо ҡаҙыу
Башҡорт халыҡ мәҡәле

Learning is digging a well with a needle
Bashkir folk proverb

List of Papers

This thesis is based on the following papers, which are referred to in the text by their Roman numerals.

I. Kovacs, D., **Kiraev, S. R.**, Phipps, D., Orthaber, A., Borbas, K. E. (2020) Eu(III) and Tb(III) Complexes of Octa- and Nonadentate Macrocyclic Ligands Carrying Azide, Alkyne and Ester Reactive Groups. *Inorg. Chem.,* 59(1):106–117

II. Kovacs, D.,‡ Mathieu, E.,‡ **Kiraev, S. R.**,‡ Wells, J. A. L., Demeyere, E., Sipos, A., Borbas, K. E. (2020) Coordination Environment-Controlled Photoinduced Electron Transfer Quenching in Luminescent Europium Complexes. *J. Am. Chem. Soc*., 142(30):13190–13200

III. **Kiraev, S. R.**, Mathieu, E., Siemens, F., Kovacs, D., Demeyere, E., Borbas, K. E. (2020) Lanthanide(III) Complexes of Cyclen Triacetates and Triamides Bearing Tertiary Amide-Linked Antennae. *Molecules*, 25(22):5282

IV. **Kiraev, S. R.**, Weber R. R., Wells J. A. L., Orthaber A., Kovacs D., Borbas K. E. (2022) Analysis of Anion Binding Effects on the Sensitized Luminescence of Macrocyclic Europium(III) Complexes. *Anal. Sens*., 2:e202200015

V. Mathieu, E.,‡ **Kiraev, S. R.**,‡ Kovacs, D., Wells, J. A. L., Tomar, M., Andres, J., Borbas, K. E. (2022) Sensitization pathways in NIR-emitting Yb(III) complexes bearing 0, +1, +2, or +3 charges. *J. Am. Chem. Soc*. 144(46): 21056–21067

VI. **Kiraev, S. R.**, Mathieu, E., Kovacs, D., Wells, J. A. L., Tomar, M., Andres, J., Borbas K. E. (2022) Improved emission of Yb(III) ions in triazacyclononane-based macrocyclic ligands compared to cyclen-based ones. *Dalton Trans.*, 51(43): 16596–16604

‡ These authors contributed equally. Reprints were made with permission from the respective publishers. Papers I–III were previously discussed in the context of a licentiate thesis defence presented on 19 April 2021: *Competing Pathways of Quenching in Sensitised Lanthanide Luminescence*

Contribution report

Paper I	Synthesised and characterised CF_3-functionalised ligand. Contributed to the synthesis of the nonadentate ligand, Ln(III) complexes characterisation and photophysical measurements. Corrected the manuscript and the ESI.
Paper II	Measured extra luminescent and paramagnetic ^{1}H NMR spectra, crystallised Ln(III) complexes. Contributed to the chemical characterisation of synthetic precursors and Ln(III) compounds. Measured Ln(III) complexes fluorescence lifetimes. Assisted with writing the manuscript and compiling the ESI.
Paper III	Contributed to the synthesis and characterisation of new ligands. Performed the synthesis, chemical and photophysical characterisation of new Ln(III) carbostyril complexes. Measured ^{1}H NMR spectra and cyclic voltammograms of Ln(III) compounds. Performed photophysical measurements with added fluoride. Contributed to the writing of the manuscript and prepared the ESI.
Paper IV	Synthesised and characterised new ligands and their Ln(III) complexes. Measured paramagnetic ^{1}H NMR and photophysical properties of new Ln(III) compounds. Performed the control, fluoride- and cyanide-added photophysical experiments of Eu(III) complexes. Co-wrote the manuscript and put together the ESI.
Paper V	Performed ^{1}H NMR and extra steady-state emission spectroscopy experiments of Ln(III) compounds. Measured ligand fluorescence lifetimes on ns time scale of Yb and Lu complexes. Contributed to the characterisation of compounds, data analysis, manuscript writing and ESI preparation.
Paper VI	Synthesised and characterised Yb(III) complexes and model compounds. Crystallised Yb complexes and studied their paramagnetic ^{1}H NMR spectroscopy. Measured extra ligand-based emission spectra and lifetimes of Yb(III) compounds. Contributed to the manuscript writing, data analysis and shaped the ESI.

Papers not included in this thesis

VII. Kovacs, D., Kocsi, D., Wells, J. A. L., Kiraev S. R., Borbas K. E. (2021) Electron transfer pathways in photoexcited lanthanide(III) complexes of picolinate ligands. *Dalton Trans.*, 50(12):4244–4254

Contents

Abbreviations

A	Absorbance
$Ant^{+\cdot}$	Antenna radical cation
BET	Back energy transfer
BeT	Back electron transfer
COSY	NMR correlation spectroscopy
cyclen	1,4,7,10-tetraazacyclododecane
r_{ion}	Effective ionic radius
DBCO-NH_2	Dibenzocyclooctyne-amine
DO3A	Cyclen-1,4,7-triacetate
DOTA	Cyclen-1,4,7,10-tetraacetate
DTPA	Diethylenetriaminepentaacetate
ED	Electric dipole
ET	Energy transfer
EXSY	NMR exchange spectroscopy
$hv_{abs/L,Eu}$	Energy of absorbed/emitted photon
I	Integrated emission intensity
IC	Internal conversion
ICT	Internal charge transfer
ISC	Intersystem crossing
$k_{ET(S_1)}$	Singlet-mediated energy transfer rate constant
$k_{f,L}$	Ligand fluorescence rate constant
$k_{nr,L}$	Non-radiative ligand decay rate constant
k_{PeT}	Photoinduced electron transfer rate constant
$k_{rad,L}$	Radiative ligand fluorescence rate constant
HPLC-MS	High-performance liquid chromatography-mass spectrometry
Ln	Lanthanide
Ln(II)	Lanthanide(II) ion
Ln(III)	Lanthanide(III) ion
MD	Magnetic dipole
Me	Methyl
MOM	Methoxymethyl
n	Refractive index of the medium
NHE	Normal hydrogen electrode
NIR	Near-infrared

NMR	Nuclear magnetic resonance
PAET	Phonon-assisted energy transfer
PeT	Photoinduced electron transfer
q	Hydration state of Ln(III)
r.t.	Room temperature
S/N	Signal-to-noise ratio
S_0	Ground state
S_1	First singlet excited state
SAP	Square-antiprismatic
tacn	1,4,7-triazacyclononane
T_1	First triplet excited state
TSAP	Twisted-square-antiprismatic
VT	Variable temperature
ΔG_{PeT}	Free energy change of photoinduced electron transfer
ΔE_{Coul}	Coulombic attraction
$E_{\mathrm{ox}}^{\mathrm{Ant}}$	Antenna oxidation potential
$E_{1/2}^{\mathrm{Ln}}$	Ln(III)/Ln(II) half-wave potential
$E_{\mathrm{red}}^{\mathrm{Ln}}$	Ln(III)/Ln(II) reduction potential
ε	Molar absorption coefficient
η_{sens}	Sensitization efficiency of Ln(III)
λ_{abs}	Local absorption maximum, absorption wavelength
λ_{em}	Local emission maximum, emission wavelength
λ_{em}	Local excitation maximum, excitation wavelength
ν	Vibrational energy level
τ	Luminescence lifetime
$\tau_{\mathrm{D_2O}}$	Observed luminescence lifetime in D_2O
$\tau_{\mathrm{f,L}}$	Ligand fluorescence lifetime
$\tau_{\mathrm{H_2O}}$	Observed luminescence lifetime in H_2O
τ_{obs}	Observed luminescence lifetime
τ_{rad}	Radiative lifetime
$\tau_{\mathrm{rad,L}}$	Radiative ligand fluorescence lifetime
Φ_{L}	Residual ligand fluorescence quantum yield
Φ_{Ln}	Ln(III) overall luminescence quantum yield
$\Phi_{\mathrm{Ln}}^{\mathrm{Ln}}$	Ln(III) intrinsic quantum yield
φ_{L}	Relative ligand fluorescence quantum yield
φ_{Ln}	Relative Ln(III) emission quantum yield
ψ	NCCN torsion angle
ω	$NCCN_{py}$/NCCO torsion angle

1. Introduction

1.1 General information on lanthanides

Lanthanides (Ln) are intriguing and attractive chemical elements for many researchers worldwide due to their multiple unique properties. Ln are a group of metal elements that occupy the first row of the f-block from La ($Z = 57$) to Lu ($Z = 71$) in the periodic table. The first representative has given the original name of the group "lanthanoids," meaning "similar to lanthanum," despite the absence of f-electrons in the valence orbitals of La. Nevertheless, "lanthanides" is a commonly used term, including La and the 4f elements (from Ce to Lu).[1] Together with Sc and Y, they are referred to as rare-earth metals – the traditional name of these elements commonly found within the same ores. The history of these metals began in the Swedish village of Ytterby with the discovery of the mineral ytterbite by the army officer Carl Axel Arrhenius in 1787.[2] Later on, this ore was analysed by Johan Gadolin, who extracted yttria (Y_2O_3), which contained the first known rare-earth metal.[3] The mineral, subsequently renamed after him to gadolinite, was also composed of Ln.[4]

Every lanthanide has a stable +3 oxidation state in aqueous solutions. Examples of unusual oxidation states are Ce(IV) and Eu(II), stabilised due to unoccupied and half-filled 4f orbitals, respectively.[5] In Ln(III) ions, the more diffuse 5s and 5p orbitals shield the inner 4f orbitals, preventing their interaction with the ligand field,[6] which explains the chemical similarities of these elements.[7] The shielding of 4f orbitals also contributes to a smaller effect of balancing out the nuclear charge by the 5s and 5p orbitals. Consequently, the latter orbitals have a larger attraction to the nucleus across the series, causing the shortening of the Ln effective ionic radius (r_{ion}).[8] This phenomenon, called lanthanide contraction, is observed for 4f ions of the same oxidation state and coordination number (CN, Table 1).

Table 1. Ln(III) electron configurations and r_{ion} [Å] with CN = 9.[1] Pm is omitted.

Ln	La	Ce	Pr	Nd	Sm	Eu	Gd	Tb	Dy	Ho	Er	Tm	Yb	Lu
(III)	$4f^0$	$4f^1$	$4f^2$	$4f^3$	$4f^5$	$4f^6$	$4f^7$	$4f^8$	$4f^9$	$4f^{10}$	$4f^{11}$	$4f^{12}$	$4f^{13}$	$4f^{14}$
r_{ion}	1.22	1.20	1.18	1.16	1.13	1.12	1.11	1.10	1.08	1.07	1.06	1.05	1.04	1.03

Most Ln(III) ions are luminescent. The electrons of the 4f orbitals endow Ln(III) with photophysical properties different to those of d-block metals.

Ln(III) are nearly unaffected by crystal field splitting,[7] which means that the 4f-4f electron transitions are not energetically influenced by the ligand environment.[9] Moreover, these transitions are Laporte forbidden.[10] As a result, luminescence spectra of Ln(III) compounds consist of sharp and line-like peaks with local emission maxima (λ_{em}) at fixed wavelengths, often called "spectral fingerprints." The molar absorption coefficients (ε) of Ln(III) are small (ε = 0.20–12.5 $M^{-1}cm^{-1}$),[11] and their direct excitation is inefficient in solution.[12] These reasons explain why Ln(III) inorganic salts are mainly colourless or of faint colour, unlike those of d-block metal ions. The forbidden nature of 4f-4f transitions is also the cause of the long-lived Ln(III) emission lifetimes ($\tau = 10^{-6}$–10^{-3} s).[13]

Ln(III) luminescence becomes efficient when the 4f ion is coupled to a chromophore, serving as a light-harvesting antenna. The antenna has large ε ($> 10^4$ $M^{-1}cm^{-1}$) and sensitises Ln(III) emission by the energy transfer to the metal centre.[14] This approach combines the benefits of Ln(III) luminescence with strong chromophore absorption. A suitable overlap between Ln(III) and antenna excited states yields efficient Ln(III) sensitisation.

1.2 Sensitised Ln(III) luminescence

1.2.1 Origin of Ln(III) emission

All Ln(III) except La(III) and Lu(III) are luminescent, as the former has no f-electrons, and the latter has filled 4f orbitals.[10] Since Ln(III) are polyelectronic, they have multiple configurations of different energetic levels defined as microstates.[7] Term symbols of Ln(III) for these microstates are composed of the following quantum numbers:

$$^{2S+1}L_J$$

where S and L are total spin and total orbital angular momenta quantum numbers, respectively, and J is the spin-orbit coupling between L and S. The corresponding Ln(III) ground and excited states are denoted using their term symbols.[7,12]

Ln(III) energetic levels were observed experimentally and explained theoretically, and extensive work has been performed to attribute the intensities of energy transitions between them.[15–17] The 4f-4f transitions are of electric dipole (ED) or magnetic dipole (MD) nature.[18] The Laporte rules permit MD transitions and forbid ED ones. Nevertheless, in emission spectra of molecular Ln(III) complexes, the Ln(III) luminescence is still observed. This phenomenon is explained by the impact of the ligand field, which facilitates the mixing of 4f orbitals with higher electronic states of opposite parity, and relaxes

selection rules.[12] The formally prohibited ED transitions become induced ED ones that are partially allowed;[10] the lower the symmetry of the ligand field, the more likely the effect of induced ED transitions can take place.[12] In complexes of centrosymmetric point groups, the vibronic coupling is responsible for lifting the site symmetry; therefore, ED transitions are still observable.[7]

Figure 1 shows the energy diagram with the lowest excited and ground states of several Ln(III).[15,16] Among these ions, Sm^{3+}, Eu^{3+} and Tb^{3+} are phosphorescent in the visible region, Yb^{3+} is fluorescent in the near-infrared (NIR), and Gd^{3+} has no 4f-4f emissions in molecular complexes.[19] The excited state of Gd(III) ($^6P_{7/2}$, 32200 cm^{-1}) is energetically higher than that of the commonly used antennae. Hence, at room temperature (r.t.), one can observe only the antenna fluorescence of the Gd(III) compound. At 77 K, the emission spectrum of the same Gd(III) complex features fluorescence and phosphorescence bands, which is beneficial for determining the energy levels of the antenna excited states.[20] Thus, the appropriate controls for the antenna spectroscopic properties are Gd(III) complexes, lacking sensitised lanthanide luminescence.

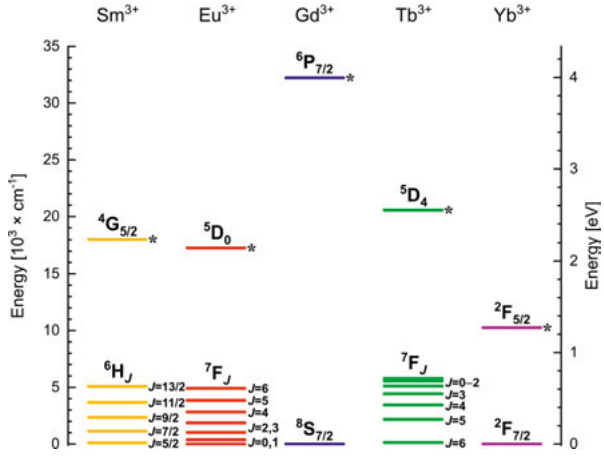

Figure 1. Energy diagram showing the lowest excited (marked with *) and ground states (^6F_J for Sm^{3+} are omitted) of chosen Ln^{3+} ions taken from (Ln^{3+}:LaF_3).[15,16]

The assignment of a typical Eu(III) compound emission spectrum in water is shown in Figure 2.[21] The radiative relaxation happens via the transition from Eu^{3+} lowest excited state $^5D_0$ (17300 cm^{-1}) to the final states ^7F_J (J = 0–5). In Eu(III) spectra, the energy transition $^5D_0 \rightarrow {}^7F_1$ (or $\Delta J = 1$) is MD, whereas the others are of ED origin.[22] The splitting of an energy transition into several spectral bands is generated by the Stark effect, which is dependent on the site symmetry of Ln(III).[22] The overall colour of the emission is governed by the most intense transition of the spectrum, e.g., for Eu(III) in Figure 2, it is red (λ_{em} = 700 nm, $^5D_0 \rightarrow {}^7F_4$). Similarly, the emission colour is green for Tb(III)

complexes due to the most intense peak at λ_{em} = 546 nm of the $^5D_4 \rightarrow {}^7F_5$ transition.[21]

The radiative lifetime (τ_{rad}) is a significant parameter specific for the particular Ln(III) emitting state in the given coordination environment and solvent. If the observed lifetime (τ_{obs}) is smaller than τ_{rad}, then it is direct evidence for the occurrence of non-radiative deactivation decreasing Ln(III) emission intensity. Using Eq. (1),[23,24] τ_{rad} of the Eu(III) single emitting level is calculated with the help of the steady-state emission spectrum, as in the assigned example (Figure 2):

$$\frac{1}{\tau_{rad}} = A_{MD,0} \cdot n^3 \cdot \left(\frac{I_{tot}}{I_{MD}}\right) \quad (1)$$

where $A_{MD,0}$ (a constant equal to 14.65 s^{-1})[22] is the spontaneous emission probability for the $^5D_0 \rightarrow {}^7F_1$ transition in vacuo, n is the refractive index of the solvent, and I_{tot}/I_{MD} is the integrated ratio of the total corrected Eu(III) emission spectrum to the area of $\Delta J = 1$.[23,24] Apart from Eu(III), the determination of τ_{rad} for other Ln(III) is not straightforward.[19,23]

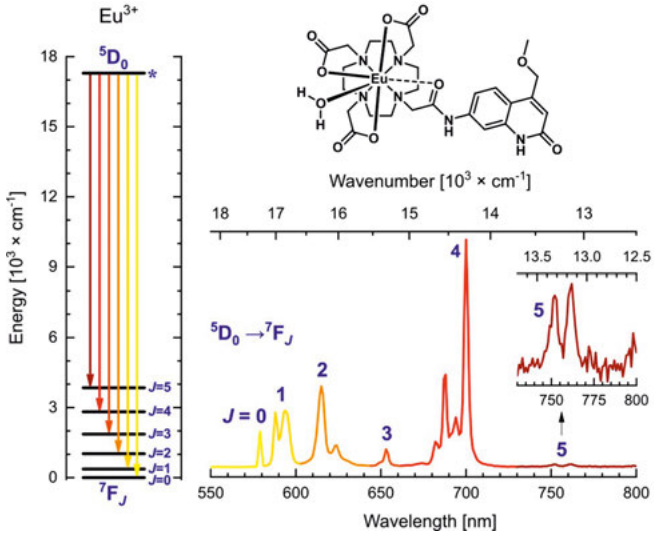

Figure 2. Energy levels diagram of $^5D_0 \rightarrow {}^7F_J$ (J = 0–5) transitions (left) and steady-state emission spectrum (right) of a Eu(III) complex (top right).[21] Energy transition arrow colours on the left diagram correspond to band colours of the right spectrum.

1.2.2 Ln(III) luminescence sensitisation

In 1942, Weissman discovered that Eu(III) luminescence could be sensitised by organic ligands.[14] Since then, the antenna effect has been ubiquitously implemented to upgrade the emission properties of 4f elements. However, different ligands gave unequal intensities of Ln(III) luminescence.[14]

The optimised ligand structures amplify sensitised 4f-4f emission intensity and afford highly luminescent Ln(III) complexes. Among the requirements for the chelating ligands is the judicious choice of antenna, providing efficient Ln(III) sensitisation and the high affinity for the Ln(III). Furthermore, the organic ligand should provide the chemical stability of the resulting complex and protect the Ln(III) from outer-sphere luminescence quenchers, such as water molecules.[25] For biological applications, Ln(III) complexes should also stay intact in harsh conditions, such as at low or high pH and in the presence of other competing metal ions.[26]

Several macrocyclic ligands can efficiently chelate Ln(III).[27] The core framework 1,4,7,10-tetraazacyclododecane (cyclen) is one of the most widely used.[19] N-alkylation of cyclen with substituents carrying coordinating groups further increases the complex stability.[28] Moreover, the light-harvesting antenna can be attached to cyclen by similar N-alkylation reactions.[29] In such a way, appropriate kinetic stability can be accessed via a macrocyclic binding site, and intense light absorption is achieved through the antenna coupled to a macrocycle.

Figure 3 shows major sensitisation pathways for Ln(III) luminescence in Eu(III) cyclen-1,4,7-triacetate (DO3A)-based compound with a 4-methoxymethyl-7-aminocarbostyril antenna.[21] The first singlet excited state (S_1) of the ligand is populated after exciting the Ln(III) complex at the antenna local absorption maximum (λ_{abs}). From here, direct energy transfer (ET) from S_1 to the Ln(III) excited state or intersystem crossing (ISC) from S_1 to the first triplet excited state (T_1) with subsequent ET from T_1 to the Ln(III) receiving level is possible. While both routes can be efficient,[30] triplet-mediated ET is considered the primary pathway for most Ln(III) complexes.[31] Finally, the sensitisation terminates with luminescence from the Ln(III) emissive state. Residual antenna fluorescence may also be observed (Figure 3, bottom right).

The Ln(III) emission intensity is quantified in the units of overall quantum yield of luminescence (Φ_{Ln}). From the measured Φ_{Ln}, one can estimate the sensitisation efficiency of the Ln(III) ion (η_{sens}) via Eq. (2):[22]

$$\eta_{\mathrm{sens}} = \frac{\Phi_{\mathrm{Ln}}}{\Phi_{\mathrm{Ln}}^{\mathrm{Ln}}} = \Phi_{\mathrm{Ln}} \cdot \frac{\tau_{\mathrm{rad}}}{\tau_{\mathrm{obs}}} \qquad (2)$$

where $\Phi_{\mathrm{Ln}}^{\mathrm{Ln}}$ is the Ln(III) intrinsic quantum yield, equal to $\tau_{\mathrm{obs}}/\tau_{\mathrm{rad}}$.[22] The overall η_{sens} depends on the combined ISC and ET efficiencies in sensitised Ln(III) luminescence.[32] The $\Phi_{\mathrm{Ln}}^{\mathrm{Ln}}$ value defines the maximum quantum yield for a given coordination environment upon direct Ln(III) excitation.[24] Thus, η_{sens} and $\Phi_{\mathrm{Ln}}^{\mathrm{Ln}}$ describe the effectiveness of the Ln(III) luminescence sensitisation and the ligand structure impact on 4f-4f emission properties, respectively.

Many research groups focus their work on the optimisation of ET from the ligand to the 4f ion in Ln(III) compounds. Latva et al. observed that to achieve

maximum Φ_{Ln}, ligand T_1 level should be energetically higher than the Ln(III) lowest excited state by more than 1850 cm^{-1} for Tb^{3+} and 2500–4000 cm^{-1} for Eu^{3+}.[31] Raymond et al. confirmed the sensitivity of Φ_{Tb} to the T_1 level in a series of analogous Tb(III) complexes, and up to 1600 cm^{-1} energy gap between $^5D_4$ and T_1 was found to be a compromise.[33] However, to obtain highly luminescent Ln(III) complexes, the non-radiative decay processes should be considered and minimised.

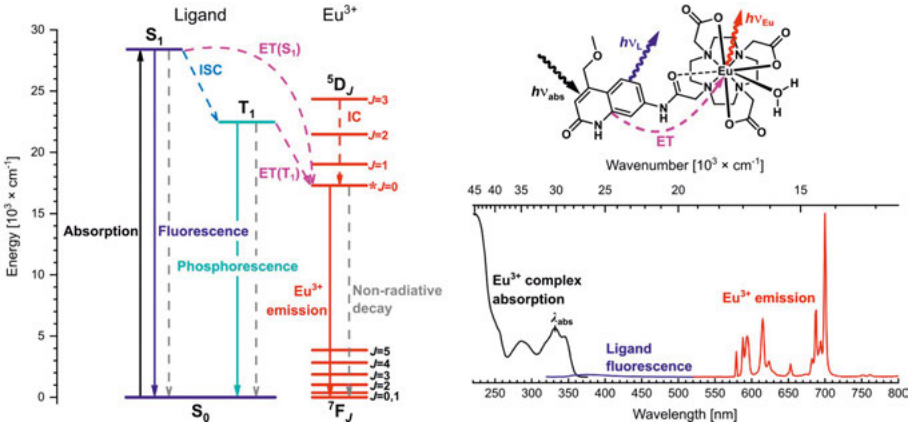

Figure 3. Jablonski diagram (left) of luminescence sensitisation in Eu(III) DO3A-based complex (top right) and its normalised absorption and steady-state emission spectra in water (bottom right). Solid and dashed arrows depict radiative and non-radiative processes, respectively. Energy levels are taken from [21]. S_0 = ground state, IC = internal conversion, $h\nu_{abs/L,Eu}$ = energy of absorbed/emitted photons.

1.2.3 Quenching of sensitised Ln(III) emission

Part of the energy that excites the Ln(III) complex is dissipated non-radiatively (grey dashed arrows in Figure 3, left). The quenching of Ln(III) luminescence is generally dependent on the initial and final states energy levels.

The X-H oscillators (X = O, N, C) from solvent and organic ligands quench the excited states of many luminescent Ln(III).[34] The most prominent O-H vibrations (ν = 3600 cm^{-1}) depopulate Ln(III) emissive levels via phonon coupling.[35] Quenching is less favoured when the energy gap between the initial and final states of the Ln(III) is larger.[22] According to that principle, Tb^{3+} luminescence is the most intense among molecular Ln(III) complexes, followed by Eu^{3+} (Figure 4, left). When it comes to NIR emitting Ln(III) ions, an inner-sphere water molecule is detrimental to Er^{3+} luminescence, as only one phonon is enough for quenching.[19] The presence of N-H (ν = 3300 cm^{-1}) and C-H (ν = 2900 cm^{-1}) oscillators in the Ln(III) coordination sphere also decreases 4f-4f emission, but to a lesser extent than O-H bonds.[36]

With a proper ligand design, water molecules can be kept outside the Ln(III) coordination sphere. One way to preserve Ln(III) luminescence is to

switch protonated solvent to a deuterated one, as X-D phonons (for X = O, ν = 2200 cm^{-1}) are lower in energy.[37] Thus, more phonon levels are required to quench Ln(III) emissive states upon inner sphere solvent molecule exchange.[34] In deuterated solvents, N-H oscillators are replaced by N-D bonds in the coordination environment of Eu(III) complexes.[38,39] Deuteration is applied to determine the Ln(III) hydration states (q) from Eq. (3) and (4)[34] in the absence of other prominent quenching pathways:

$$q(\mathrm{Tb}) = 5\left(1/\tau_{\mathrm{H_2O}} - 1/\tau_{\mathrm{D_2O}} - 0.06\right) \quad (3)$$

$$q(\mathrm{Eu}) = 1.2\left(1/\tau_{\mathrm{H_2O}} - 1/\tau_{\mathrm{D_2O}} - 0.25 - m \cdot 0.075\right) \quad (4)$$

where $\tau_{\mathrm{H_2O}}$ and $\tau_{\tau_{\mathrm{D_2O}}}$ are observed lifetimes in H_2O and D_2O, respectively, and m is the number of N-H bonds in the Eu(III) coordination sphere.[34]

Another route is the substitution of C-H bonds in the ligand structure with energetically lower oscillators, for instance, C-D[34,40–44] or halogenated carbon atoms.[45–47] Yet, selective ligand deuteration does not always lead to decreased oscillator quenching, as demonstrated for Pr(III)[48] and Tb(III)[34] emission. Fluorination alters the energetics of the ligand excited states and affects the Ln(III) luminescence sensitisation.[49–51]

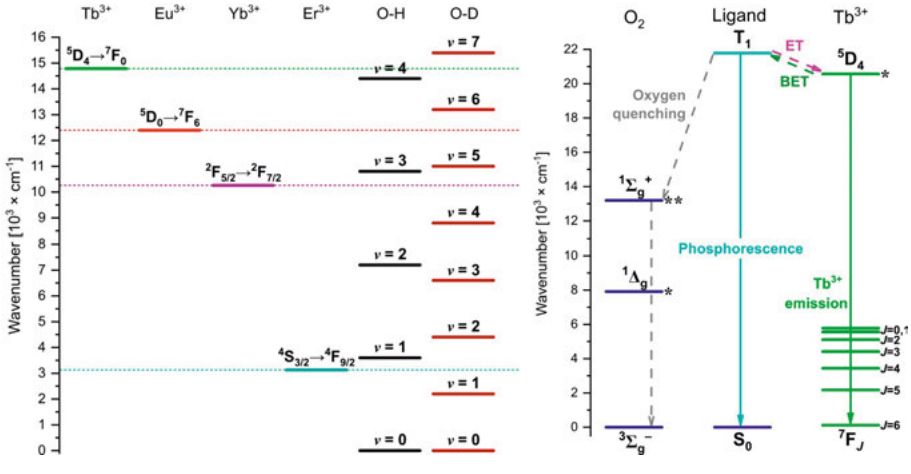

Figure 4. Diagram of Ln(III) initial-final state energy gaps vs O-H and O-D phonon levels (left)[35] and a scheme of T_1 thermal repopulation by BET from $^5D_4$ emissive state of Tb^{3+} leading to O_2 quenching (right).[52]

The second prominent quenching agent of Ln(III) emission is molecular oxygen. It is noteworthy that there is no direct ET between Ln(III) and O_2 excited states, whether Ln(III) is bound to a complex.[37,53] The sensitivity of Ln(III) emission to O_2 is due to the susceptibility of the antenna T_1 to molecular oxygen quenching. When T_1 is within 2000 cm^{-1} [31,33] of the Tb^{3+} long-lived

emissive state ($^5D_4$, 20600 cm^{-1}, $\tau = 10^{-3}$ s), it stimulates thermal repopulation by back energy transfer (BET) from the latter to the former excited state (Figure 4, right).[31,53–57] While a solution of such Tb(III) complex is exposed to air, the long-lived T_1 is quenched[52] via O_2 excited states.[58] If the Ln(III) receiving level is short-lived, the quenching by O_2 is not favoured even when the T_1-Ln(III) emissive state energy gap is small, as for Dy^{3+} ($^4F_{9/2}$, 21100 cm^{-1}, $\tau = 10^{-6}$ s).[59]

Collisional quenching with O_2 of the long-lived antenna T_1 is one of the processes deactivating phosphorescence at r.t. in emission spectra of the Gd(III) complexes. On the other hand, in luminescent Ln(III), the competition between O_2 quenching and ET may occur if T_1-mediated ET to the Ln(III) excited state is slower than the deactivation by the molecular oxygen. Then, quenching is irrespective of the energy gap between T_1 and the Ln(III) receiving level.[60–63] The fate of O_2 quenching by slow ET or via BET depends on the distance between the Ln(III) ion and the sensitising chromophore.[64]

1.2.4 Photoinduced electron transfer in Ln(III) compounds

Excitation of the antenna increases its reducing ability, making it susceptible to react with an electron acceptor. Photoinduced electron transfer (PeT) can occur intramolecularly, during which an electron is transferred from the excited antenna to Ln(III), leaving them formally oxidised ($Ant^{+\cdot}$) and reduced (Ln(II)), respectively.[65,66] PeT is followed by the subsequent charge recombination via back electron transfer (BeT). Only the more reducible Ln(III) ions are affected by PeT (Table 2). Such charge migration forms $Ant^{+\cdot}$-Ln^{2+} intermediate state and depopulates the antenna S_1 (Figure 5, left). Therefore, PeT is a competitive pathway to ligand fluorescence, decreasing the intensity of the latter.[67,68] As for the emission of Ln(III), PeT from the antenna excited states to Ln(III) can quench or sensitise 4f-4f emission.[69] BeT yields ground state Ant-Ln^{3+}, or in the case of Yb, excited Ln(III).[69]

Table 2. Ln(III)/Ln(II) half-wave potentials ($E_{1/2}^{Ln}$ [V vs NHE]) and the resulting Ln(II) electron configurations. $E_{1/2}^{Ln}$ values for Sm, Eu and Yb are measured in aqueous media, the rest are estimated.[70] Pm is omitted.

Ln	Ce	Pr	Nd	Sm	Eu	Gd	Tb	Dy	Ho	Er	Tm	Yb
$E_{1/2}^{Ln}$	–3.2	–2.7	–2.6	–1.55	–0.35	–3.9	–3.7	–2.6	–2.9	–3.1	–2.3	–1.15
(II)	$4f^2$	$4f^3$	$4f^4$	$4f^6$	$4f^7$	$4f^8$	$4f^9$	$4f^{10}$	$4f^{11}$	$4f^{12}$	$4f^{13}$	$4f^{14}$

PeT is mainly ascribed to complexes with Eu(III)[21,71–76] and Yb(III),[61,68,77–80] as these ions are the most readily reducible among the Ln(III) species (Table 2). The luminescence of Yb(III), which has a single low-lying excited state ($^2F_{5/2}$, 10260 cm^{-1}), can be sensitised by a stepwise PeT-BeT process. The latter was first demonstrated by Horrocks in a parvalbumin protein, where the

sensitising antenna was a tryptophan moiety (Trp).[69] There is no spectral overlap between the sensitising Trp S_1 or T_1 and the Yb(III) $^2F_{5/2}$ excited states. The $Trp^{+\cdot}$-Yb^{2+} intermediate is higher in energy than the $^2F_{5/2}$ excited state, resulting in the population of the latter and eventual NIR emission. In contrast, the Eu(III) $^5D_0$ excited state is higher in energy than $Trp^{+\cdot}$-Eu^{2+} and the emission is quenched (Figure 5, right).[69]

The feasibility of PeT upon excitation of the Ln(III) complex can be estimated from the Weller equation (Eq. (5)):[66,81,82]

$$\Delta G_{\mathrm{PeT}} = E_{\mathrm{ox}}^{\mathrm{Ant}} - E_{\mathrm{red}}^{\mathrm{Ln}} - E_{\mathrm{S_1}} - \Delta E_{\mathrm{Coul}} \qquad (5)$$

where ΔG_{PeT} is the free energy change of photoinduced electron transfer, $E_{\mathrm{ox}}^{\mathrm{Ant}}$ is the antenna oxidation potential, $E_{\mathrm{red}}^{\mathrm{Ln}}$ is the Ln(III)/Ln(II) reduction potential, $E_{\mathrm{S_1}}$ is the energy level of S_1 and ΔE_{Coul} is the Coulombic attraction between $Ant^{+\cdot}$ and the lanthanide(II) ion (Ln(II)).[66] Consequently, a more reducible Ln(III) combined with a more oxidable antenna promotes PeT.

Apart from Eu(III) and Yb(III), PeT may also diminish the emission intensities of the harder-to-reduce Sm(III), Dy(III) and Nd(III).[21,66] Gd^{3+} has the lowest $E_{1/2}^{\mathrm{Ln}}$ and, hence, the residual ligand fluorescence quantum yield (Φ_{L}) in Gd(III) complexes would be the largest across the series of analogous Ln(III) compounds, in the absence of other processes depleting S_1. Φ_{Tb} is unaffected by PeT quenching ($E_{1/2}^{\mathrm{Tb}} = -3.7$ V vs NHE).[66] In exceptional cases, PeT can also sensitise Eu(III) emission. Then the sensitisation happens through a ligand-to-metal charge transfer state populating the $^5D_1$ receiving level[83] or forming a higher-energy $Ant^{+\cdot}$-Eu(II) intermediate, followed by the recombination.[84]

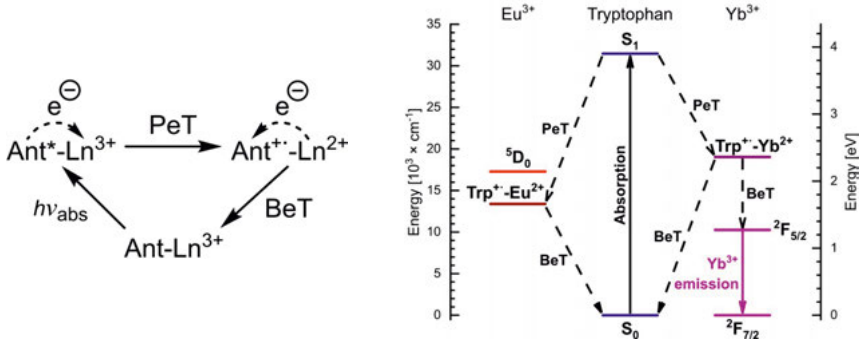

Figure 5. General scheme of antenna-to-Ln(III) PeT-BeT upon complex excitation (left) and the Horrocks' energy diagram showing the effect of PeT on Eu^{3+} and Yb^{3+} luminescence (right).[69]

1.3 Structural characterisation of macrocyclic Ln(III) complexes

The complete characterisation of Ln(III) compounds is essential to correlate the structure of the coordination complexes with the observed photophysical properties. Ln(III) compounds based on macrocyclic ligands with pendant arms form several species in solution due to their intrinsic structural dynamics.[85] The macrocycle ring inversion or pendant arm rotation results in the presence of several stereoisomers in solution.[85] Depending on the time scale of the spectroscopic experiment, the signals from two isomers or their weighted average can be detected. For example, Ln(III) complexes of cyclen-1,4,7,10-tetraacetate (DOTA) can adopt capped square antiprismatic (SAP) or twisted SAP (TSAP) geometry (Figure 6, left).[85]

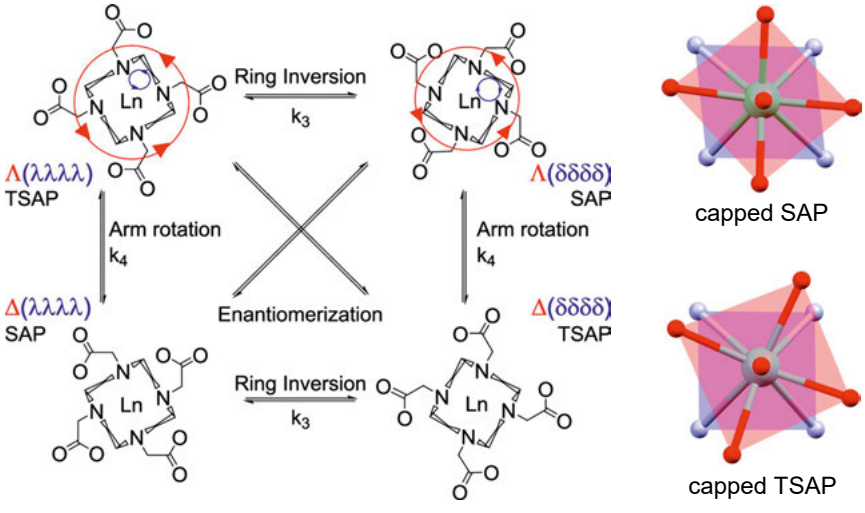

Figure 6. Scheme of structural dynamics for LnDOTA isomers in solution (left),[85] top view of capped SAP (top right)[86] and TSAP (bottom right)[87] polyhedra from solid-state structures. Figures were reprinted or reproduced with permission.[85–87] *Copyright © 2020/1984/1997, American Chemical Society*.

Both diastereomers were observed in solution via ^{1}H NMR spectroscopy, with SAP as a major and TSAP as a minor isomer for Eu and Yb complexes.[88–93] The conformation of the isomer is described by cyclen ring chirality (*δδδδ*/*λλλλ*, inner blue circle) or pendant arms helicity (*Δ*/*Λ*, outer red circle). The distinction between the two conformers in the ^{1}H NMR spectrum is established via proton signals of the 12-membered ring: the SAP CH_2 resonances are more deshielded than those of the TSAP. The structure-signal assignment was achieved by COSY spectra,[89,90] while EXSY[89–91] and VT experiments[88,89,92–94] revealed that these species interconvert on the NMR time scale.

The geometry of the isomers can be investigated via X-ray crystallography to provide further support for the structural data obtained from the studies in solution. In the structural analysis of single crystalline DOTA-based Ln(III) compounds, both SAP or TSAP geometries can be observed,[95] and several SAP or TSAP enantiomers may be found in the crystal lattice (Figure 6, right). The identity of the isomer can be determined by measuring the NCCN (ψ) and NCCO (ω) torsion angles, which correspond to cyclen ring and pendant arms helicities, respectively.[38,94,96,97] A positive or negative pair of torsion angles agrees with the TSAP structure, while two torsion angles of the opposite sign indicate the SAP isomer (Table 3).

For EuDOTA (Figure 6, top right)[86] and LaDOTA (Figure 6, bottom right)[87] complexes, exhibiting the opposite type of isomers, the structural data obtained from NMR spectroscopy were in perfect agreement with solid-state structures. Thus, these two techniques are complementary to the luminescent characterisation, as fluorescence spectroscopy cannot be utilised as a standalone method to determine the structure of the complex in solution.[93]

Table 3. Signs of ψ and ω torsion angles and the type of isomers that they form.

Parameter	Sign of ψ and ω torsion angles and type of helicity			
ψ helicity	+, $\delta\delta\delta\delta$	−, $\lambda\lambda\lambda\lambda$	+, $\delta\delta\delta\delta$	−, $\lambda\lambda\lambda\lambda$
ω helicity	+, Δ	−, Λ	−, Λ	+, Δ
Isomer	$\Delta(\delta\delta\delta\delta)$, TSAP	$\Lambda(\lambda\lambda\lambda\lambda)$, TSAP	$\Lambda(\delta\delta\delta\delta)$, SAP	$\Delta(\lambda\lambda\lambda\lambda)$, SAP

1.4 Applications of Ln(III) compounds photophysical properties

The luminescence of Ln ions has found applications in many optical-related fields. The materials containing 4f ions are components of phosphors in television sets, lamps for lightning, lasers,[12] and even security inks for anti-counterfeiting.[98] Molecular Ln(III) complexes require fine-tuning to enable their use in cells for probing biological systems[65] or in solutions for analyte detection.[99] This part briefly describes the latter cases of Ln(III) applications (Figure 7), as the thesis is devoted to luminescence studies of molecular complexes in solution.

Ln(III) compounds offer spectroscopic tools that are complementary to organic fluorophores. While the latter have short-lived (10^{-9} s time scale) fluorescence and broad emission profiles, Ln(III) luminophores are amenable to time-resolved detection up to milliseconds; their characteristic narrow spectral peaks are readily distinguished from the background in complex media.[100] Before entering cells, Ln(III) complexes can be equipped with reactive groups for conjugation to target biomolecules.[100–102] In cells, Ln(III) probes can measure the local pH[103] or the concentration of key metabolites[104] and enzymes.[105,106] At the same time, Ln(III) emission allows cellular imaging via

luminescence microscopy[107–109] and the tracking of Ln complex localisation in different organelles.[110]

Analyte detection can occur by a variety of mechanisms.[99] The analytes may react with the Ln(III) complex changing its structure and affecting Ln ion sensitisation. Ln(III) emission changes were observed after analyte-assisted antenna formation,[111] the displacement of inner sphere H_2O molecules by various anions,[99,112] ligand protonation[54] or deprotonation.[113] Antenna excited state quenching by O_2 can be utilised for ratiometric molecular oxygen sensing.[54,60,61,64] Quenching by O_2 can form reactive oxygen species, which are useful in photodynamic therapy.[56,114,115]

Ln(III) complexes of 1,4,7-triazacyclononane (tacn) found their use in cellular microscopy imaging.[116,117] The ligand platform based on tacn-1,4,7-trispicolinate derivative with the π-conjugated system provided the complex with immense ε = 60000 $M^{-1}cm^{-1}$. The latter increased the brightness of highly emissive complexes, which allowed the staining of cellular mitochondria by the visible luminescence of Eu(III).[116] The NIR emission of the analogous Yb(III) complexes was applied for in-depth tissue imaging via two-photon scanning laser microscopy.[117] As with cyclen derivatives, Ln(III) complexes based on tacn ligands can also be pH sensitive[118,119] or generate singlet oxygen upon light irradiation.[120]

As described in this part of the thesis, Ln(III) luminescence is beneficial in many aspects of life sciences, proving the necessity of further development in the design of bright lanthanide(III) compounds.

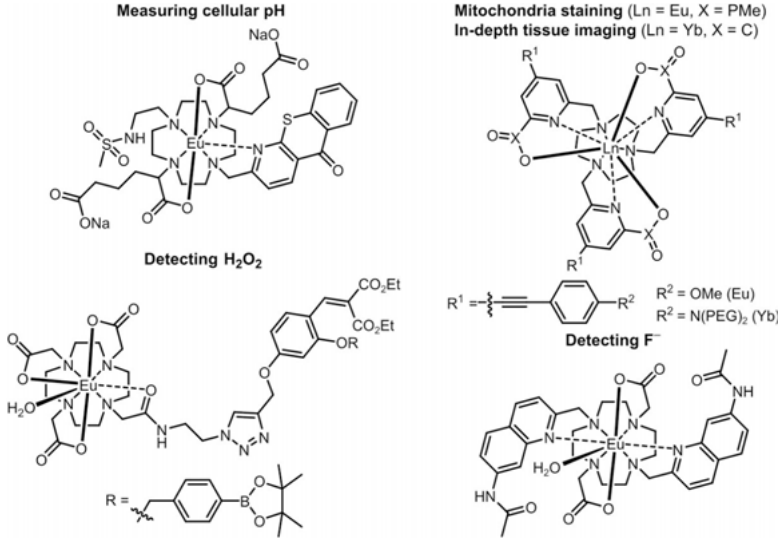

Figure 7. Ln(III) complexes for probing biological systems (top)[103,116,117] and for analyte detection (bottom).[105,112]

1.5 Aims of the doctoral thesis

The thesis aimed to establish structure-property relationships in luminescent Ln(III) complexes based on cyclen and tacn binding sites. By unravelling this connection, we intended to distinguish the processes leading to the quenching of 4f-4f emission intensity, estimate the proportion of excitation energy lost to the non-radiative decay and propose ways to preserve Ln(III) luminescence. To do so, we have set the following plan:

- Study the solution structures of a library of Ln(III) compounds via ^{1}H NMR spectroscopy to perceive their possible isomers;
- Examine their crystal structures utilising X-ray crystallography to define the preferential conformers in the solid state;
- Determine Ln(III)/Ln(II) reduction potentials through cyclic voltammetry to find out which ligands better stabilise the +3 oxidation state;
- Investigate their photophysical properties using steady-state and time-resolved luminescence spectroscopy to reveal and explain quenching trends of the luminophores with the least and the most intense emission;
- Analyse the sensitisation pathways based on photophysical data coupled to calculated rate constants of deactivating or sensitising processes.

2. Lanthanide complexes of bioconjugable ligands (Paper I)

One of the existing challenges in using Ln(III) complexes for biological visualisation is the targeted delivery of these luminophores into cells. Such Ln(III) compounds should have both advantageous photophysical properties and sufficient stability in cellular media and cells. Previous reports were on the synthesis and cellular studies of Ln(III) complexes based on linear polyaminocarboxylate ligands with carbostyril antennae functionalised with azide or alkyne bioconjugable groups.[121]

Ln(III) compounds based on macrocyclic ligands are kinetically more stable than their linear polyaminocarboxylate analogues.[122,123] Thus, the Ln(III) complexes of DO3A binding site previously studied in the group (**LnL1^{Me}**, Figure 8, left),[21,49] could represent a more beneficial alternative. In this chapter, we aimed to functionalise **LnL1^{Me}** complexes with the abovementioned bioconjugable groups and to improve their spectroscopic properties for better cellular detection.

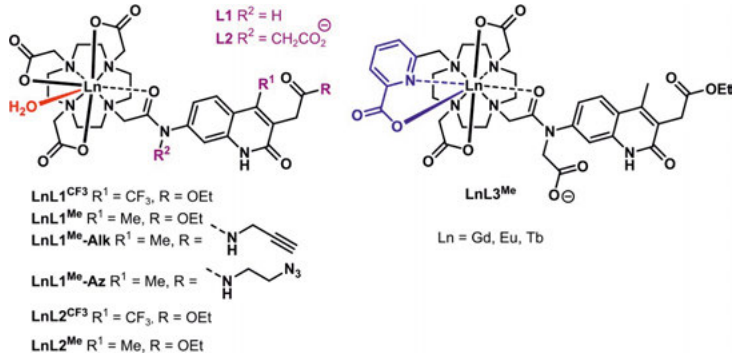

Figure 8. Ln(III) complexes of octa- (left) and nonadentate (right) ligands studied in Paper I. Adapted with permission.[124] *Copyright © 2020 American Chemical Society.*

The azide or alkyne reactive handles were connected to the carbostyril by a methylene spacer to keep the electronic properties of the antenna in the Ln(III) compounds unaltered (**LnL1^{Me}-Alk**/**Az**, Figure 8, left). At the same time, we focused on increasing the emission intensities of Eu(III) complexes for a larger signal-to-noise ratio (S/N) upon cellular detection. The first approach was to set an electron-withdrawing CF_3 substituent in the 4-position of the

carbostyril (**LnL1^{CF3}**), which would diminish PeT quenching in Eu(III) compounds by making antenna less reducing.[21] Second, we replaced one of the monodentate methylcarboxylate arms with a bidentate picolinate pendant arm in the macrocyclic binding site to remove the coordinated water molecule. The resulting nonadentate ligand should saturate the Ln(III) coordination sphere (**LnL3^{Me}**, Figure 8, right).

2.1 Reactivity of bioconjugable groups

The bioconjugable compounds were prepared by Dr. Daniel Kovacs. Strain-promoted azide-alkyne cycloadditions of the Eu(III) and Tb(III) complexes were performed with dibenzocyclooctyne-amine (DBCO-NH_2). After 5 h, the conversion reached up to 90%, according to HPLC-MS analysis. We observed two regioisomers with different retention times, which was consistent with the reported cyclooctyne reactivity (Figure 9).[125] We compared the photophysical properties of the formed triazole compounds with their parent molecules (Figure 10).

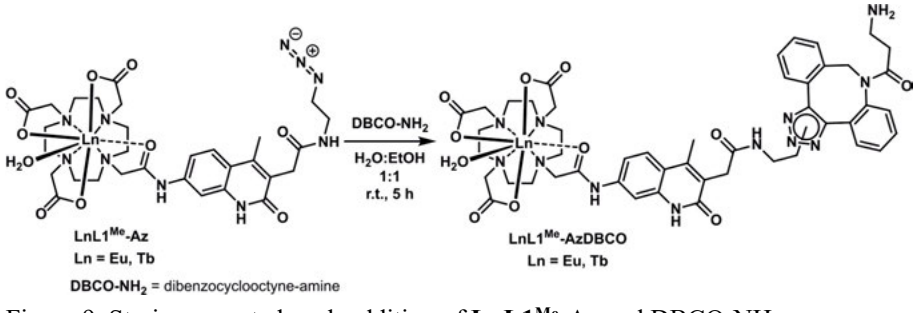

Figure 9. Strain-promoted cycloaddition of **LnL1^{Me}-Az** and DBCO-NH_2.

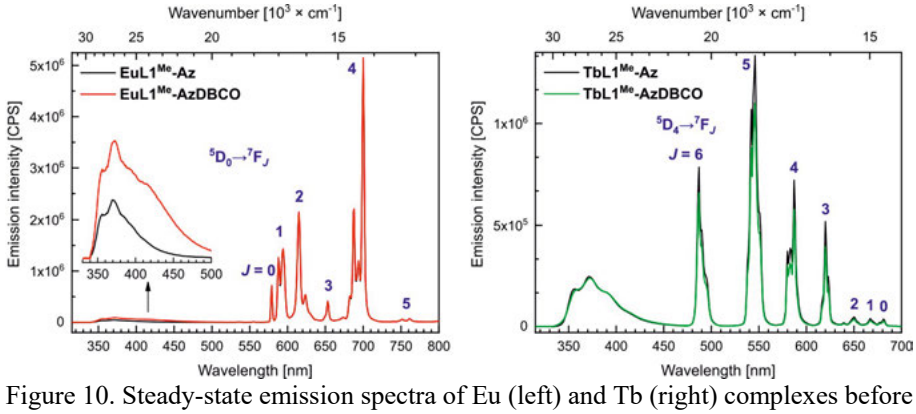

Figure 10. Steady-state emission spectra of Eu (left) and Tb (right) complexes before and after cycloaddition measured with identical sample absorbance (λ_{ex} = 345 nm) and slit widths. [**LnL1^{Me}-Az**] = 10 µM in 10 mM PIPES-buffered aqueous solutions (pH 6.5).

The absorption spectra of complexes were similar despite the formation of the DBCO-adduct. Steady-state emission spectra of both compounds were superimposable, with slight intensity differences of ligand fluorescence for Eu(III) and lanthanide emission for Tb(III) species (Figure 10). Triazole complexes had comparable τ_{H_2O} and τ_{D_2O} to those of the original compounds. Hence, the conjugation with cyclooctyne did not substantially alter the luminescent properties of the parent complexes as the methylene spacer separated the modified linker from the antenna.

2.2 Photophysical characterisation of Ln(III) compounds

All photophysical measurements were performed in aqueous 10 mM PIPES-buffered solutions (pH 6.5) with 10 μM complex concentration. The absorption spectra of **LnL1^{Me}** were not affected by the functional groups attached to the antenna or Ln(III) type. Replacing the Me with the CF_3 substituent in the 4-position of the carbostyril chromophore led to a 15 nm red shift of λ_{abs} for both secondary and tertiary amide complexes. The picolinate donor increased the absorbance of **LnL3^{Me}** at 275 nm compared to those of the octadentate ligand-based complexes; however, the absorption corresponding to the antenna region remained unchanged.

Table 4. **LnL** ligand-based and Ln(III) emission quantum yields, Ln(III) lifetimes and hydration states.

Complex	Φ_L [%] [a]	Φ_{Ln} [%] [a]	τ_{H_2O} [ms] [b]	τ_{D_2O} [ms] [b]	q [c]
EuL1^{CF3}	2.0 [d]	11 [d]	0.613	2.03	1.0
GdL1^{CF3}	4.0 [d]	/	/	/	/
EuL2^{CF3}	2.5	12	0.640	2.14	1.0
GdL2^{CF3}	2.7	/	/	/	/
EuL2^{Me}	1.7 [e]	5.7 [e]	0.652	2.16	1.0
GdL2^{Me}	7.6 [e]	/	/	/	/
TbL2^{Me}	6.9 [e]	40 [e]	1.57	2.47	0.9
EuL3^{Me}	0.78 [d]	5.8 [d]	1.00	1.38	0
GdL3^{Me}	7.2 [d]	/	/	/	/
TbL3^{Me}	6.2 [d]	45 [d]	1.83	1.95	0

The values carry relative experimental error of 10%. [a] Relative to quinine sulfate (Φ = 59% in 0.05 M H_2SO_4).[126] [b] Mean of 3 different measurements. [c] Calculated using Eq. (3) or (4). [d] Mean of 2 independent measurements. [e] Mean of 3 independent measurements.

The results of luminescence measurements are summarised in Table 4. These experiments were recorded by exciting Ln(III) complexes at the carbostyril absorption band. Along with the residual ligand fluorescence observed in all compounds, the Ln(III) emission was detected for Eu and Tb complexes. Ln(III) compounds with azide or alkyne reactive handles had luminescence

quantum yields comparable to their parent **LnL1^{Me}** species; the differences were within 15% of the average Φ_{Ln} (3.3% and 11.3% for Eu and Tb complexes, respectively). While Φ_L for Tb(III) compounds were similar (mean 6.1%), Eu(III) complexes with bioconjugable functions had a smaller intensity of ligand fluorescence than **EuL1^{Me}** (0.15% vs 0.42%).

Eu(III) compounds with CF_3-modified antenna had the largest Φ_{Eu} in the series. The electron-withdrawing CF_3 substituent might diminish PeT from the carbostyril to Eu(III),[21] which was supported by identical Φ_L in **LnL2^{CF3}** regardless of Ln(III) and η_{sens} close to unity (Table 5). Furthermore, a lower T_1 of the antenna (21300 cm^{-1}) could provide a better overlap between the carbostyril and Eu(III) excited states and, thus, more efficient ET. A combination of these factors increased Eu(III) emission intensity in **EuL1^{CF3}** and **EuL2^{CF3}** 4-fold and 2-fold, respectively, compared to their Me-substituted analogues. The decreased energy level of T_1 was detrimental to Tb(III) emission, as it enabled thermal BET and, consequently, O_2 quenching of the antenna triplet.

Complexes with the nonadentate ligand were almost as luminescent as their **LnL2^{Me}** rivals. While Φ_{Tb} was slightly larger than that of the octadentate ligand-based compound, Eu(III) emission intensity was identical in both complexes. This result contradicted our expectations from eliminated inner sphere O-H oscillators. Notably, Φ_L in **EuL3^{Me}** was half of that in **EuL2^{Me}**, alongside a similar ligand fluorescence intensity in Tb(III) compounds.

The removal of the coordinated H_2O was confirmed by $q = 0$ for **LnL3^{Me}**, whereas **LnL2^{Me}** had $q = 1$ (Ln = Eu, Tb). Other structural changes were indicated by altered Ln(III) electronic transitions in steady-state emission spectra (Figure 11). Thus, $\Delta J = 2/\Delta J = 1$ (r or asymmetry of the Eu^{3+} site,[24] Table 5) increased 2.7-fold in Eu(III) spectra, and Stark splitting of Tb(III) $^5D_4 \rightarrow {}^7F_{5,4}$ transitions was decreased. The methylcarboxylate and water donor replacement by the picolinate pendant arm transformed the Ln(III) coordination environment.

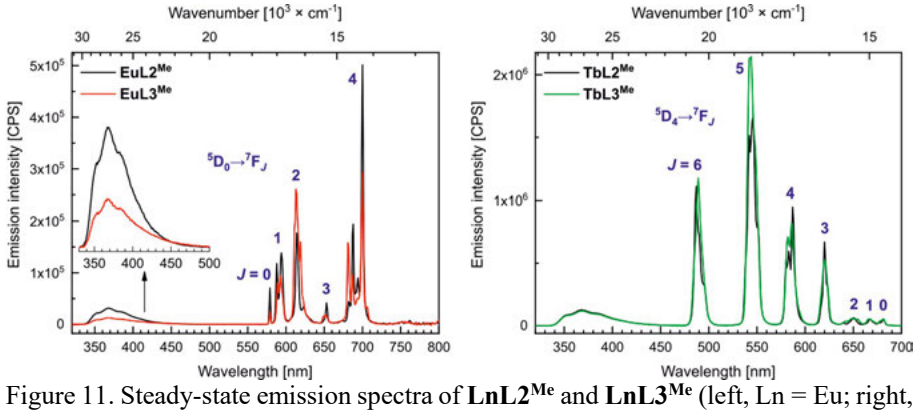

Figure 11. Steady-state emission spectra of **LnL2^{Me}** and **LnL3^{Me}** (left, Ln = Eu; right, Ln = Tb) measured with identical sample absorbance (λ_{ex} = 314 nm) and slit widths. Reproduced with permission.[124] *Copyright © 2020 American Chemical Society.*

To assess why Φ_{Eu} was not improved for **EuL3^{Me}**, we investigated the differences in photophysical properties between **EuL2^{Me}** and **EuL3^{Me}** (Table 5). A 2.3-fold enhanced intrinsic quantum yield was in line with an eliminated inner sphere H_2O molecule; however, η_{sens} was reduced to the same extent. PeT from a similar carbostyril antenna could quench Φ_{Eu}.[21] Moreover, picolinic acid is known to accept an electron from Eu(II).[127] Therefore, a likely explanation is intraligand PeT from the excited carbostyril to the picolinate via intermediate Eu(II) formation. We estimated that 42% of the excitation energy could be recovered in the nonadentate complex upon removing the coordinated H_2O molecule, based on the difference in the energetic loss from O-H quenching between **EuL2^{Me}** and **EuL3^{Me}**.

Table 5. **EuL** photophysical properties.

Complex	τ_{rad} [ms] [a]	Φ_{Ln}^{Ln} [%] [b]	η_{sens} [%] [b]	r [c]	*Loss* [%] [d]
EuL1^{CF3}	5.06	12.1	84	1.30	70
EuL2^{CF3}	5.26	12.2	95	1.19	70
EuL2^{Me}	5.38	12.1	48	1.16	70
EuL3^{Me}	3.79	27.2	21	3.08	28

The values carry relative experimental error of 10%. [a] Calculated using Eq. (1). [b] Calculated using Eq. (2). [c] Calculated as a ratio of $I_{J=2}/I_{J=1}$, where $I_{J=2}$ and $I_{J=1}$ are the integrated emission intensities of $^5D_0 \rightarrow {}^7F_2$ (604–644 nm) and $^5D_0 \rightarrow {}^7F_1$ (582–603 nm) transitions, respectively. [d] Calculated as $(\tau_{D_2O} - \tau_{H_2O})/\tau_{D_2O}$.[34]

2.3 Conclusions

Luminescent Ln(III) complexes with bioconjugable groups were prepared by modification of octadentate ligands. The products of the reactions between azide-functionalised compounds and cyclooctyne had similar photophysical properties to those of the parent molecules. Eu(III) complexes with CF_3-substituted carbostyril antennae had the largest 4f-4f emission quantum yield (11–12%) in the set of compounds with the same lanthanide(III) ion. A water molecule removal from the Ln(III) coordination sphere in nonadentate ligand-based complexes resulted in a slight increase of Tb emission intensity, but the Eu luminescence quantum yield was unchanged. The latter outcome was ascribed to intraligand photoinduced electron transfer from the excited antenna to picolinate moiety through a reducible Eu(III) centre that could offset the effects of removed inner sphere O-H oscillators.

3. Ligand-controlled photoinduced electron transfer quenching of Eu emission intensity (Paper II)

Several examples of unexpectedly small Eu(III) emission quantum yields were interpreted as a consequence of PeT quenching to date.[66] However, this mechanism remains an often underestimated deactivation pathway in Ln(III) luminescence sensitisation. While energy loss from X-H oscillators is routinely determined via luminescent measurements in protonated and deuterated solvents,[34] PeT contribution to decreased Ln(III) emission intensity has not been evaluated. In several cases, the effect of PeT quenching cannot be assuredly estimated as the cause of diminished Φ_{Ln} due to changes in the antenna S_1 energy levels[54] or undetermined $E_{\mathrm{ox}}^{\mathrm{Ant}}$.[21]

An alternative scenario of tuning PeT by varying $E_{\mathrm{red}}^{\mathrm{Ln}}$ through the coordination environment but keeping the same antenna and macrocycle has not yet been proposed. In the work of Selvin et al., Ln(III) ions were encapsulated by ligands based on DO3A and diethylenetriaminepentaacetate (DTPA).[73] Eu(III) emission was sensitised by 4-methyl-7-aminocarbostyril in both complexes. However, Φ_{Eu} in the DO3A-based emitter was 1.7 times weaker than in the DTPA complex. While these species had a single coordinated water molecule, an extra negative charge of the DTPA ligand better stabilised the Eu(III) oxidation state. Thus, the significant reduction of Eu(III) luminescence intensity in the DO3A compound was because of more favourable PeT quenching than that in the DTPA luminophore.[66]

To estimate the part of excitation energy lost to PeT quenching, we studied the effect of structural variations on photoluminescent properties in the series of Ln(III) complexes shown in Figure 12. We chose a known Ln(III) compound of DO3A ligand with a 4-methoxymethylcarbostyril ($\mathbf{L^{MOM}}$, Figure 12) antenna as a charge-neutral reference point.[21] We introduced increasing amounts of positive charge (balanced by chloride counterions) into a series of Ln(III) complexes by successively substituting a negatively charged carboxylate donor with a neutral amide pendant arm. In the molecules carrying +3 charge, methylation of primary amides afforded secondary and tertiary amide complexes with decreased N-H vibrational quenching. The compounds had the same antennae, hydration states, and Ln(III)-carbostyril distances to keep

Eu sensitisation unchanged. We studied the structural and photophysical behaviour of the Ln(III) complexes in detail.

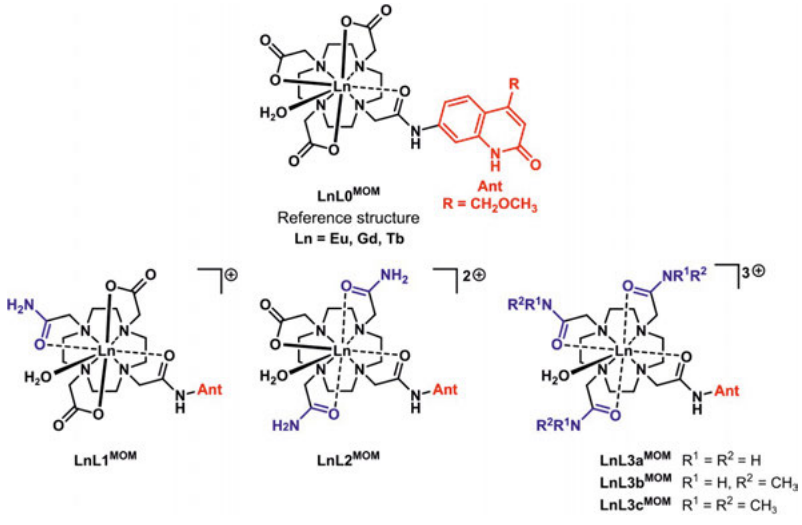

Figure 12. Ln(III) compounds of increasing charge and identical antennae in Paper II. Adapted with permission.[128] *Copyright © 2020 American Chemical Society.*

3.1 Structural characterisation of $\mathbf{LnL^{MOM}}$ compounds

Ln(III) compounds were prepared by Dr. Daniel Kovacs. Eu(III) complexes of DO3A ligands behave similarly in solution as their DOTA-based analogues (Figure 6).[85] Hence, up to two types of conformers were expected: SAP and TSAP. To determine the isomeric composition of our Ln(III) complexes, we explored their structures in solution and solid-state by ^{1}H NMR spectroscopy and X-ray crystallography, respectively.

^{1}H NMR spectra of $\mathbf{EuL^{MOM}}$ were recorded in CD_3OD at 0 °C to acquire well-resolved signals (Figure 13). The resonances of axial cyclen protons belonging to SAP and TSAP isomers were found in their designated regions.[85] While $\mathbf{EuL0–2^{MOM}}$ were present as mixtures of SAP and TSAP conformers, their +3 charged analogues had only SAP geometries in solution (Table 6). Nevertheless, the predominant structure in the former compounds was SAP, a proportion of which increased from $\mathbf{EuL0^{MOM}}$ (SAP:TSAP = 1:0.39) to $\mathbf{EuL1^{MOM}}$ and $\mathbf{EuL2^{MOM}}$ (1:0.22 and 1:0.20, respectively). The most deshielded chemical shifts of SAP-related CH_2 protons were for the neutral complex at 35.61–41.97 ppm, followed by $\mathbf{EuL1,2^{MOM}}$ and $\mathbf{EuL3c^{MOM}}$ (29.12–37.72 ppm) and the remaining +3 charged species (28.42–33.15 ppm) reflecting different ligand field effects. TSAP signals resonated at a relatively lower frequency at 13.44–15.46 ppm.

Thus, the triamide **EuL3^{MOM}** compounds existed as SAP enantiomers, while **EuL0–2^{MOM}** complexes had SAP-TSAP isomeric mixture in solution. Based on this outcome, only single geometry of the +3 charged species is expected to contribute to the photophysical properties, whereas the other compounds would give a weighted average result of the two isomers. However, given the different temperatures (0 °C vs r.t.), solvents (CD_3OD vs H_2O), and time scales (10^{-5} s vs 10^{-9}–10^{-3} s)[85] of the NMR and fluorescence spectroscopy techniques, the isomeric composition of **EuL^{MOM}** complexes might differ between the two types of experiments.

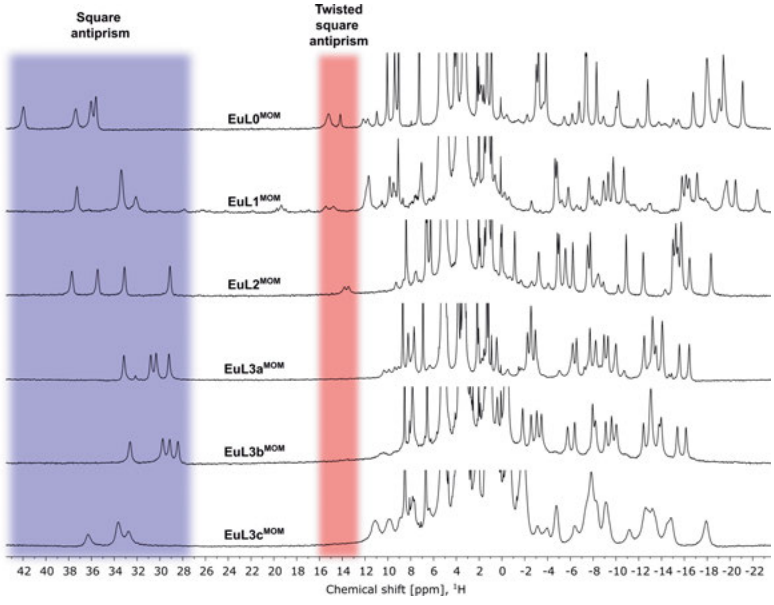

Figure 13. Stacked ^{1}H NMR spectra of **EuL^{MOM}** (400 MHz, CD_3OD, 0 °C) with cyclen axial CH_2 protons of SAP and TSAP isomers highlighted in blue and red, respectively. Adapted with permission.[128] *Copyright © 2020 American Chemical Society.*

Table 6. Data of **EuL^{MOM}** isomers extracted from ^{1}H NMR spectra. First row: spectral regions of SAP and TSAP isomers signals, second row: their integrated ratios.

Parameter	**EuL0^{MOM}**	**EuL1^{MOM}**	**EuL2^{MOM}**	**EuL3a^{MOM}**	**EuL3b^{MOM}**	**EuL3c^{MOM}**
SAP and	35.61–41.97	32.10–37.27	29.12–37.72	29.20–33.15	28.42–32.62	32.75–36.27
TSAP, ppm	14.17–15.19	14.77–15.46	13.44–13.81	-	-	-
SAP:TSAP	1:0.39	1:0.22	1:0.20	-	-	-

X-ray crystallography was performed by Dr. Jordann Wells. Single crystals were obtained for the three types of complexes by slow diffusion of 1,2-dimethoxyethane into their concentrated aqueous solutions. Among **LnL^{MOM}**, **EuL1^{MOM}** crystallised as a dimeric molecule with water and methylcarboxylate bridge (μ-AcO^-) capping Eu1 and Eu2 centres, respectively (Figure 14, left). The polyhedra about the metal atoms were formed by N_4 and O_4 planes

from the cyclen ring and pendant arms, respectively (Figure 14, right). **Gd,TbL2^{MOM}** and **EuL3a^{MOM}-F** had similar nonacoordinate environments to **EuL1^{MOM}**, except they were monomeric structures with capping H_2O or F^- on Ln(III) centres. KF (4 equiv.) was added to solutions of **EuL3a^{MOM}** to facilitate crystallisation.

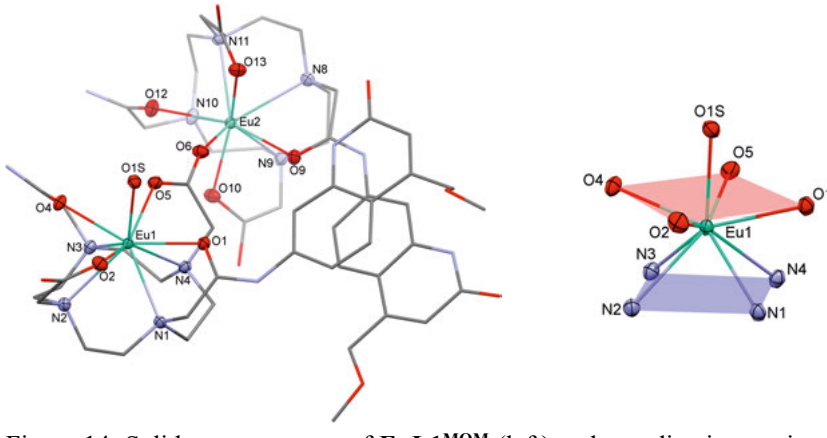

Figure 14. Solid-state structure of **EuL1^{MOM}** (left) and coordination environment of Eu1 centre (right) with O_4 and N_4 planes highlighted in red and blue, respectively. Protons, chloride counterions, and water molecules were omitted for clarity. Eu1 and Eu2 coordinating atoms are ellipsoids at 50% probability, while the rest are capped sticks. Reprinted with permission.[128] *Copyright © 2020 American Chemical Society.*

To reveal which isomers were in the single crystals, we measured mean ψ and ω torsion angles from Ln(III) coordination environments (Figure 14, right).[96] Since all pairs of ψ and ω torsion angles were of opposite signs between each other in our crystal structures, the defined isomers were $\Delta(\lambda\lambda\lambda\lambda)$ or $\Lambda(\delta\delta\delta\delta)$ configurations attributable to SAP enantiomers (Table 7). Such isomeric composition correlates with the previously obtained solid-state structures of DO3A-based carbostyril complexes containing both molecules related to the SAP isomer.[49,124] Crystal structures of Ln(III) compounds exhibiting only SAP geometry support the predominance of this isomer in solution as found by ^{1}H NMR spectroscopy. Most probably, the SAP conformer made a decisive contribution to the observed photophysical properties of Ln(III) complexes.

Table 7. Data of **LnL^{MOM}** isomers extracted from X-ray structures.

Parameter	**EuL1^{MOM}**		**GdL2^{MOM}**		**TbL2^{MOM}**		**EuL3a^{MOM}-F**	
Metal centre	Eu1	Eu2	Gd1	Gd2	Tb1	Tb2	Eu1	Eu2
Capping ligand	H_2O	μ-AcO^-	H_2O	H_2O	H_2O	H_2O	F^-	F^-
ψ, °	−58.7	60.4	58.4	−59.0	−58.0	59.5	58.6	−59.1
ω, °	24.3	−24.2	−20.8	23.9	25.3	−24.6	−31.5	29.4
Isomer	$\Delta(\lambda\lambda\lambda\lambda)$	$\Lambda(\delta\delta\delta\delta)$	$\Lambda(\delta\delta\delta\delta)$	$\Delta(\lambda\lambda\lambda\lambda)$	$\Delta(\lambda\lambda\lambda\lambda)$	$\Lambda(\delta\delta\delta\delta)$	$\Lambda(\delta\delta\delta\delta)$	$\Delta(\lambda\lambda\lambda\lambda)$

3.2 Photophysical properties of **LnL^{MOM}** complexes

To compare the photophysics of the Ln(III) compounds, we characterised their absorption and steady-state and time-resolved emission in aqueous PIPES-buffered (10 mM, pH 6.5) solutions. The installation of amide arms instead of acetates increased **LnL^{MOM}** relative absorption in the medium UV (260–310 nm), whereas the antenna region was unaltered (Figure 15, left). Therefore, Ln(III) complexes were excited at λ_{abs} for luminescence studies. **LnL^{MOM}** had superimposable absorption and excitation spectra in the carbostyril region, verifying Ln(III) sensitisation from the antenna (Figure 15, right). The carbostyril T_1 energy levels were at 22600±100 cm^{-1}, as determined from antenna phosphorescence transitions in the steady-state emission spectra of **GdL^{MOM}** at 77 K. Thus, antenna and Ln(III) excited states were identical in **LnL^{MOM}**.

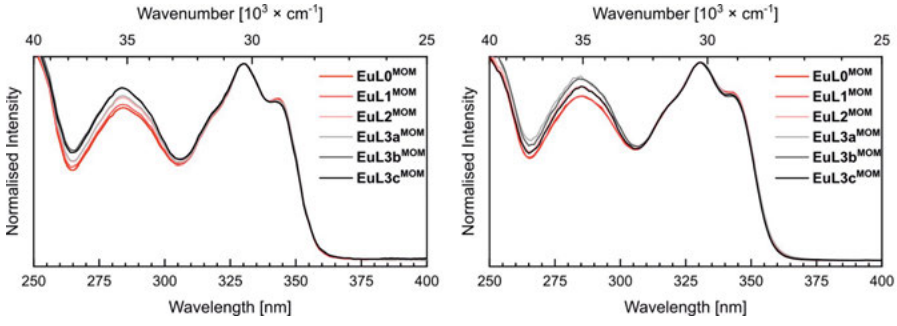

Figure 15. Superimposed and normalised absorption (left, λ_{abs} = 330 nm) and excitation (right, λ_{em} = 615 nm) spectra of **EuL^{MOM}**. Reproduced with permission.[128] *Copyright © 2020 American Chemical Society.*

First, we investigated the emissive properties of **LnL^{MOM}** with hard-to-reduce Gd(III) and Tb(III) (Figure 16). The ligand fluorescence intensity varied by 7% within the mean Φ_L in Gd and Tb compounds (6.7% and 5.1%, respectively). The deviation from the average Φ_{Tb} of 26.8% was only 4% (Table 8). **TbL^{MOM}** emission profiles resembled each other, which is expected if the Tb(III) ions were in similar coordination environments (Figure 16, right). The Φ_L differences in **Gd** and **TbL^{MOM}** were within the expected 10% relative experimental error; however, the ligand fluorescence quantum yield was still smaller in Tb complexes than in the Gd ones.

Singlet-mediated EnT to Tb(III) excited state is possible in **TbL^{MOM}** (Figure 3),[21,30] and the same pathway is closed in compounds of Gd(III) due to its inaccessible $^6P_{7/2}$ level. To investigate this possibility, we recorded ligand fluorescence lifetimes ($\tau_{f,L}$) of **Gd,TbL^{MOM}**. Tb complexes had shorter $\tau_{f,L}$ than the Gd ones (mean 0.33 ns vs 0.41 ns, respectively). By assuming that the rest of the non-radiative decay in these compounds is identical, we could estimate the rate constants of EnT(S_1) ($k_{EnT(S_1)}$) in **TbL^{MOM}** from the radiative ligand

fluorescence lifetimes ($\tau_{\mathrm{rad,L}}$) using Eq. (6), and $k_{\mathrm{EnT(S_1)}}$ could be determined from Eq. (7):

$$\tau_{\mathrm{rad,L}} = \frac{\tau_{\mathrm{f,L}}}{\Phi_{\mathrm{L}}} \tag{6}$$

$$k_{\mathrm{EnT(S_1)}} = \frac{1}{\tau_{\mathrm{f,L(Tb)}}} - \frac{1}{\tau_{\mathrm{rad,L(Tb)}}} - \left(\frac{1}{\tau_{\mathrm{f,L(Gd)}}} - \frac{1}{\tau_{\mathrm{rad,L(Gd)}}}\right) \tag{7}$$

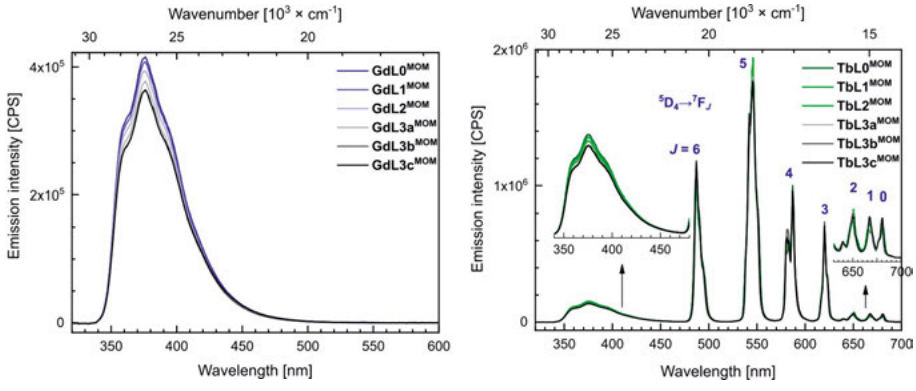

Figure 16. Steady-state emission spectra of **GdL$^{\mathbf{MOM}}$** (left) and **TbL$^{\mathbf{MOM}}$** (right) measured with identical sample absorbance (λ_{ex} = 329.5 nm) and slit widths. Reproduced with permission.[128] *Copyright © 2020 American Chemical Society.*

Table 8. **GdL$^{\mathbf{MOM}}$** and **TbL$^{\mathbf{MOM}}$** ligand photophysical properties and Φ_{Tb}.

Complex	Φ_{L} (φ_{L}) [%] [a]	$\tau_{\mathrm{f,L}}$ [ns] [b]	$\tau_{\mathrm{rad,L}}$ [ns] [c]	$k_{\mathrm{EnT(S_1)}}$ [ns^{-1}] [d]	Φ_{Ln} (φ_{Ln}) [%] [a]
GdL0$^{\mathbf{MOM}}$	7.21 (100)	0.426	5.91	-	/
GdL1$^{\mathbf{MOM}}$	7.01 (97)	0.419	5.98	-	/
GdL2$^{\mathbf{MOM}}$	6.81 (95)	0.413	6.06	-	/
GdL3a$^{\mathbf{MOM}}$	6.52 (91)	0.410	6.29	-	/
GdL3b$^{\mathbf{MOM}}$	6.36 (88)	0.406	6.39	-	/
GdL3c$^{\mathbf{MOM}}$	6.45 (90)	0.409	6.34	-	/
TbL0$^{\mathbf{MOM}}$	5.39 (100)	0.349	6.47	0.53	27.6 (100)
TbL1$^{\mathbf{MOM}}$	5.25 (97)	0.332	6.32	0.64	27.2 (99)
TbL2$^{\mathbf{MOM}}$	5.06 (94)	0.322	6.36	0.69	26.4 (96)
TbL3a$^{\mathbf{MOM}}$	4.84 (90)	0.317	6.55	0.72	26.0 (94)
TbL3b$^{\mathbf{MOM}}$	4.87 (90)	0.328	6.74	0.59	25.7 (93)
TbL3c$^{\mathbf{MOM}}$	4.87 (90)	0.327	6.71	0.62	27.7 (100)

The values carry relative experimental error of 10%. [a] Relative to quinine sulfate (Φ = 59% in 0.05 M H_2SO_4).[126] φ_{L} and φ_{Ln} are relative (to **LnL0$^{\mathbf{MOM}}$**) ligand and Ln(III) emission quantum yields, respectively. [b] Mean of 2 independent measurements, λ_{ex} = 315 nm. [c] Calculated using Eq. (6). [d] Calculated using Eq. (7).

Thus, larger $\tau_{\mathrm{f,L}}$ and Φ_{L} resulted in larger $\tau_{\mathrm{rad,L}}$ in Gd complexes than that of the Tb analogues (6.2 ns vs 6.5 ns on average). The $k_{\mathrm{EnT(S_1)}}$ differed from the smallest for **TbL0$^{\mathbf{MOM}}$** to the largest for **TbL3a$^{\mathbf{MOM}}$** (Table 8, 0.53 ns^{-1} and 0.72 ns^{-1}, respectively). Nevertheless, these rate constants diverted from an

average of 0.63 ns^{-1} only by 13−19%, suggesting some variations in Ln(III) sensitisation via antenna S_1 in the series of Tb compounds.

The ligand fluorescence quantum yields for **EuL^{MOM}** were drastically smaller than that of Gd and Tb species (Table 9). Φ_L decreased by 94–98% in Eu(III) complexes compared to **GdL^{MOM}** and **TbL^{MOM}** values. Eu(III) ligand fluorescence intensity gradually diminished from neutral to +3 charged molecules; it was slightly recovered only in dimethylated **EuL3c^{MOM}**. These changes somewhat correlated with Φ_{Eu}, which dropped by 27% on average (rel. to **EuL0^{MOM}**) with each methylcarboxylate arm replaced by an amide. The mono- and dimethylation of **EuL3a^{MOM}** increased Eu(III) emission intensity by 11% and 34% (rel. to **EuL0^{MOM}**) for **EuL3b^{MOM}** and **EuL3c^{MOM}**, respectively, due to N-H oscillator removal. However, in the absence of other quenching pathways, one would expect Φ_{Eu} of **EuL3c^{MOM}** to resemble that of **EuL0^{MOM}**, as both compounds had the same number of N-H bonds. Thus, the 47% smaller Φ_{Eu} in **EuL3c^{MOM}** than that of **EuL0^{MOM}** was caused by PeT.

Table 9. **EuL^{MOM}** ligand-based and Eu(III) emission quantum yields, Eu(III) lifetimes and hydration states.

Complex	Φ_L (φ_L) [%] [a, b]	Φ_{Ln} (φ_{Ln}) [%] [a, b]	τ_{H_2O} [ms] [c]	τ_{D_2O} [ms] [c]	q [d]
EuL0^{MOM}	0.322 (100)	5.07 (100)	0.605	2.16	1.0
EuL1^{MOM}	0.212 (66)	3.57 (70)	0.572	2.14	1.0
EuL2^{MOM}	0.168 (52)	2.55 (50)	0.522	1.95	0.9
EuL3a^{MOM}	0.114 (35)	0.980 (19)	0.439	1.44	1.0
EuL3b^{MOM}	0.100 (31)	1.54 (30)	0.498	1.68	1.0
EuL3c^{MOM}	0.232 (72)	2.71 (53)	0.549	1.65	1.1
EuL3a^{MOM}-F [e]	0.298 (92)	7.47 (147)	0.980	2.37	0

The values carry relative experimental error of 10%. [a] Relative to quinine sulfate (Φ = 59% in 0.05 M H_2SO_4),[126] φ_L and φ_{Ln} are relative to **EuL0^{MOM}**. [b] Mean of 2 or 3 independent measurements. [c] Mean of 3 different measurements. [d] Calculated using Eq. (4). [e] Measured with 0.1 M KF.

To further support the impact of PeT quenching of Eu(III) luminescence quantum yields, we investigated the photophysical properties of the complexes in depth (Table 10). Eu(III) emission bands were alike, showing the same Stark splitting of the transitions (Figure 17, left), and τ_{rad} was similar in **EuL^{MOM}**, which, together with q = 1, supported the structural analogy of Eu(III) compounds. Except for **EuL3a^{MOM}**, τ_{H_2O} values were within the 10% experimental error. In the +3 charged species, τ_{D_2O} were significantly reduced even if these were decoupled from X-H quenching (Table 9). As Φ_{Ln}^{Ln} is dependent on the coordination environment, it decreased from 11.8% to 8.85% due to the increasing number of N-H oscillators; Φ_{Ln}^{Ln} increased to 11.2% in dimethylated **EuL3c^{MOM}**. The latter was in contrast to trends seen for η_{sens}, which was still 1.8-fold larger in **EuL0^{MOM}** than in **EuL3c^{MOM}**. Thus, Eu(III) emission intensity in **EuL3c^{MOM}** was diminished due to less populated antenna S_1. As calculated using Eq. (5) for similar compounds,[129] ΔG_{PeT} is thermodynamically

downhill for the charge-neutral complex (–1.04 eV), and increased E_{red}^{Ln} in +3 charged species would only facilitate this process further (up to –1.32 eV, Table 10).

Table 10. Photophysical properties, E_{red}^{Eu} and ΔG_{PeT} of **EuL^{MOM}**.

Complex	τ_{rad} [ms] [a]	Φ_{Ln}^{Ln} [%] [b]	η_{sens} [%] [b]	r [c]	E_{red}^{Eu} [d]	ΔG_{PeT} [eV] [e]
EuL0^{MOM}	5.14	11.8	43.0	1.21	–0.908	–1.04
EuL1^{MOM}	5.14	11.1	32.2	1.23	–0.800	–1.16
EuL2^{MOM}	4.93	10.6	24.1	1.53	–0.684	–1.28
EuL3a^{MOM}	4.96	8.85	11.1	1.53	–0.643	–1.32
EuL3b^{MOM}	5.11	9.75	15.8	1.30	–0.676	–1.26
EuL3c^{MOM}	4.91	11.2	24.2	1.41	–0.771	–1.18
EuL3a^{MOM}-F [f]	4.84	20.3	36.8	2.25	-	-

The values carry relative experimental error of 10%. [a] Calculated using Eq. (1). [b] Calculated using Eq. (2). [c] Calculated as a ratio of $I_{J=2}/I_{J=1}$, where $I_{J=2}$ and $I_{J=1}$ are the integrated emission intensities of $^5D_0 \rightarrow {}^7F_2$ (604–640 nm) and $^5D_0 \rightarrow {}^7F_1$ (582–603 nm) transitions, respectively. [d] V vs NHE, measured in H_2O (0.1 M LiCl, pH 6.4–6.7, 0.10 V/s) with [**EuL^{MOM}**] = 1 mM.[128] [e] Calculated using Eq. (5), with E_{ox}^{Ant} = 1.76 V vs NHE,[130] E_{red}^{Eu} from the previous column, E_{S1} = 3.56 eV,[128] and ΔE_{Coul} = 0.15 eV.[80] [f] Measured with 0.1 M KF.

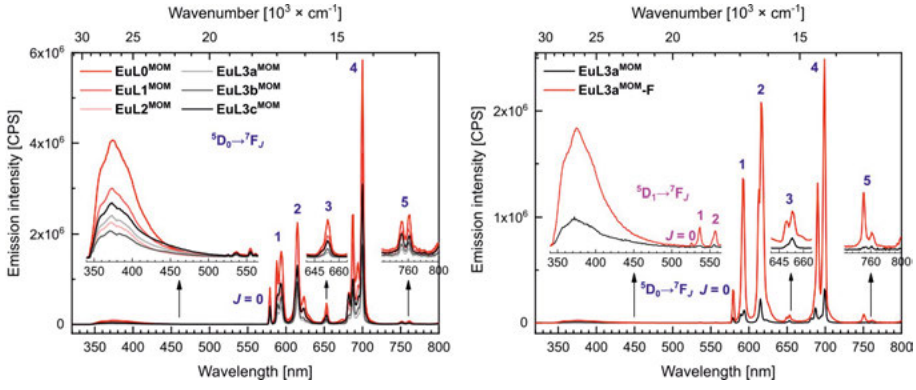

Figure 17. Steady-state emission spectra of **EuL^{MOM}** (left, λ_{ex} = 335 nm) and **EuL3a^{MOM}** with and without added excess F^- (right, λ_{ex} = 330 nm) measured with identical sample absorbance and slit widths. Reproduced with permission.[128] *Copyright © 2020 American Chemical Society.*

To stabilise Eu(III) and reduce PeT quenching, we studied the luminescent properties of the least emissive **EuL3a^{MOM}** upon added excess of fluoride (10^4 equiv. KF). Fluoride stoichiometrically replaced Eu-bound H_2O, as proved by calculated q = 0 and the changes in the steady-state emission spectrum (Figure 17, right). The decreased Stark splitting was observed for ΔJ = 1, 4 transitions, while ΔJ = 2/ΔJ = 1 was 1.5-fold larger. Furthermore, fluoride binding boosted Φ_L and Φ_{Eu} 2.6-fold and 7.6-fold, respectively, compared to H_2O-capped **EuL3a^{MOM}** (Table 9). The origin of the improved Eu(III) emission intensity was found in the 2.3-fold increased Φ_{Ln}^{Ln} and the 3.4-fold

enhanced η_{sens} (Table 10). The increased intrinsic quantum yield was due to O-H oscillator removal, while the enhanced sensitisation efficiency was attributed to diminished PeT quenching, as Φ_{Eu} of **EuL3a$^{\mathbf{MOM}}$-F** was still 1.5-fold larger than that of **EuL0$^{\mathbf{MOM}}$**.

3.3 Conclusions

We thoroughly studied the connection between structural modifications and photophysical properties in Ln(III) complexes of increasing charges and identical sensitising antennae. All compounds had one major SAP isomer in solution and crystals; this conformer was expected to contribute the most to the photoluminescent behaviour. The spectral overlap between the antenna and Ln(III) excited states was similar in all complexes. The quantum yields of compounds with non-reducible Gd(III) and Tb(III) were close within the set of molecules with the same Ln(III) ion. The differences between estimated rate constants of singlet-mediated energy transfer in Tb species were minor, highlighting the structural similarities of the Ln(III) complexes.

Eu(III) emission quantum yield was decreased by 47% in the +3 charged compound due to PeT quenching since the complex had the same number of N-H oscillators as the neutral species. The decrease of Eu(III) emission intensity via PeT was comparable in magnitude with the quenching from a coordinated water molecule (42%, see Chapter 2). Hence, PeT was found to quench as much excitation energy as an inner sphere water molecule. Fluoride binding boosted the quantum yield of Eu(III) in the compound with primary amide arms 7.6-fold via both removed O-H oscillators and reduced PeT quenching. The former accounted for a 2.3-fold increased intrinsic quantum yield, while the latter was relevant for 3.4-fold raised sensitisation efficiency.

Apart from few Ln(III), most of them are generally considered redox inactive, and PeT from the excited antenna to the Ln(III) is rarely proposed as the cause of the 4f-4f emission intensity decrease. This study shows that this nevertheless can be the case for Eu(III), one of the most commonly used Ln in luminophores. We also reveal that the PeT quenching effect can be diminished by increasing the anionic ligand coordination sites or by fluoride binding, which is beneficial for brighter Eu(III) complexes.

4. Lanthanide compounds with tertiary amide-linked antennae (Paper III)

In the previous two chapters, we showed that the Ln(III) emission intensity was affected by varying the electronic properties of the antenna or the coordination environment of the 4f ion. Through these changes, we could control the effect of PeT quenching on the Eu(III) emission intensity. However, to obtain brighter complexes, we intended to improve the ability of the antenna to sensitise Ln(III) ion. Tertiary amides connecting carbostyril antennae to the DO3A framework promoted 38–94% more excitation energy to Eu(III) than secondary amides (Figure 18a).[49]

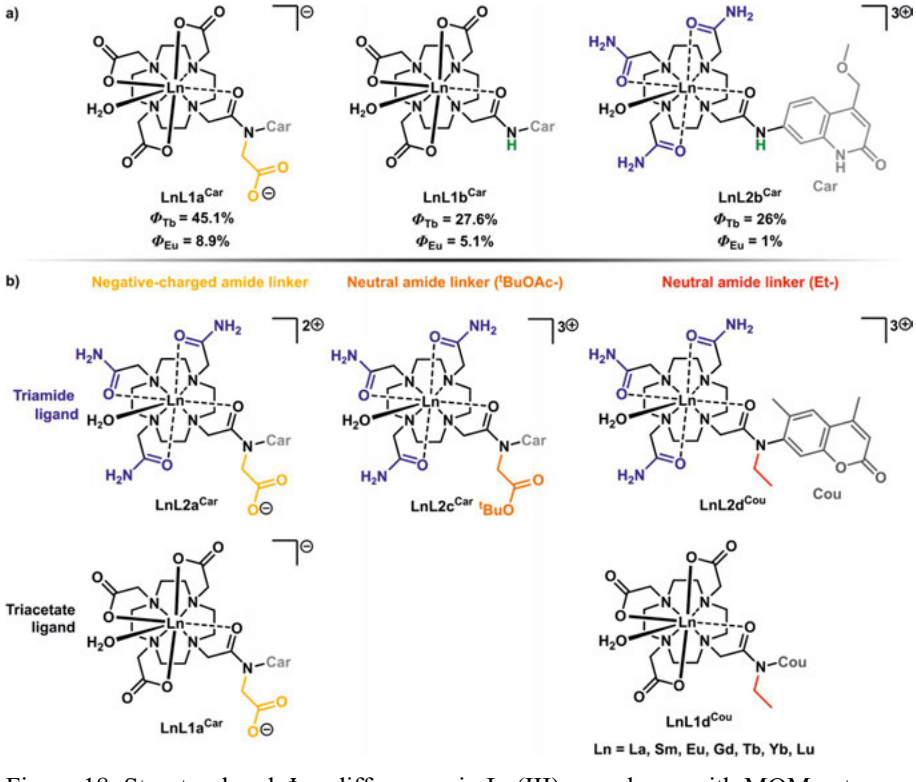

Figure 18. Structural and Φ_{Ln} differences in Ln(III) complexes with MOM antennae attached via secondary or tertiary amide linkers (a).[21,49] Ln(III) compounds with three kinds of tertiary amide linkers and two antennae types explored in Paper III (b).[131]

While the acetate substituent on the amide linker did not coordinate Ln(III), it still enhanced Ln(III) emission. We decided to investigate this phenomenon further and enlarge the tertiary amide-linked antennae compounds library to triamide complexes, as well as vary the substituent charge on the linker amide from negative to neutral and the sensitising antennae from 4-methoxymethyl-carbostyril to coumarin 2 (Figure 18b).

4.1 Synthesis of new ligands and their Ln(III) complexes

Triacetate **LnL1** complexes were synthesised as reported.[21,49] The preparation of triamide **LnL2c^{Car}** and **LnL2d^{Cou}** followed similar methods (Figure 19). Trialkylation of antenna-appended cyclen molecules **1** and **3** with 2-bromoacetamide **2a** and an appropriate base-solvent mixture (DIPEA in DMF and K_2CO_3 in CH_3CN, respectively) afforded **L2c^{Car}** and **L2d^{Cou}** with high yields (79–83%). Acidic cleavage of ^{t}Bu from tertiary amide linker substituent in a 1:1 mixture of trifluoroacetic acid (TFA) and CH_2Cl_2 resulted in the formation of **L2a^{Car}** with an excellent yield. Ln(III) complexation by the three ligands using $LnCl_3$ in H_2O:EtOH (1:1) yielded Ln(III) compounds with moderate to quantitative yields. The reaction product between protected **L2c^{Car}** and $LnCl_3$ was a mixture of **LnL2a^{Car}** and **LnL2c^{Car}** in a 1:2 ratio according to HPLC-MS analysis.

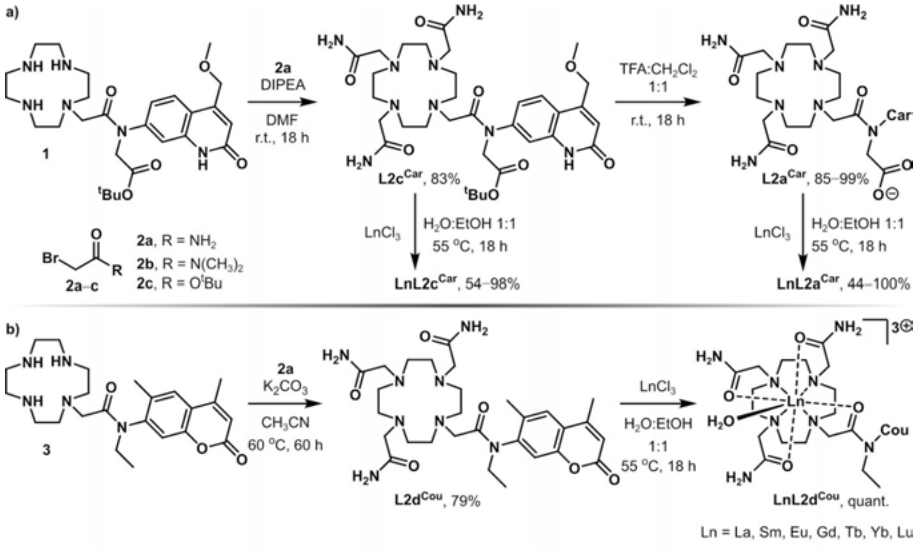

Figure 19. Synthesis of triamide carbostyril (a) and coumarin (b) Ln(III) complexes.[131]

4.2 ^{1}H NMR spectroscopy studies of paramagnetic compounds

We investigated the ^{1}H NMR spectra of paramagnetic Eu(III) and Yb(III) complexes to establish their solution structures. The spectra of Eu(III) species were recorded at lower temperatures to increase S/N, while those of Yb(III) compounds could be obtained at r.t. As expected, triacetate **EuL1a^{Car}** and **EuL1d^{Cou}** in D_2O at 10 °C had CH_2 cyclen ring signals which could be assigned to the SAP and TSAP isomers (Figure 20). The spectra of their triamide analogues **EuL2a^{Car}** and **EuL2d^{Cou}** in CD_3OD at 0 °C contained chemical shifts of only SAP species, and so did **EuL2c^{Car}**. The proportion of the TSAP conformer was more pronounced in **EuL1d^{Cou}** (SAP:TSAP = 1:0.34) than in **EuL1a^{Car}** (1:0.22). All SAP isomers had resonances at larger frequencies than the TSAP ones, with the former stretched from 29.85 ppm to 36.33 ppm and the latter resonated at 11.86–13.50 ppm (Table 11).

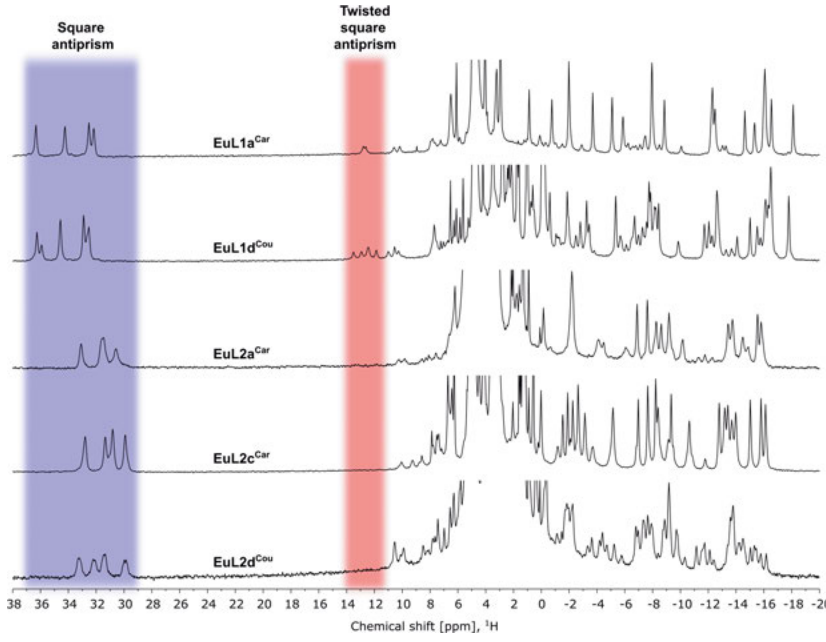

Figure 20. Stacked ^{1}H NMR spectra (400 MHz) of **EuL1** in D_2O at 10 °C and **EuL2** in CD_3OD at 0 °C with cyclen axial CH_2 protons of SAP and TSAP isomers highlighted in blue and red, respectively.[131]

Table 11. Data of **EuL** isomers extracted from ^{1}H NMR spectra. First row: spectral regions of SAP and TSAP isomers signals, second row: their integrated ratios.

Parameter	**EuL1a^{Car}**	**EuL1d^{Cou}**	**EuL2a^{Car}**	**EuL2c^{Car}**	**EuL2d^{Cou}**
SAP and TSAP, ppm	32.17–36.33 12.61–12.79	32.53–36.26 11.86–13.50	30.58–33.08 -	29.91–32.80 -	29.85–33.24 -
SAP:TSAP	1:0.22	1:0.34	-	-	-

Yb(III) complexes had chemical shifts solely from SAP conformers (Figure 21). Tricarboxylate **YbL1a^{Car}** and **YbL1d^{Cou}** had the most deshielded signals of SAP-related protons at 112.46–133.54 ppm, while those of triamide compounds extended from 95.03 ppm to 112.27 ppm. The presence of only one isomer type for Yb(III) complexes, as opposed to two for Eu(III) tricarboxylates, indicated a faster pendant arm rotation relative to the cyclen ring in **YbL**, presumably due to Ln(III) contraction.[89,132] SAP signals of coumarin compounds had 5 and 8 peaks in Eu(III) and Yb(III) spectra, respectively. No more than four chemical shifts were observed in the SAP region for carbostyril complexes. The steric hindrance between the 6-Me coumarin substituent and the carbonyl group of the tertiary amide linker could point to several SAP rotamers in **Eu,YbL^{Cou}**.

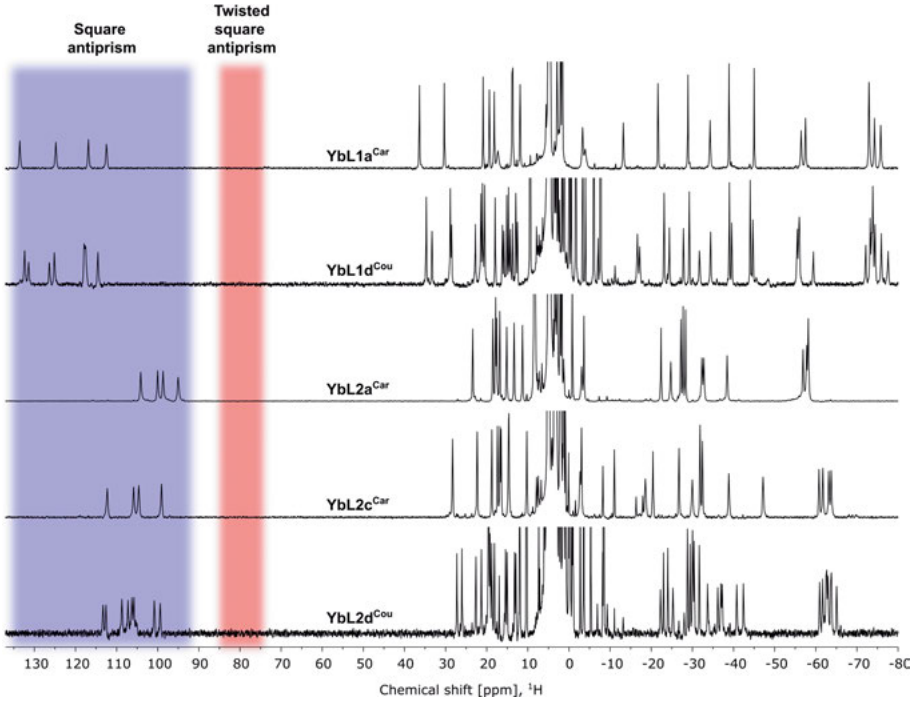

Figure 21. Stacked ^{1}H NMR spectra (400 MHz) of **YbL1**,**2a^{Car}** and **YbL1d^{Cou}** in D_2O, **YbL2c^{Car}** and **YbL2d^{Cou}** in CD_3OD at r.t. with cyclen axial CH_2 protons of SAP and TSAP isomers highlighted in blue and red, respectively.[131]

4.3 Cyclic voltammetry of Eu(III) complexes

The electrochemical properties of Eu(III) in different ligand environments and the influence of tertiary amide linker substituent on $E_{1/2}^{Ln}$ were studied by cyclic voltammetry of the compounds in aqueous solutions (0.1 M LiCl, pH 6.5,

100 mV/s scan rate). The one-electron reduction of Eu^{3+} in **EuL1a^{Car}** happened at –948 mV vs NHE, while that in **EuL2a^{Car}** occurred at more positive potentials (–612 mV vs NHE, Figure 22, left). The latter values were 109 mV and 58 mV more cathodic than those of secondary amide-linked **EuL1b^{Car}** and **EuL2b^{Car}**, respectively. The coumarin-appended complexes had Eu^{3+} reductions at –854 mV vs NHE for **EuL1d^{Cou}** and –565 mV vs NHE for **EuL2d^{Cou}**.

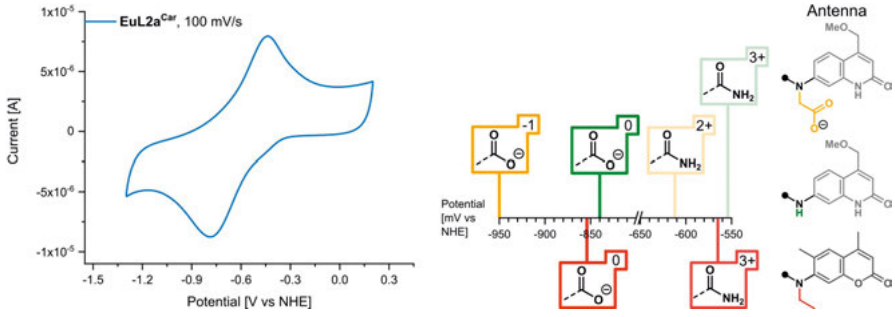

Figure 22. Cyclic voltammogram of **EuL2a^{Car}** (1 mM) measured in H_2O (left, 0.1 M LiCl, pH 6.5, 100 mV/s). Effect of coordination environment (tricarboxylate vs triamide) and amide linker (tertiary vs secondary) on $E_{1/2}^{Ln}$ in Eu(III) complexes (right).[131]

As the **EuL2^{Car}** series had the same coordination environment and carbostyril antenna, we assessed the impact of $-CH_2CO_2^-$, $-CH_2CO_2{}^tBu$, and -H substituents on the amide linker to Eu(III) reduction (Figure 22, right). The $-CH_2CO_2^-$ substituent resulted in the most cathodic shift of $E_{1/2}^{Ln}$ in the series. The difference in Eu(III)/Eu(II) reduction potentials between **EuL2c^{Car}** and **EuL2b^{Car}** was within measurement error (–564 mV vs NHE and –554 mV vs NHE, respectively). $E_{1/2}^{Ln}$ was identical for **EuL2c^{Car}** and **EuL2d^{Cou}**, reflecting the analogical contribution of the ligand field to Eu^{3+} reduction. Hence, the negatively charged substituent on the tertiary amide linker had the most stabilising effect on Eu(III), which might improve the emissive properties of corresponding complexes due to diminished PeT.

4.4 Photophysical studies of Ln(III) compounds

The photophysical properties of Ln(III) complexes were measured in aqueous PIPES-buffered solutions (10 mM, pH 6.5). The absorption spectra of compounds with the same antennae were similar regardless of the ligand binding site or Ln(III). Carbostyril and coumarin-based λ_{abs} were at 328 nm and 319 nm, respectively. The profile of the excitation spectra of the metal-based luminescence matched the respective absorption of Ln(III) complexes in the

antenna region (Figure 23). Thus, Ln(III) emission was sensitised by either carbostyril or coumarin antenna.

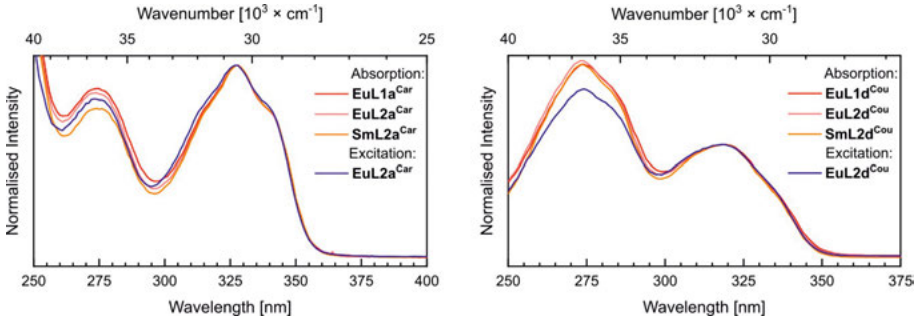

Figure 23. Superimposed normalised absorption and excitation (λ_{em} = 615 nm) spectra of **LnL^{Car}** (left, λ_{abs} = 328 nm) and **LnL^{Cou}** (right, λ_{abs} = 319 nm) complexes.[131]

To verify the similar sensitisation in Ln(III) complexes by the same antennae, we defined their T_1 energy levels from steady-state emission spectra of Gd(III) compounds at 77 K. Excitation at λ_{abs} resulted in ligand-based fluorescence and phosphorescence (Figure 24). The T_1 levels were estimated from 0–0 phonon transitions at 23000 cm^{-1} and 22200 cm^{-1} for **GdL^{Car}** and **GdL^{Cou}** complexes, respectively. The former T_1 was 400 cm^{-1} larger than that in the corresponding secondary amide-linked carbostyril antenna.[128] Thus, these ligands had appropriate excited state levels to sensitise several Ln(III).[21]

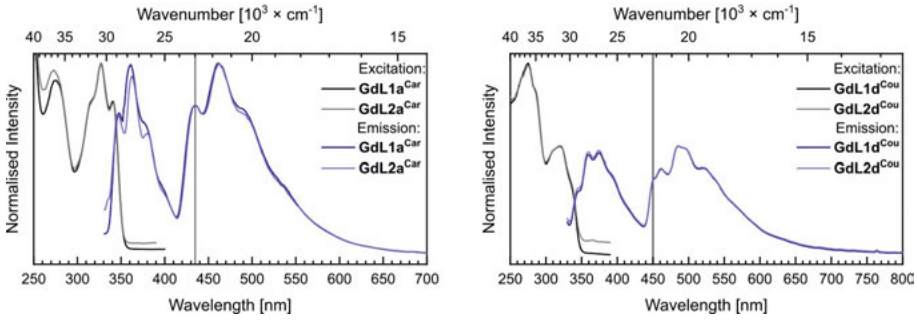

Figure 24. Superimposed normalised excitation (left, λ_{em} = 435 nm; right, λ_{em} = 462 nm) and steady-state emission spectra of **GdL^{Car}** (left, λ_{ex} = 327 nm) and **GdL^{Cou}** (right, λ_{ex} = 315 nm) complexes at 77 K. Dark grey lines are at 0–0 phonon transitions of phosphorescent bands (**GdL^{Car}** λ_{em} = 435 nm, **GdL^{Cou}** λ_{em} = 450 nm).[131] **GdL1a^{Car}** spectra were plotted for comparison.[49]

For Ln(III) compounds (Ln = La, Gd, Lu) with ligand-based fluorescence alone, the values of Φ_L were similar within experimental error (mean 4.6% for **LnL^{Car}** and 0.64% for **LnL^{Cou}**). Yb(III) complexes had the same ligand fluorescence intensity as the latter compounds. Φ_L varied greatly in carbostyril molecules with 4f-4f emission, while that in coumarin complexes was

identical (0.63% on average) regardless of the Ln(III) identity. A smaller Φ_L in Sm(III) and Eu(III) carbostyril compounds than that in Tb(III) ones might be due to PeT from the excited antenna to a more reducible Ln(III). The latter effect is even more prominent in triamide **EuL2a^{Car}**, which retained just 31% of the ligand fluorescence intensity of **EuL1a^{Car}** (Table 12).

Table 12. Ligand-based and Ln(III) emission quantum yields, Ln(III) lifetimes and hydration states of carbostyril and coumarin complexes.

Complex	Φ_L [%] [a]	Φ_{Ln} [%] [a]	τ_{H_2O} [ms] [b]	τ_{D_2O} [ms] [b]	q [c]
SmL1a^{Car}	3.6 [d]	0.19 [d]	0.009	0.032	-
EuL1a^{Car} [e]	2.5	8.9	0.66	2.17	1.0
TbL1a^{Car} [e]	4.5	45.1	1.81	2.92	0.8
SmL2a^{Car}	3.4 [d]	0.21 [d]	0.010	0.032	-
EuL2a^{Car}	0.77 [f]	2.7 [f]	0.51	2.05	0.9
TbL2a^{Car}	4.1	36.6	1.50	2.70	1.2
SmL1d^{Cou}	0.64 [d]	0.059 [d]	0.010	0.031	-
EuL1d^{Cou}	0.62 [f]	2.2 [f]	0.62	1.96	1.0
TbL1d^{Cou}	0.62	1.7	0.47	0.61	-
SmL2d^{Cou}	0.64 [d]	0.067 [d]	0.012	0.032	-
EuL2d^{Cou}	0.58 [f]	1.5 [f]	0.54	2.01	0.8
TbL2d^{Cou}	0.67	1.0	0.29	0.45	-

The values carry relative experimental error of 10%. [a] Relative to quinine sulfate (Φ = 59% in 0.05 M H_2SO_4).[126] [b] Mean of 3 different measurements. [c] Calculated using Eq. (3) or (4). [d] Mean of 2 independent measurements. [e] Reprinted data.[49] [f] Mean of 3 independent measurements.

The Ln(III) emission spectral shapes were similar in carbostyril and coumarin compounds, underscoring their similar Ln(III) coordination environments (Figure 25). The replacement of the tricarboxylate with a triamide binding site diminished Φ_{Ln} in the case of Eu(III) and Tb(III) complexes, whereas Sm(III) emission intensity had a minor change upon increasing molecular charge. The latter was due to increased uncertainty in measuring small Φ_{Sm}, comparable to the values of secondary amide-linked compounds.[21] Eu(III) emission intensity was 70% smaller in **EuL2a^{Car}** than in **EuL1a^{Car}**, while **TbL2a^{Car}** preserved 81% of Φ_{Tb} in **TbL1a^{Car}**. The latter was supported by the moderate sensitivity of Tb(III) emission to N-H oscillators; however, the reduction of Φ_{Eu} was still too much, considering only the vibrational quenching involved. Hence, part of the excitation energy could be lost to PeT in +2 charged **EuL2a^{Car}**. In coumarin complexes, Eu(III) emission intensity was decreased only by 32% in **EuL2d^{Cou}** relative to Φ_{Eu} of **EuL1d^{Cou}**.

Carbostyril compounds had q = 1, which agreed with an octadentate ligand structure. The same q value was obtained for Eu(III) complexes with coumarin antennae. However, for **TbL1,2d^{Cou}** q could not be determined. The latter was due to a small energy gap (1600 cm^{-1}) between coumarin T_1 and the $^5D_4$ receiving level of Tb^{3+}, which facilitated thermal BET and quenching of

antenna triplet by molecular O_2. For a similar reason, **TbL1d^{Cou}** and **TbL2d^{Cou}** had small Φ_{Tb} (1.7% and 1.0%, respectively).

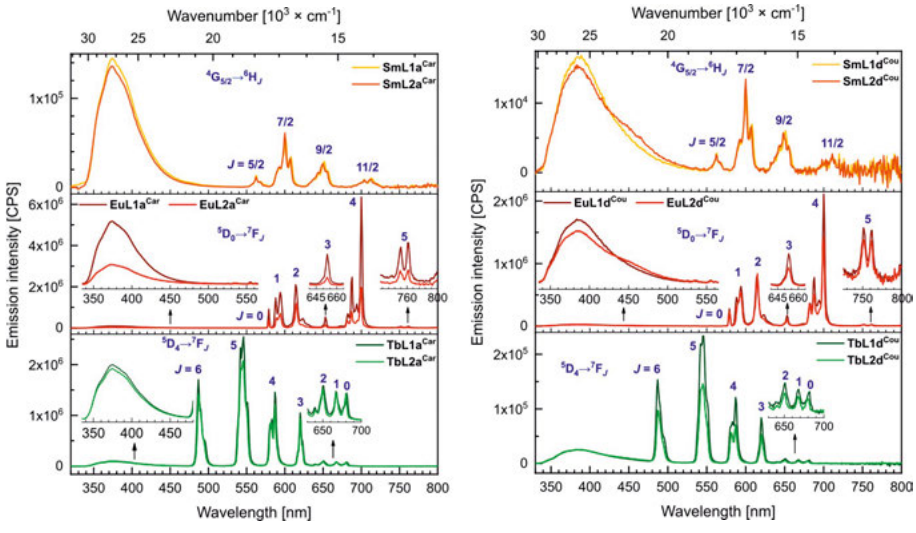

Figure 25. Steady-state emission spectra of **LnL^{Car}** (left, λ_{ex} = 327 nm) and **LnL^{Cou}** (right, λ_{ex} = 315 nm) complexes measured with identical sample absorbance and slit widths. Sm and Eu spectra are from 10 mM PIPES-buffered D_2O solutions (pD 6.9).[131] **Eu,TbL1a^{Car}** spectra were plotted for comparison.[49]

As the coumarin compounds were less emissive than the carbostyril analogues, we studied the photophysical properties of the Eu(III) species in more detail. Eu(III) emission spectral shape was the same in all molecules having similar τ_{rad} in H_2O and D_2O (mean 5.2 ms, Table 13). The average Φ_{Ln}^{Ln} for **EuL1** and **EuL2** complexes was 12% and 10.4%, respectively, due to increased X-H quenching in the latter. The largest η_{sens} was found for the most emissive **EuL1a^{Car}**, while that of **EuL2a^{Car}** was 2.6-fold smaller. Despite more destabilised Eu^{3+} in **EuL2d^{Cou}** than in **EuL1d^{Cou}**, both compounds had almost equal η_{sens}, which were the smallest in the series (mean 15.9%).

To decouple from the contribution of X-H oscillators in photophysical parameters measured in H_2O, we performed similar measurements in D_2O. While ligand fluorescence intensity was not altered upon deuteration, Φ_{Eu} increased in all complexes 4-fold on average. Even without X-H oscillators, Eu(III) emission intensity in **EuL2a^{Car}** was 63% smaller than in **EuL1a^{Car}**. For coumarin compounds, the difference between **EuL2d^{Cou}** and **EuL1d^{Cou}** was only a quarter. Φ_{Ln}^{Ln} in D_2O were equal (mean 39.1%, Table 13), and η_{sens} had the same trends as in H_2O, except for an 11% larger gap between the coumarin species. Since Eu(III) emission of tricarboxylate and triamide complexes was decoupled from X-H quenching in D_2O, the 63% and 26% reduced Φ_{Eu} in carbostyril and coumarin compounds, respectively, were due to PeT.

Table 13. Photophysical properties of Eu(III) carbostyril and coumarin complexes.

Parameter	**EuL1a^{Car}**	**EuL2a^{Car}**	**EuL1d^{Cou}**	**EuL2d^{Cou}**
τ_{rad} [ms] [a]	5.36	5.11	5.26	5.03
Φ_{Ln}^{Ln} [%] [b]	12.2	10.0	11.8	10.7
η_{sens} [%] [b]	72.8	27.6	17.6	14.1
$\Phi_L(D_2O)$ [%] [c]	2.6	0.83	0.66	0.60
$\Phi_{Ln}(D_2O)$ [%] [c]	32.3	11.8	8.5	6.3
$\tau_{rad}(D_2O)$ [ms] [a]	5.39	5.16	5.31	5.11
$\Phi_{Ln}^{Ln}(D_2O)$ [%] [b]	40.3	39.7	36.9	39.3
$\eta_{sens}(D_2O)$ [%] [b]	80.3	29.8	23.0	16.0

The values carry relative experimental error of 10%. [a] Calculated using Eq. (1). [b] Calculated using Eq. (2). [c] Relative to quinine sulfate (Φ = 59% in 0.05 M H_2SO_4).[126]

To compare the effects of PeT quenching in the carbostyril and coumarin compounds of Eu(III), we performed analogical luminescence experiments with added excess fluoride (10^4 equiv. KF). While fluoride binding was indicated through altered steady-state emission spectra (Figure 26) and by q = 0 determined for the triamide species, the tricarboxylates retained the H_2O ligand. The latter was established via the unchanged q = 1 and the superimposable emission spectra of **EuL1** measured in the presence and absence of fluoride. Hence, F^- binding in negatively charged **EuL1a^{Car}** and neutral **EuL1d^{Cou}** was ineffective.

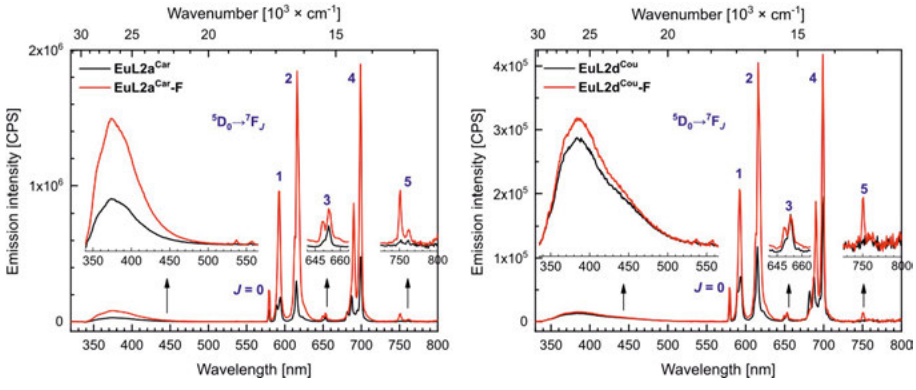

Figure 26. Steady-state emission spectra of **EuL2a^{Car}** (left, λ_{ex} = 327 nm) and **EuL2d^{Cou}** (right, λ_{ex} = 315 nm) with and without added excess F^- measured with identical sample absorbance and slit widths.[131]

Triacetate compounds had similar photophysical properties with and without fluoride, while triamide complexes were more emissive upon F^- addition (Table 14). For **EuL2a^{Car}-F**, the increase in Φ_L was 2.7-fold in light and heavy water; Eu(III) emission intensity was enhanced 4.6-fold in H_2O and 2.7-fold in D_2O. The former improvement was due to doubled Φ_{Ln}^{Ln} and η_{sens} as the outcome of the replaced inner-sphere water molecule and reduced PeT,

respectively. The enlargement of Φ_{Eu} in D_2O was due to doubled η_{sens} via hindered PeT quenching, as Eu^{3+} was more stabilised due to fluoride coordination. These effects were less pronounced than in secondary amide-linked **EuL2b^{Car}**; however, in **EuL2d^{Cou}-F**, the enhancement in emission intensity was even more moderate. While Φ_L remained unchanged in both solvents, Φ_{Eu} increased by a factor of 2.2 in H_2O and 1.4 in D_2O. This modest improvement was associated with removed O-H vibrations in both cases, as η_{sens} values were comparable to those without added fluoride. Hence, Eu(III) emission in coumarin complexes was the least affected by PeT quenching in the series of triamide compounds.

Table 14. Photophysical properties of Eu(III) carbostyril and coumarin complexes in the presence of excess fluoride (0.1 M KF).

Complex	Φ_L [%] [a]	Φ_{Ln} [%] [a]	τ_{obs} [ms] [b]	τ_{rad} [ms] [c]	Φ_{Ln}^{Ln} [%] [d]	η_{sens} [%] [d]
EuL1a^{Car}-F	2.5	9.5	0.68	5.33	12.8	73.4
EuL2a^{Car}-F	2.1	12.3	1.01	4.86	20.7	58.9
EuL1d^{Cou}-F	0.64	2.3	0.69	5.19	13.3	17.3
EuL2d^{Cou}-F	0.65	3.3	1.01	4.81	21.0	15.7
EuL1a^{Car}-F (D_2O)	2.6	32.3	2.29	5.38	42.6	75.7
EuL2a^{Car}-F (D_2O)	2.2	31.3	2.40	4.89	49.1	63.7
EuL1d^{Cou}-F (D_2O)	0.67	8.2	2.25	5.29	42.6	19.2
EuL2d^{Cou}-F (D_2O)	0.69	8.7	2.39	4.88	48.9	17.8

The values carry relative experimental error of 10%. [a] Relative to quinine sulfate (Φ = 59% in 0.05 M H_2SO_4).[126] [b] Mean of 3 different measurements. [c] Calculated using Eq. (1). [d] Calculated using Eq. (2).

4.5 Conclusions

Ln(III) complexes of cyclen triamide or triacetate binding sites and carbostyril or coumarin antennae were developed, and their photophysical properties were investigated. After the antennae were connected to the cyclen rings via tertiary amide linkers, we studied the impact of the amide substituent on the electrochemical and photophysical properties. The paramagnetic ^{1}H NMR spectra of the coumarin-based compounds indicated the presence of several rotamers in solution, while carbostyril-appended complexes had either one species or several isomers rapidly interconverting on the NMR time scale. The presence of rotamers was ascribed to the steric hindrance between the coumarin 6-Me and the amide carbonyl groups. By contrast, the carbostyril 6-position was unsubstituted, allowing the free rotation around the N-C(Ar) bond.

The largest stabilisation of Eu^{3+} was induced by a negatively charged methylcarboxylate compared to other substituents on a tertiary amide linker. Ln(III) carbostyril compounds with a methylcarboxylate group on the linker amide were more emissive than their secondary amide-connected analogues of the same binding sites. The replacement of tricarboxylate with a triamide

ligand facilitated PeT in the latter; however, the quenching effect was less significant than in the corresponding complex with a secondary linker amide. The diminution of PeT was achieved by 4.6-fold increased Eu(III) emission intensity upon fluoride binding of the triamide carbostyril compound in aqueous solutions. However, the Eu(III) emission quantum yield of coumarin-sensitised molecules was improved by only 2.2-fold after fluoride addition in water. The latter was solely accounted for the O-H vibrations removal, as the sensitisation efficiency remained the same.

This study provides insight into the structure-property relationship of compounds comprising carbostyril and coumarin chromophores. These heterocycles are closely related, but the emissive properties of their complexes can be very different. Since coumarin and carbostyril antennae are among the most widely used sensitisers of Ln(III) emission, understanding the conformations of emitting species is key to finding the correlation between desired luminescent properties and structures of respective compounds.

5. Analysis of anion binding effects on the sensitised Eu luminescence (Paper IV)

The quenching by PeT of Eu(III) luminescence intensity was suppressed by fluoride binding in triamide cyclen-based complexes, as shown in the previous two chapters. We noticed that the structural modifications outside the metal binding site still modulate the extent of PeT quenching. Thus, in the secondary amide-linked **EuL3a^{MOM}**, fluoride binding boosted Eu(III) emission intensity 1.7 times more than in the analogous complex with a tertiary amide linker (**EuL2a^{Car}**). The latter was caused by a similar difference in the increase of sensitisation efficiencies, so the luminescence of secondary amide-linked complexes was more affected by PeT quenching than that of the tertiary amide ones. Hence, we aimed to explore the outcome of anion binding on photophysical parameters and how they change with the varying size of the Ln(III) binding site, the sensitising antenna, and the overall complex charge. Moreover, changes in Φ_{Ln}^{Ln} and η_{sens} could differentiate negatively charged anions such as fluoride and cyanide, provided that the same compound shows different responses upon analyte binding.

We prepared two series of Ln(III) complexes based on cyclen and tacn ligand platforms (Figure 27). The first series (**Lc**) was the *N,N*-dimethylated amide versions of +1 and +2 charged compounds studied in Chapter 3. These new structures did not have N-H oscillators in their pendant arms, which diminished the vibrational quenching of Ln(III) excited states. The second series (**Lt**) was based on tacn-1,4-diacetate with 4-methyl (Me) or 4-MOM carbostyril antenna connected via a secondary or tertiary amide linker (**s** or **t**, respectively). The ligands were octa- and hexadentate, affording one or three available coordination sites for anion binding.[133]

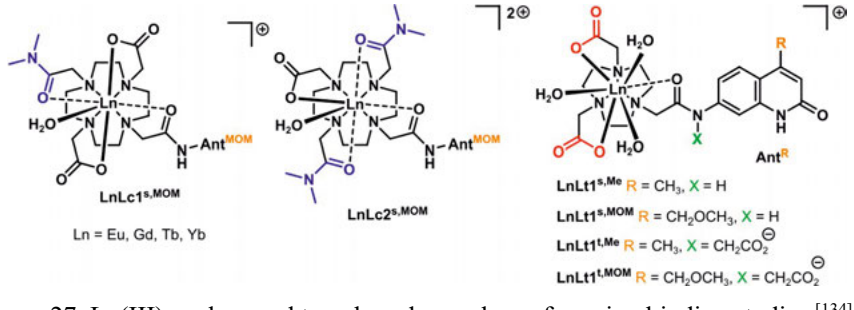

Figure 27. Ln(III) cyclen- and tacn-based complexes for anion binding studies.[134]

5.1 Synthesis of **Lc**- and **Lt**-based Ln(III) complexes

The preparation of **LnLc** complexes based on cyclen derivatives was similar to the synthesis of their analogues containing primary amide arms.[128] The alkylation of the known precursors **4** and **5**[128] by 2-bromo-*N,N*-dimethylacetamide **2b** in the presence of DIPEA in DMF at r.t. formed protected ligands **6** and **7**, respectively, in quantitative yields. In the following step, the *tert*-butyl and ethyl groups were cleaved via acidic (TFA in CH_2Cl_2) and basic (NaOH in CH_3CN:H_2O 1:1 mixture) hydrolyses at r.t. yielding **Lc1^{s,MOM}** and **Lc2^{s,MOM}**, respectively. Semi-preparative HPLC purification of **Lc1^{s,MOM}** resulted in a 58% yield, while **Lc2^{s,MOM}** could be obtained almost quantitively in pure form after column chromatography. Complexation of the ligands with a slight excess of Eu, Gd, Tb and Yb trichlorides in a water-ethanol 1:1 mixture at 45 °C supplied target Ln(III) compounds (Figure 28).

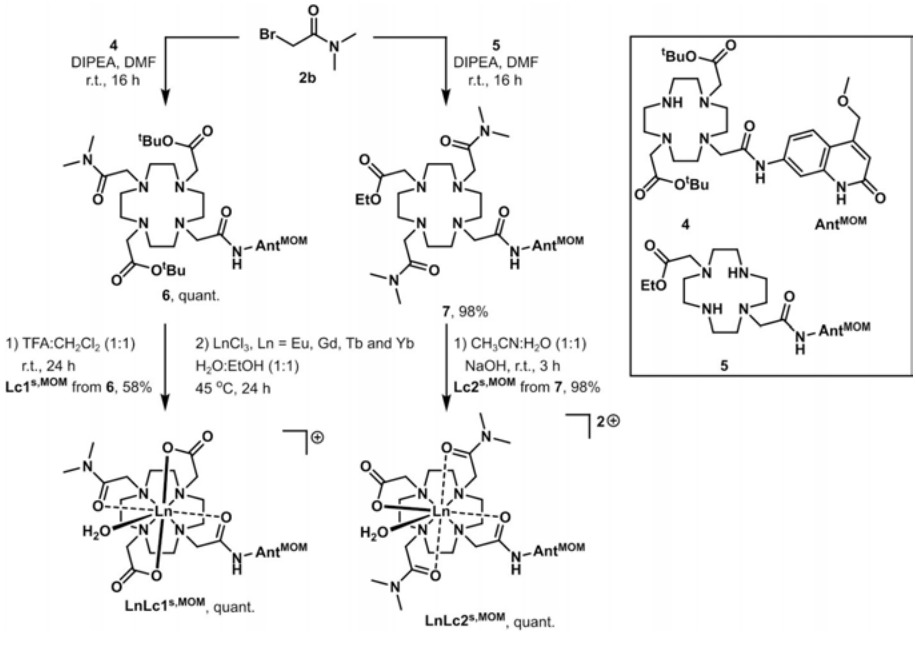

Figure 28. Synthesis of cyclen-based Ln(III) complexes.[134]

The synthesis of **LnLt** complexes commenced with commercially available free base tacn (Figure 29). The cyclic 9-membered triamine **8** was reacted with chloroacetylated antenna **9^{t,MOM}** in $CHCl_3$:DMF (8:1) at r.t. to obtain monoalkylated tacn **10^{t,MOM}** in a satisfactory yield of 60%. We afforded only a third of the expected amount for the **12^{t,MOM}** product (29%) by stirring the monoalkylated tacn **10^{t,MOM}** with two equiv. of *tert*-butyl bromoacetate **2c** in the mixture of DIPEA in DMF at r.t. This reaction resulted in the formation of tetra-*N*-alkylated species, and the yield of **12^{s,MOM}** via the described procedure was too small.

Instead of the previous method, we first attached two *tert*-butyl methylcarboxylate groups to the tacn **8**. We then alkylated the remaining secondary amine in building block **11** with the appropriate chloroacetylated antenna $\mathbf{9^{s/t,R}}$ (R = Me, MOM) in the presence of K_2CO_3 in CH_3CN at 60 °C. The Me-antenna-containing products $\mathbf{12^{s/t,Me}}$ of these reactions had moderate yields (53%), and that of $\mathbf{12^{s,MOM}}$ was 84%. The deprotection in an acidic environment by TFA in CH_2Cl_2 at r.t. removed ^{t}Bu groups forming a family of **Lt** compounds. In the final ligands, it was crucial to eliminate leftover TFA, which negatively affected the complexations with Ln(III). Hence, the ligands were precipitated by Et_2O from their concentrated solutions in MeOH, allowing the isolation of pure **Lt** in acceptable yields (>57%). Ln(III) were complexed with the ligands adapting the same procedure from the synthesis of cyclen-based compounds. **LnLt** (Ln = Eu, Gd, Tb and Yb) were isolated in quantitative yields.

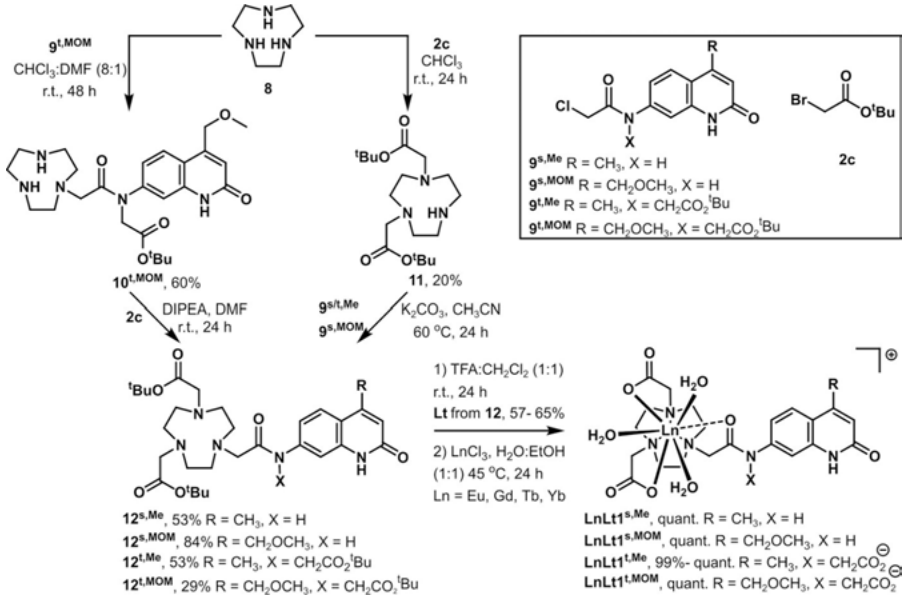

Figure 29. Synthesis of tacn-based Ln(III) complexes.[134]

The molecular structures of $\mathbf{12^{s,Me}}$ and $\mathbf{Lt1^{t,MOM}}$ were confirmed by single-crystal X-ray crystallography (Figure 30). The protected ligand $\mathbf{12^{s,Me}}$ crystallised from aqueous-CH_3CN filtrate after washing the filter cake from the reaction mixture, and the crystals of $\mathbf{Lt1^{t,MOM}}$ were found in an NMR tube containing a concentrated D_2O solution. The angle between the least square planes of the linker amide and the carbostyril was 85.9° in $\mathbf{Lt1^{t,MOM}}$, which is comparable to the value in the cyclen derivative with the tertiary amide-linked antenna.[49] The same parameter was found to be 13.7° for $\mathbf{12^{s,Me}}$, reflecting the better alignment between the secondary linker amide and the antenna. The

latter value is expected to be larger in the Ln(III) complexes of **Lt1^{s}** ligands.[49] Notably, the tilt of the carbostyril unit relative to the linker amide was dependent on the nature of the latter (89.0° for the tertiary[135] and 28.8° for the secondary[130]) in picolinate-appended tacn-based Gd(III) complexes of MOM-antenna. Thus, the orbital overlap of the heterocycle and the tertiary amide is much smaller than that of the secondary linker, which could affect carbostyril orientation and the rate of ET from the antenna to Ln(III).

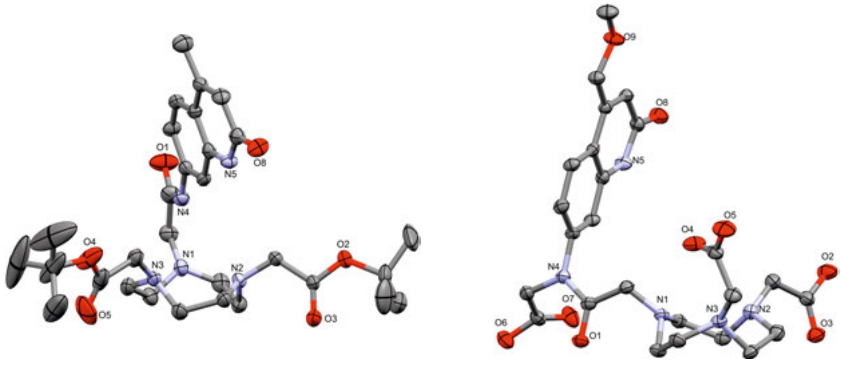

Figure 30. Solid-state structures of **12^{s,Me}** (left) and **Lt1^{t,MOM}** (right). Depicted as ellipsoids at 50% probability, protons and H_2O molecules were omitted for clarity.[134]

5.2 Solution structures of **LnLt** and **LnLc** compounds

The solution structures of cyclen and tacn-based Ln(III) complexes were studied by NMR spectroscopy. ^{1}H NMR spectra of **EuLc** compounds were measured in similar conditions as their NH_2 versions (400 MHz, CD_3OD, 0 °C) to enable comparison of their structures. As expected, the axial cyclen protons of SAP isomers resonated at higher frequencies at 31.11–40.03 ppm than those of the TSAP-attributed signals (14.21–19.63 ppm, Figure 31). The isomer ratios were 1:0.54 and 1:0.36 (SAP:TSAP) for +1 and +2 charged complexes, respectively (Table 15). The proportion of the TSAP isomer vs the SAP one was 2.5 and 1.8 times larger in **EuLc1^{s,MOM}** and **EuLc2^{s,MOM}**, respectively, than in the analogous structures with primary amides (see Chapter 3). The latter can be explained by the increased steric demand from *N*-methyl groups, which could slow down the rotation of pendant arms and change their helicity (*Δ*↔*Λ*), favouring the TSAP structure.[136]

Yb(III) complexes exhibited pronounced paramagnetic induced shifts in the ^{1}H NMR spectra.[137] **YbLc** had proton signals from 125 ppm to –70 ppm, with axial CH_2 cyclen resonances of SAP isomers at 108.10–123.41 ppm. Unlike their Eu(III) versions, no TSAP conformers were observed for **YbLc** compounds, likely because of the smaller r_{ion} of Yb^{3+} (Chapter 1, Table 1).[89,92]

The fully *N*-methylated Yb(III) cyclen-1,4,7,10-tetraamide also contained only SAP isomer in D_2O.[138]

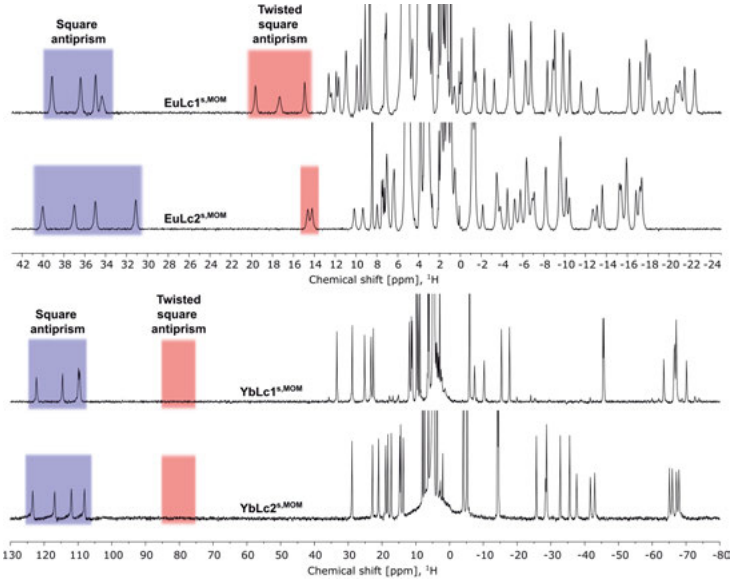

Figure 31. ^{1}H NMR spectra (400 MHz) of **EuLc** (top, 0 °C, CD_3OD) and **YbLc** (bottom, 10 °C, D_2O) complexes. The highlighted area in blue and red correspond to cyclen axial CH_2 protons from SAP and TSAP isomers, respectively.[134]

Table 15. ^{1}H NMR data extracted from **EuLc** and **YbLc** spectra. First row: spectral regions of SAP and TSAP isomers signals, second row: their integrated ratios.

Parameter	**EuLc1^{s,MOM}**	**EuLc2^{s,MOM}**	**YbLc1^{s,MOM}**	**YbLc2^{s,MOM}**
SAP	34.35–39.12	31.11–40.03	109.50–122.32	108.10–123.41
and TSAP, ppm	14.92–19.63	14.21–14.63	-	-
SAP:TSAP	1:0.54	1:0.36	-	-

Among the tacn-based complexes, only **EuLt1^{t}** had well-resolved signals in the ^{1}H NMR spectra to examine their structures in solution (400 MHz, D_2O). The number of major peaks observed in the ^{1}H NMR spectra of **EuLt1^{1}** corresponded to the theoretically expected signals of a single conformer in solution. Hence, 15 and 16 resonances were counted for **EuLt1^{t,Me}** and **EuLt1^{t,MOM}**, respectively. The ^{1}H NMR spectrum from the heated solution of **EuL1^{t,MOM}** (50 °C, Figure 32, left) allowed a more precise integration of signals, which had a better separation than the r.t. spectral pattern. The four aromatic CH protons of the carbostyril were assigned to the resonances with the highest chemical shifts (7.20–8.33 ppm), followed by CH_2 and CH_3 of the MOM-substituent (5.25 ppm and 3.89 ppm) and CH_2 signals from tacn and methylcarboxylate groups (from 3.50 ppm to –3.34 ppm). Further support for this assignment was established by the COSY NMR spectrum at r.t., where a single cross-peak was observed for adjacent aromatic protons, and the rest five

peaks were attributed to ^{1}H-^{1}H cross-couplings between the CH_2 protons of the tacn ring (Figure 32, right).

Thus, in solution, **EuLt1^{t}** complexes had one major conformer, while **EuLc** compounds were present as a mixture of major and minor isomers. The results of luminescence measurements can be treated from the single species of complexes with tacn binding sites, and those of the cyclen-based compounds will give a weighted average of two geometries observed by ^{1}H NMR spectroscopy.

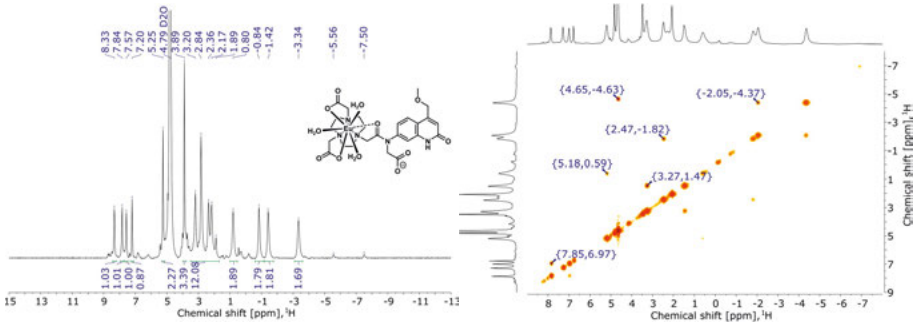

Figure 32. ^{1}H (left, 50 °C) and COSY (right, r.t.) NMR spectra (400 MHz, D_2O) of **EuLt1^{t,MOM}**. The symmetrical peaks relative to the diagonal ones were kept in the COSY spectrum. The peaks in COSY spectrum are not referenced to D_2O signal.[134]

5.3 Photophysical studies of Ln(III) complexes

5.3.1 Characterisation of new compounds

The photophysical characterisation of new **Lc** and **Lt**-based Ln(III) complexes was performed in aqueous 10 mM PIPES buffer solutions (pH 6.5) with absorbance (A) set to 0.10 at λ_{ex}. **LnLc** complexes resembled their NH_2 versions in the absorption spectra, and the differences between the spectral profiles were negligible. The carbostyril π–π* absorption band was superimposable in all cyclen-based compounds regardless of the Ln(III) ion or the metal binding site with λ_{abs} = 332 nm (Figure 33, left).

The absorption of **LnLt** complexes was dependent on the linker amide structure (**s**/**t**) and the antenna substituent (Me/MOM). In the spectra with the same carbostyril moiety, the secondary amide red-shifted λ_{abs} of n–π* C=O and π–π* antenna transitions by 12 nm and 4 nm, respectively, compared to their tertiary linker analogues. These bands (258–306 nm and 294–365 nm) underwent only a 3 nm hypsochromic shift upon changing the carbostyril substituent from MOM to Me while keeping the linker amide unaltered. These changes were small, considering that only the antenna-centred absorption was used to excite Ln(III) complexes (λ_{abs} = 324–331 nm, Figure 33, right). **LnLt**

compounds of a single ligand type had uniform absorption spectra despite the presence of different Ln(III) in their structures.

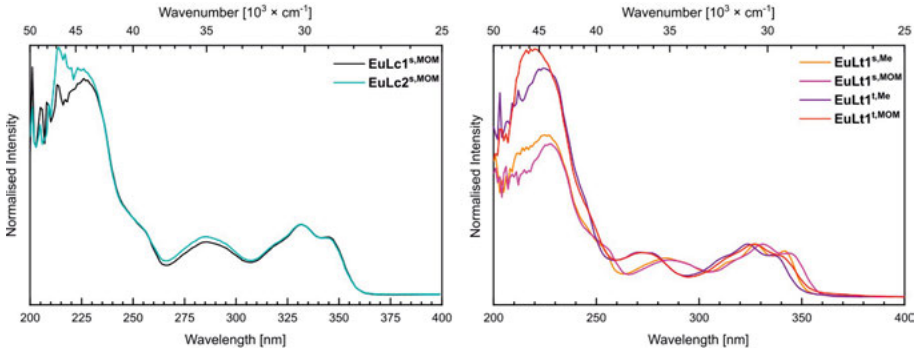

Figure 33. Normalised superimposed absorption spectra of **EuLc** (left, λ_{abs} = 332 nm) and **EuLt** (right, λ_{abs} = 324 nm, 327 nm, 328 nm and 331 nm) complexes.[134]

The ligand excited state levels were estimated from 0–0 phonon transitions of the phosphorescent bands observed in the steady-state emission spectra of Gd(III) complexes at 77 K (Figure 34). The triplets of secondary amide-linked compounds with MOM antenna were within the 22520–22620 cm^{-1} range, while those of **Lt1^{s,Me}** and tertiary amide-containing ligands had T_1 at 22900–23000 cm^{-1}. The T_1 levels of **GdLt1^{s,Me}** and **GdLt1^{s,MOM}** decreased by 100 cm^{-1} and 400 cm^{-1} than those of their alkylated amide linker analogues. Thus, ligand T_1 levels of tacn complexes with the same linker amide and antenna were identical to those of cyclen-based compounds (see Chapter 3 and 4),[21,49,131] pointing out that the size of the binding site does not affect carbostyril excited state levels.

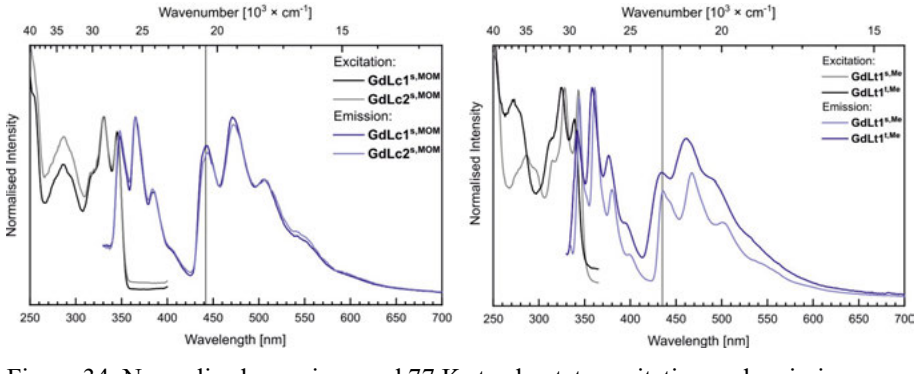

Figure 34. Normalised superimposed 77 K steady-state excitation and emission spectra of **GdLc** (left, λ_{ex} = 331 nm, λ_{em} =442–444 nm) and **GdLt1^{Me}** (right, λ_{ex} = 324–327 nm, λ_{em} =435–436 nm) complexes with A = 0.10 sample absorption. Dark grey lines are at 0–0 phonon transitions of phosphorescent bands (442 nm and 435 nm).[134]

Antenna-based (Ln = Eu, Gd, Tb, Yb) and 4f-4f emissions (Ln = Eu, Tb) were observed by exciting Ln(III) complexes at appropriate λ_{ex}. The ligand fluorescence region contained two features in **EuLc** and all the tacn-based compounds (Figure 35). The first band was identified as $S_1 \rightarrow S_0$ transition based on Stokes shifts (mean 3300 cm^{-1} for Me- and 3700 cm^{-1} for MOM-carbostyril) that were similar to the related compounds.[21]

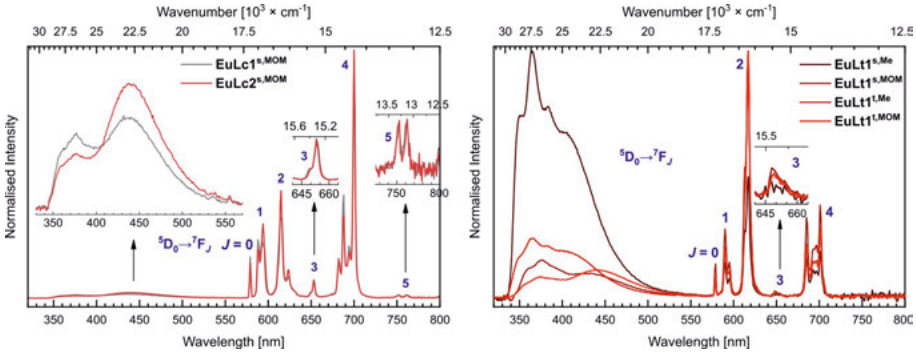

Figure 35. **EuLc** (left, λ_{ex} = 330 nm) and **EuLt** (right, λ_{ex} = 324–329 nm) normalised superimposed steady-state emission spectra with A = 0.10 sample absorption.[134]

The second feature was at longer wavelengths, which varied with the antenna substituent. The intensity of this band declined with the increasing amounts of DMF in H_2O:DMF solutions until it was not observable in 100% DMF media. Moreover, the steady-state excitation spectrum measured at λ_{em} = 475 nm showed an energetically lower emitting level than antenna S_1 (λ_{ex} = 352–361 nm). These data were consistent with emissions from an internal charge transfer (ICT) state.[139–141] For Me-functionalised carbostyrils, λ_{ICT} was at 417–423 nm, while for complexes with MOM antenna, λ_{ICT} was red-shifted to 442–445 nm. The ICT state energy levels were estimated at >25500 cm^{-1}, making them unlikely to be involved in the sensitisation of Ln(III) emission due to a better overlap of the antenna T_1 with Eu(III) and Tb(III) excited states.

The Ln(III) emission spectral profiles of cyclen and tacn-based complexes were not the same. The most pronounced differences were observed in the Eu(III) spectra for the coordination environment-sensitive ΔJ = 2 and 4 bands, with the former transition being the most intense in **EuLt**, and the latter in the **EuLc** compounds (Figure 35). The peaks of ΔJ = 5 were detected only for complexes with cyclen ligands in aqueous solutions. In **TbLc** emission spectra, the $^5D_4 \rightarrow {}^7F_J$ (J = 3, 4) transitions were split into several peaks, while those of **TbLt** appeared as singlets (Figure 36).

Φ_L values were calculated with the help of scaled emission spectra of Gd(III) cyclen-based complexes that did not have ICT emission bands (Table 16).[21,49,128] Overall, the complexes of Gd(III) had the largest values of Φ_L in both series. The latter was expected, as Gd(III) can neither be involved in PeT

nor luminesce in these conditions. The ligand fluorescence intensities of **YbLc** were the second biggest in the **LnLc** series, as there is no spectral overlap between $^2F_{5/2}$ and antenna excited states, but a 22% decrease in Φ_L relative to **GdLc** might indicate the PeT contribution.

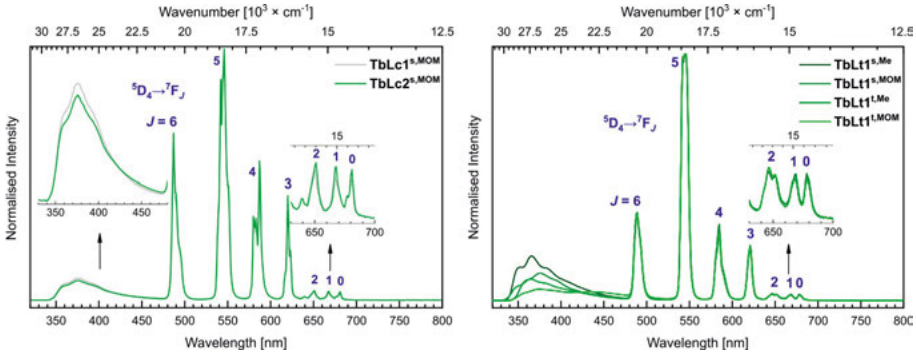

Figure 36. **TbLc** (left, λ_{ex} = 330 nm) and **TbLt** (right, λ_{ex} = 324–329 nm) normalised superimposed steady-state emission spectra with A = 0.10 sample absorption.[134]

Table 16. Ligand fluorescence and Ln(III) emission quantum yields, lifetimes and hydration states of **LnL** complexes.

Complex	Φ_L [%] [a]	Φ_{Ln} [%] [a]	τ_{H_2O} [ms] [b]	τ_{D_2O} [ms] [b]	q [c]
EuLc1^{s,MOM}	0.24	4.3	0.601	2.03	1.0
EuLc2^{s,MOM}	0.17	3.9	0.602	1.83	1.0
EuLt1^{s,Me}	2.0	0.30	0.259	1.47	3.4
EuLt1^{s,MOM}	0.61	1.1	0.265	1.54	3.4
EuLt1t^{,Me}	1.7	1.6	0.266	1.51	3.4
EuLt1t^{,MOM}	2.1	4.1	0.267	1.55	3.4
TbLc1^{s,MOM}	4.9	22.5	0.904	1.42	n.d. [d]
TbLc2^{s,MOM}	4.8	24.3	0.979	1.40	1.2
TbLt1^{s,Me}	4.6	9.9	0.730	0.873	n.d. [d]
TbLt1^{s,MOM}	4.9	15.3	0.643	0.774	n.d. [d]
TbLt1t^{,Me}	4.5	17.7	0.920	1.67	2.1
TbLt1t^{,MOM}	4.0	24.5	0.930	2.25	2.9

The values carry relative experimental error of 10%. [a] Relative to quinine sulfate (Φ = 59% in 0.05 M H_2SO_4).[126] [b] Mean of 3 different measurements. [c] Calculated using Eq. (3) or (4). [d] Not determined due to BET.

TbLc retained 69–75% of **GdLc** antenna emission intensity, and the rest might have been lost to S_1-mediated ET to Tb(III) excited states. **EuLc** had significantly diminished Φ_L, only 3% of that in Gd(III) compounds (Table 16). Such a drastic difference was not accompanied by a robust Eu(III) emission, which suggested PeT quenching of antenna S_1. Moreover, Φ_{Eu} values were 16% and 23% smaller for **EuLc1^{s,MOM}** and **EuLc2^{s,MOM}**, respectively, than in their tricarboxylate analogue (see Chapter 3). These compounds had the same number of X-H oscillators and similar ligand S_1 and T_1 energy levels, providing a close overlap between the former and Eu(III) excited states. Hence,

EuLc complexes have comparable ET efficiencies, and the reduced Φ_{Eu} ought to come from PeT quenching. **TbLc** quantum yields were within 16% of mean Φ_{Tb} for **TbL^{MOM}**, consistent with the inaccessible Tb(II) oxidation state (Table 2) for PeT quenching. The Ln(III) coordination environment in the **LnLc** complexes was completed by a single inner-sphere water molecule, established by $q = 1$.

The analysis of ligand fluorescence intensity for tacn-based compounds was not trivial, as the interference from the ICT emission could also depopulate antenna S_1 apart from other processes quenching Φ_L. **YbLt1^{s}** and **YbLt1^{t}** complexes preserved 45–60% and 88–93% of Φ_L in corresponding Gd(III) species, respectively. The average antenna fluorescence quantum yield was 4.5% for **TbLt** compounds. Φ_L values in Eu(III) tacn-based complexes decreased in the order **EuLt1^{t,MOM}** ≈ **EuLt1^{s,Me}** > **EuLt1^{t,Me}** > **EuLt1^{s,MOM}**. The tendencies seen in antenna fluorescence intensities for Eu and Tb compounds with tacn ligands did not correlate with those of Φ_{Ln}.

Ln(III) emission quantum yields increased from more to less electron-donating carbostyril substituent (Me vs MOM) and from secondary to tertiary amide linker. In **EuLt**, these phenomena could be explained by the diminished reducing ability of the antenna, which disfavoured PeT quenching. By assuming that positively charged **EuLt1^{s}** and neutral **EuLt1^{t}** (overall complex charges) would have similar E_{red}^{Eu} to those of **EuL1^{MOM}** and **EuL0^{MOM}**, respectively, we calculated the driving force of PeT in each tacn-based Eu(III) compound (Table 17). The resulting values of ΔG_{PeT} followed the same course as Φ_{Eu}: the smallest Eu(III) emission quantum yield of 0.30% was for the complex with the most negative free energy change of PeT. The smaller Φ_{Tb} in **TbLt1^{s}** compounds than in **TbLt1^{t}** was likely due to BET and subsequent oxygen quenching of antenna T_1. All Eu(III) complexes of tacn binding sites and **TbLt1^{t,MOM}** had $q = 3$, confirming the presence of 3 water molecules in the first coordination sphere of the Ln(III).

Table 17. Calculation of free energy change of PeT for **EuLt1** complexes.

Parameter	**EuLt1^{s,Me}**	**EuLt1^{s,MOM}**	**EuLt1^{t,Me}**	**EuLt1^{t,MOM}**
E_{ox}^{Ant} [V vs NHE]	1.65 [a]	1.76 [b]	1.91 [c]	1.94 [c]
E_{red}^{Eu} [V vs NHE]	–0.800 [d]	–0.800 [d]	–0.908 [e]	–0.908 [e]
E_{S_1} [eV] [f]	3.60	3.56	3.64	3.61
ΔG_{PeT} [eV] [g]	–1.30	–1.15	–0.972	–0.912

[a] Value from [21]. [b] Value from [130]. [c] Value from [135]. [d] Estimated as the value of **EuL1^{MOM}**.[128] [e] Estimated as the value of **EuL0^{MOM}**.[128] [f] Estimated from the 0–0 phonon transitions in **GdLt** steady-state emission spectra at 77 K.[134] [g] Calculated using Eq. (5), with ΔE_{Coul} = 0.15 eV.[80]

5.3.2 Fluoride and cyanide binding experiments

The photophysical properties of Eu(III) complexes in the absence and presence of fluoride or cyanide were determined in 10 mM TRIS-buffered solutions (H_2O, pH 8.05) to prevent the release of HCN gas while handling KCN.

Φ_L and Φ_{Eu} of **EuLc** compounds from control experiments were smaller in TRIS buffer solutions than in PIPES-containing ones by 17% and 25% on average, respectively. The pH titrations under constant ionic strength (0.1 M KCl in H_2O) revealed that the emission intensity decreased by 12% for **EuLc1^{s,MOM}** and 23% for **EuLc2^{s,MOM}** at pH > 8.5. The drop of Φ_{Eu} at more basic pH is due to the NH deprotonation of the secondary amide linker, which was observed for similar complexes.[21,142] Eu(III) compounds of cyclen-based ligands had the same τ_{rad} = 5 ms and q = 1, verifying the similarity of their coordination environments. The intrinsic quantum yield and the sensitisation efficiency of **EuLc2^{s,MOM}** were smaller than in **EuLc1^{s,MOM}**, which was in line with the diminished Φ_{Eu} of the former emitter (Table 18).

The emission quantum yields of **EuLt** without added fluoride or cyanide were similar to those obtained at more acidic pH in PIPES buffer media. The Eu(III) complexes of tacn ligands had close values of τ_{rad}, Φ_{Ln}^{Ln} and hydration states (mean 3.2 ms, 8.2% and 3.5, respectively), supporting the structural resemblance of **EuLt** species. However, η_{sens} decreased from the most to the least Eu(III) emissive compound, which also correlated with the trends observed in ΔG_{PeT}. The largest sensitisation efficiency was for the complex with the least negative free energy change of PeT, supporting that changes in η_{sens} mirror the effects of PeT quenching in the Eu(III) emission.

Table 18. Results of control photophysical measurements for **EuLc** and **EuLt** complexes.

Complex	Φ_L [%] [a]	Φ_{Ln} [%] [a]	τ_{rad} [ms] [b]	Φ_{Ln}^{Ln} [%] [c]	η_{sens} [%] [c]	q [d]
EuLc1^{s,MOM}	0.203	3.49	5.08	11.6	30.1	1.1
EuLc2^{s,MOM}	0.139	2.69	5.07	10.0	27.1	1.3
EuLt1^{s,Me}	1.89	0.341	3.21	7.87	4.33	3.6
EuLt1^{s,MOM}	0.708	1.19	3.43	7.31	16.3	3.6
EuLt1t^{,Me}	1.73	1.67	3.13	8.70	19.2	3.3
EuLt1t^{,MOM}	1.87	4.66	3.05	8.90	52.4	3.4

The values carry relative experimental error of 10%. [a] Relative to quinine sulfate (Φ = 59% in 0.05 M H_2SO_4).[126] [b] Calculated using Eq. (1). [c] Calculated using Eq. (2). [d] Calculated using Eq. (4).

For **EuLc** complexes, 0.1 M analyte (F^- or CN^-) concentration was used for binding studies,[128] while for **EuLt** compounds, [F^-/CN^-] = 1 M to reach the maximum response in luminescence intensity.

The addition of fluoride increased the quantum yields in all complexes (Table 19). The Φ_L and Φ_{Eu} increase was 2-fold larger in +2 charged **EuLc2^{s,MOM}** than in **EuLc1^{s,MOM}** compound carrying a positive charge. The origin of

boosted Eu(III) emission intensities was in enhanced Φ_{Ln}^{Ln} and η_{sens}: these parameters had a 1.4-times stronger effect in +2 than in +1 charged species upon fluoride binding. The complete replacement of coordinated H_2O by F^- in **EuLc2^{s,MOM}** was confirmed by determining the number of lost water molecules ($\Delta q = -1$). Hence, the increased overall charge of the complex resulted in a larger emission response in the presence of fluoride, as demonstrated on Eu(III) compounds based on cyclen binding sites.

Table 19. Photophysical properties of **EuLc** and **EuLt** complexes with added excess of fluoride (0.1 M KF for **EuLc** and 1 M KF for **EuLt**).

Complex	Φ_L [%] [a]	Φ_{Ln} [%] [a]	Φ_{Ln}^{Ln} [%] [b]	η_{sens} [%] [b]	Δq [c]
EuLc1^{s,MOM}-F	0.394 (×1.9)	6.19 (×1.8)	16.1 (×1.4)	38.4 (×1.3)	–0.6
EuLc2^{s,MOM}-F	0.530 (×3.8)	10.3 (×3.8)	21.3 (×2.1)	48.4 (×1.8)	–1.1
EuLt1^{s,Me}-F	4.03 (×2.1)	2.06 (×6.0)	19.8 (×2.5)	10.4 (×2.4)	–3.1
EuLt1^{s,MOM}-F	2.15 (×3.0)	3.30 (×2.8)	19.4 (×2.7)	17.0 (×1.04)	–3.1
EuLt1t^{Me}-F	3.06 (×1.8)	7.84 (×4.7)	21.7 (×2.5)	36.1 (×1.9)	–2.7
EuLt1t^{MOM}-F	3.18 (×1.7)	16.0 (×3.4)	21.8 (×2.4)	73.3 (×1.4)	–2.8

The values carry relative experimental error of 10%. In parentheses: fold increase relative to the values from Table 18. [a] Relative to quinine sulfate (Φ = 59% in 0.05 M H_2SO_4).[126] [b] Calculated using Eq. (2). [c] Calculated as $q(F^-) - q(H_2O)$.

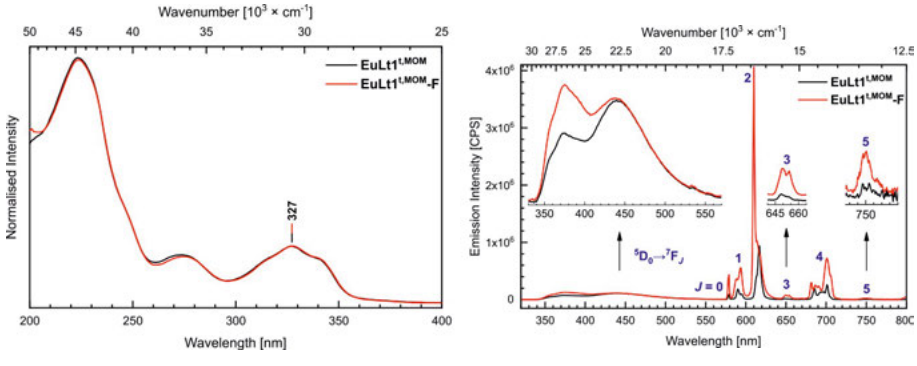

Figure 37. Normalized superimposed absorption (left) and steady-state emission spectra (right) of **EuLt1^{t,MOM}** (black, control) with excess fluoride (red, 1 M KF). λ_{ex} = 327 nm, front slit: 2 nm, exit slit: 1.5 nm.[134]

In **EuLt** complexes, the largest (6-fold) increase of Eu(III) emission quantum yield by the addition of fluoride was in **EuLt1^{s,Me}**, for which PeT quenching was calculated to be the most favourable across the series (Table 17). This improvement was reached via a 2.5-fold larger intrinsic quantum yield and sensitisation efficiency. The increase in Φ_{Ln}^{Ln} was due to $\Delta q = -3$, meaning that up to three inner-sphere water molecules were swapped with fluorides, while η_{sens} became larger because of less efficient antenna-to-Eu(III) PeT. All **EuLt-F** species had 2.5-fold increased Φ_{Ln}^{Ln} and similar τ_{rad} (mean 20.7% and 3.9 ms, respectively), revealing similar geometries of the fluoride-bound complexes. The fluoride coordination did not alter the absorption spectra of Ln(III)

compounds, and the Eu(III) emission spectral pattern was also similar to the one observed for the aqua complex (Figure 37).

Surprisingly, the addition of cyanide resulted in a significant drop in Eu(III) emission intensity, which was accompanied by decreased (**EuLc**) or increased (**EuLt**) ligand fluorescence quantum yield. While in cyclen-based complexes $\Phi_{\mathrm{Ln}}^{\mathrm{Ln}}$ and η_{sens} were smaller with added cyanide, the intrinsic quantum yields in the compounds with tacn ligands had a 1.4-fold increase on average. The larger Φ_{L} values in **EuLt** were also contrary to the previous results with fluoride. If PeT quenching was involved in diminished Φ_{Ln}, one would expect a parallel reduction in the antenna fluorescence intensity. Moreover, the cyanide addition replaced only 1 or 2 of the water molecules in **EuLt** complexes, while **EuLc** compounds retained aqua ligands according to the calculated hydration states (Table 20).

Table 20. Photophysical properties of **EuLc** and **EuLt** complexes with added excess of cyanide (0.1 M KCN for **EuLc** and 1 M KCN for **EuLt**).

Complex	Φ_{L} [%] [a]	Φ_{Ln} [%] [a]	$\Phi_{\mathrm{Ln}}^{\mathrm{Ln}}$ [%] [b]	η_{sens} [%] [b]	q [c]
EuLc1^{s,MOM}-CN	0.171 (×0.84)	1.46 (×0.42)	9.20 (×0.79)	15.8 (×0.52)	1.2
EuLc2^{s,MOM}-CN	0.075 (×0.54)	0.347 (×0.13)	7.05 (×0.71)	4.92 (×0.18)	1.5
EuLt1^{s,Me}-CN	4.28 (×2.3)	0.154 (×0.45)	10.7 (×1.4)	1.44 (×0.33)	1.2
EuLt1^{s,MOM}-CN	3.69 (×5.2)	0.435 (×0.37)	11.1 (×1.5)	3.91 (×0.24)	1.2
EuLt1t^{Me}-CN	2.86 (×1.7)	1.04 (×0.62)	11.5 (×1.3)	9.01 (×0.47)	2.2
EuLt1t^{MOM}-CN	2.12 (×1.1)	1.24 (×0.27)	12.1 (×1.4)	10.3 (×0.20)	2.2

The values carry relative experimental error of 10%. In parentheses: fold increase relative to the values from Table 18. [a] Relative to quinine sulfate (Φ = 59% in 0.05 M H_2SO_4).[126] [b] Calculated using Eq. (2). [c] Calculated using Eq. (4).

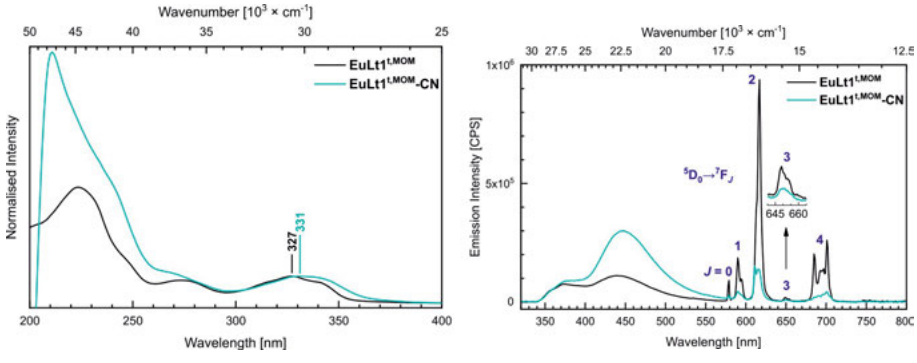

Figure 38. Normalized superimposed absorption (left) and steady-state emission spectra (right) of **EuLt1^{t,MOM}** (black, control) with excess cyanide (turquoise, 1 M KCN). λ_{ex} = 327 nm (control) and 330 nm (CN^-), front slit: 2 nm, exit slit: 1.5 nm.[134]

We attempted to identify the possible chemical interactions between the complexes and the cyanide. In the absorption spectra of the cyanide-containing samples, antenna π–π^* transitions were bathochromically shifted compared to aqua compounds (Figure 38, left), indicating the altered electronic structure

of complexes in the presence of KCN. In diamagnetic ^{1}H NMR spectra of analogous Lu(III) compounds, the aromatic carbostyril proton signals resonated at the same chemical shifts, pointing towards the intact antenna upon cyanide addition.

The cyanide binding is known to give turn-on[143] or off[144] responses with the emission of Eu(III) complexes (Figure 39). The turn-on change in Eu^{III}-Lys-HOPO emission intensity was due to the replacement of all aqua ligands with cyanides in the coordination sphere of Ln(III). The turn-off response in **Ln.1–2** was explained by the reaction between the carbonyl linker and cyanide, leading to the formation of cyanohydrin species, which were less emissive than the parent complexes. At the same time, amide-functionalised **Ln.5** did not interact with cyanide.[144]

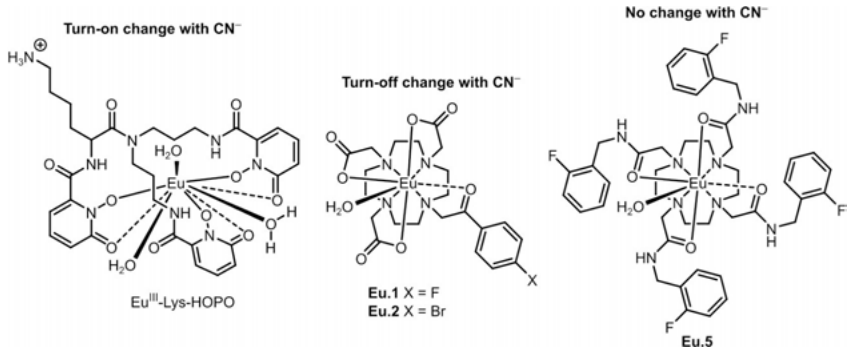

Figure 39. Eu(III) complexes with turn-on (Eu^{III}-Lys-HOPO),[143] turn-off (**Ln.1–2**) or no change (**Ln.5**)[144] upon added excess of CN^- in solution.

EuLc and **EuLt** contain a secondary or a tertiary amide linker, which can exclude the cyanohydrin formation in our complexes, based on observations of Faulkner's group.[144] Then, cyanide may react with the antenna linker and functionalise it with a stronger electron-donating group. The latter would explain the changes in the UV-Vis; however, further investigations of the covalent adducts between our complexes and cyanide are necessary to ascertain these statements.

5.4 Conclusions

We synthesised and structurally characterised two series of Ln(III) complexes designed for anion-binding studies. The first series was based on cyclen octadentate ligands, functionalised with one or two *N*,*N*-dimethylamide pendant arms, rendering the resulting compounds +1 or +2 charged. The second series was built on tacn core structure with two acetate donor groups and a secondary or tertiary amide-linked carbostyril antenna, giving the space for three labile one-donor atom ligands. The complexes of cyclen binding sites existed as

mixtures of two isomers, while a single conformer was identified for tacn-based compounds in solution.

All complexes containing Gd and Yb were fluorescent, and those with Eu and Tb also showed Ln(III) luminescence. The brightest emission of Eu(III) and Tb(III) was for the complexes of the tacn ligand containing a tertiary amide linker and a 4-methoxymethylcarbostyril antenna. These species were the least prone to PeT quenching of the Eu(III) luminescence intensity, as shown by the calculated free energy change of electron transfer. In aqueous solutions, cyclen- and tacn-based complexes had 1 or 3 coordinated water molecules, which was determined by the time-resolved studies of Ln(III) emission.

The fluoride binding increased the Eu(III) emission up to 6-fold via replaced aqua ligands and inhibited PeT quenching. The effect was the largest for the poorest emitter of the tacn series, where PeT quenching was calculated to be the most favourable. In cyclen-based compounds, the higher the overall charge of the complex, the larger the increase upon fluoride binding. However, cyanide addition quenched the luminescence of all compounds regardless of the metal binding site. These changes were attributed to a possible chemical reaction of the emitters, with the cyanide creating less emissive molecules than their parent structures. Thus, these complexes were proved to be functional to detect fluoride and cyanide via turn-on and off changes in the Eu(III) emission intensity, respectively. Further structural tuning of the complexes to make them more anion-responsive could facilitate the distinction of analytes that are still hard to detect, e.g. different halides.

6. Competing sensitisation pathways of Yb(III) NIR luminescence (Paper V)

The luminescence of Ln(III) ions in the NIR region is particularly useful for the in-depth imaging of biological tissues that are more transparent in this part of the electromagnetic spectrum (700–1200 nm).[117] Among NIR-emissive lanthanides, Yb(III) is extraordinary as it has a single $^2F_{5/2}$ excited state at 10260 cm^{-1} and a relatively large intrinsic quantum yield compared to other luminescent Ln(III).[19] As the $^2F_{5/2}$ excited state is energetically much lower than that of the UV-absorbing organic ligands, the sensitisation of Yb(III) NIR emission remains unclear in some cases.[21,145]

The PeT-BeT mechanism suggested by Horrocks (see 1.2.4)[69] was often invoked for Yb(III) emitters, where a spectral overlap between the ligand and $^2F_{5/2}$ excited states was negligible.[77–80] The PeT pathway was cited as operational because of the accessible Yb(II) oxidation state, even when the free energy change of electron transfer was not calculated.[61] In the literature, there were no examples of how the Yb(III) luminescence could be tuned by accelerating PeT if this process was sensitising. Controlling the sensitisation mechanisms through the ligand structure of the emissive Yb(III) complexes is essential to improve their photophysical properties and implement them as biological tools.

In this chapter, the strategy of regulating PeT in luminescent Yb(III) complexes is explored in two different ways: by changing either the coordination environment of the metal centre or the reducing ability of the sensitising antenna. The former was achieved by successively introducing a positive charge in the DO3A-based MOM-carbostyril appended complexes, starting from neutral **YbL0^{MOM}** and ending with +3 charged **YbL3^{MOM}** (Chapter 3, Figure 12). We functionalised carbostyrils in the 4-positions from the CF_3 substituent to Me and MOM groups in charge-neutral **YbL0** compounds (R = CF_3, Me and MOM in Figure 12, Chapter 3) to vary the electronic structure of the antenna. These approaches would modulate the contribution of PeT to the luminescence sensitisation via altered Yb(III)/Yb(II) reduction or antenna oxidation potentials. The structural composition of Yb(III) complexes was studied in solution and solid state before investigating their steady-state UV-Vis and NIR electronic spectra, as well as the ligand fluorescence lifetimes. We aimed to evaluate the contribution of PeT to the sensitisation of Yb(III) luminescence and how to control this process for brighter NIR emission.

6.1 $\mathbf{YbL^R}$ complexes solution and solid-state structures

Dr. Daniel Kovacs prepared the Yb(III) compounds. The solution structures of the Yb(III) complexes were investigated by ^{1}H NMR spectroscopy. These studies were performed to verify that neither different antenna substituents (**YbL0^{CF3,Me,MOM}**) nor carboxylate to amide arm replacement (**YbL0–3^{MOM}**) imposed significant changes in solution structures of the Yb(III) compounds.

All ^{1}H NMR spectra of **YbL^R** complexes were measured at r.t. and constant magnetic field (400 MHz, Figure 40) in D_2O. Yb^{3+} induced significant paramagnetic shifts on the ligand proton signals stretching between 130 ppm and –75 ppm. The highest frequency chemical shifts were assigned to axial cyclen CH_2 resonances belonging to SAP isomers. These signals were found at 111.63–133.60 ppm for **YbL0** compounds, and those of positively charged **YbL1–3** species were more shielded at 92.07–114.47 ppm. The tricarboxylate complexes were present as mixtures of SAP and TSAP diastereomers, and the chemical shifts of the latter resonated at 54.38–84.90 ppm. The amount of the SAP compared to the TSAP isomer was ~10-fold larger in all three compounds (SAP:TSAP = 1:0.07, 1:0.09, 1:0.08 for **YbL0^{CF3,Me,MOM}**, Table 21). Hence, **YbL0** complexes would give the weighted average result of the SAP-TSAP mixture (with less than 10% of TSAP), provided that the same equilibrium occurs during the photoluminescent measurements. At the same time, Yb(III) compounds with amide pendant arms would have single contributing species of SAP geometry.

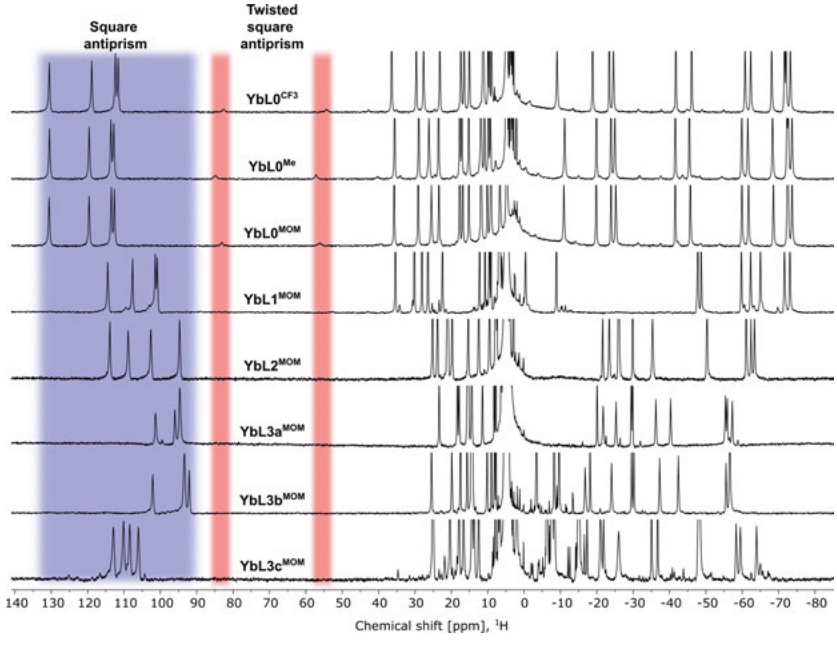

Figure 40. ^{1}H NMR spectra of **YbL^R** compounds (400 MHz, D_2O, r.t.) with the highlighted blue and red areas of SAP and TSAP axial cyclen proton signals.[146]

Table 21. Data from ^{1}H NMR spectra of **YbL^{R}** complexes. First row: spectral regions of SAP and TSAP isomers signals, second row: their integrated ratios.

Parameter	**YbL0^{CF3}**	**YbL0^{Me}**	**YbL0^{MOM}**	**YbL1–3^{MOM}**
SAP and	111.63–130.55	112.82–130.49	112.66–130.60	92.07–114.47
TSAP, ppm	54.38, 82.64	57.18, 84.90	55.91, 83.23	-
SAP:TSAP	1:0.07	1:0.09	1:0.08	-

We obtained single crystals of **YbL0^{CF3}** upon the slow diffusion of dioxane into its concentrated aqueous solution. There were two significant differences in the solid-state structure of **YbL0^{CF3}** compared to those of the other Ln(III) complexes based on DO3A ligand binding sites with the carbostyril antennae.[49,124] The central ion in **YbL0^{CF3}** had CN = 8 instead of the nonacoordinate polyhedra of lighter Dy(III)[49] or Eu(III)[124] due to the smaller r_{ion} of Yb^{3+} [r_{ion} = 0.99 Å (Yb), 1.03 Å (Dy), 1.07 Å (Eu) for CN = 8, Figure 41].[147] Both molecules of **YbL0^{CF3}** in the crystal packing were TSAP enantiomers, which was revealed by the same signs of ψ and ω torsion angles [+56.8° and +14.2° for $\Lambda(\lambda\lambda\lambda\lambda)$, and –56.8° and –14.2° for $\Delta(\delta\delta\delta\delta)$].

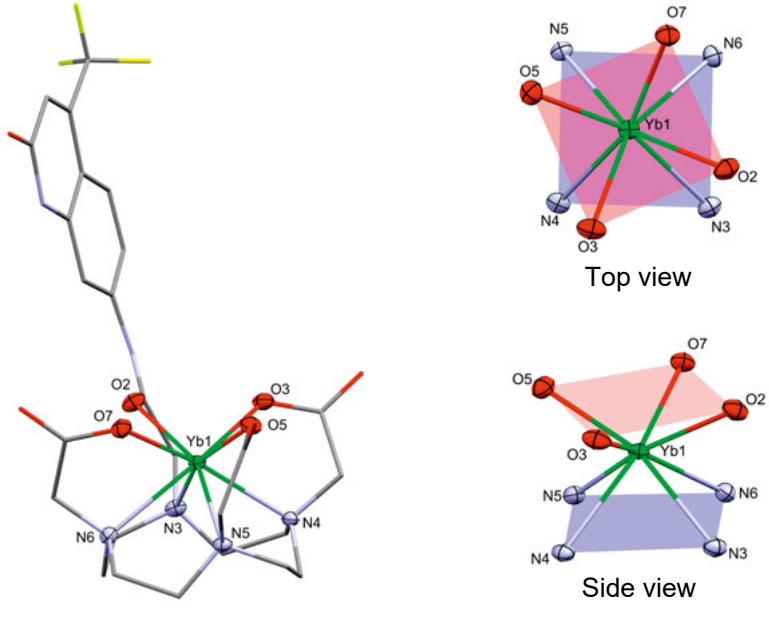

Figure 41. Solid-state structure of **YbL0^{CF3}** (left, $\Delta(\delta\delta\delta\delta)$ isomer) and the coordination environment of Yb^{3+} (right, view from the top and the side of the polyhedron). Yb and coordinating atoms are shown as ellipsoids at 50% probability, the rest of the structure is capped sticks. Protons, solvent (H_2O) and antisolvent (dioxane) molecules were omitted for clarity.[146]

YbL0^{CF3} was the first crystal structure containing TSAP isomers of Yb(III) cyclen-based complexes, as similar compounds were only reported to

crystallise in their capped SAP form.[97] As studied by ^{1}H NMR spectroscopy, the DOTA-based Ln(III) compounds could undergo capped SAP-TSAP isomerisation with the loss of coordinated water molecule, so we cannot exclude that our Yb(III) compounds may have an inner-sphere H_2O ligand in solution.[92] The ^{1}H NMR data proved that **YbL^R** complexes have the same SAP geometry of the predominant isomer in solution, affirming the major contributing species to the photophysical properties.

6.2 Ligand-based and 4f-4f emission properties of **YbL^R** compounds

All photophysical measurements were performed in 10 mM PIPES-buffered aqueous solutions at pH 6.5 unless stated otherwise. The absorption spectra of Yb(III) complexes were recorded before the emission spectroscopy experiments. The electron-donating Me and electron-withdrawing CF_3 substituents on the carbostyril of **YbL0** complexes blue- and red-shifted antenna π–π* transitions by 3 and 10 nm, respectively, compared to the MOM group (Figure 42, left). Yb(III) compounds carrying the same 4-MOM-carbostyril had identical λ_{abs} = 331 nm, and small intensity differences were observed in the absorbance of the higher energy region corresponding to n–π* carbonyl absorptions (Figure 42, right). **YbL^{MOM}** absorption and excitation spectra were similar to those of the Eu(III) complexes containing the same ligands (see Chapter 3), which means that identical antenna excited states are involved in the sensitisation of Yb(III) complexes.

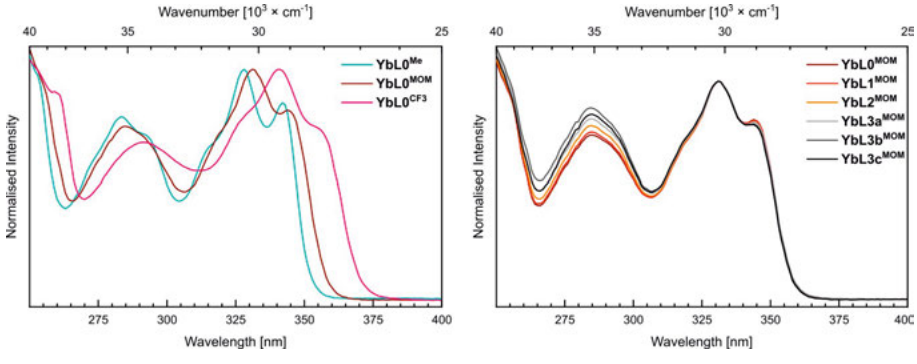

Figure 42. Normalised superimposed absorption spectra of **YbL0** (left, λ_{abs} = 328 nm, 331 nm and 341 nm) and **YbL^{MOM}** (right, λ_{abs} = 331 nm) complexes with A = 0.10.[146]

All steady-state and time-resolved luminescence spectroscopy experiments were performed with A = 0.10 of the solutions at λ_{ex} to ensure that the samples absorbed equal amounts of light. The ligand fluorescence peak positions of **YbL0** compounds in the steady-state emission spectra correlated well with their respective absorptions. While **YbL0^{MOM}** had λ_{em} = 376 nm, complexes

with 4-Me and 4-CF_3 auxochromes on the carbostyril antenna emitted at 10 nm lower and 15 nm higher wavelengths, respectively. In the **YbL^{MOM}** series, all representatives had the same λ_{em} as the neutral species, differing only in the intensities of the fluorescence bands (Figure 43).

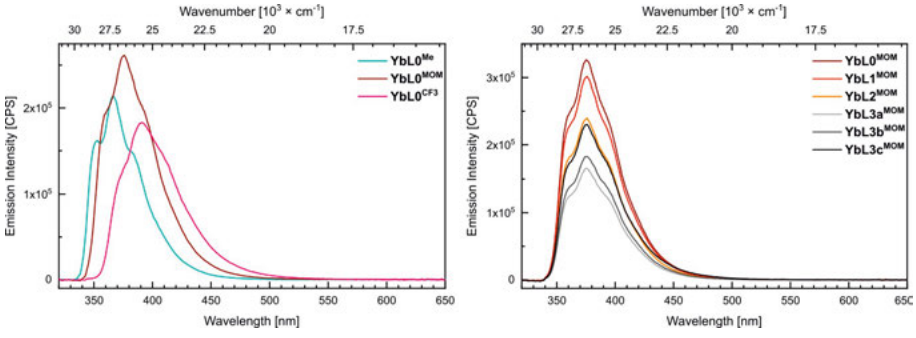

Figure 43. Steady-state emission spectra of **YbL0** (left, λ_{ex} = 329 nm) and **YbL^{MOM}** (right, λ_{ex} = 329.5 nm) complexes. Front slit: 2 nm, exit slit: 1.5 nm.[146]

Along with Yb(III) compounds, we also studied the photophysical properties of the analogous Lu(III) complexes with 4-MOM-carbostyrils. Lu(III) was chosen as it is the closest neighbour of Yb(III) in r_{ion};[147] hence, these metals were supposed to have minimal differences in their complex structures.[89,92] Moreover, the ligand photophysics of **LuL^{MOM}** compounds was not expected to be perturbed by PeT or ET to the Ln(III).

Of the neutral complexes, **YbL0^{MOM}** had the largest Φ_L = 5.9%, while the CF_3 and Me-derivatives had smaller ligand fluorescence quantum yields (4.8% and 4.2%, respectively). Each extra positive charge decreased Φ_L in the **YbL^{MOM}** series by 16% on average from the tricarboxylate to the triamide compound. The smallest ligand fluorescence quantum yield of **YbL3a^{MOM}** was increased by 7% and 22% after consecutive methylation in **YbL3b^{MOM}** and **YbL3c^{MOM}**, respectively. Contrary to Yb(III) complexes, Φ_L of **LuL^{MOM}** varied by 10% of the mean 7.9%, confirming the inactivity of Lu(III) in the photo- and redox processes in these conditions (Table 22).

The **LnL^{MOM}** antenna fluorescence lifetimes were also measured. The $\tau_{f,L}$ values were determined to estimate the rate constants of the processes that depopulate antenna S_1 in Yb(III) compounds compared to the Lu(III) analogues. The ligand fluorescence lifetimes of **LuL^{MOM}** were within ±5% of the average 0.45 ns, which was consistent with negligible differences in Φ_L across the series. The smallest $\tau_{f,L}$ in the set of **YbL^{MOM}** was for the +3 charged complex, concordant with the more efficient quenching of the antenna S_1 than in the other Yb(III) compounds. The radiative ligand fluorescence lifetimes of **LnL^{MOM}** were calculated using Eq. (6). While for Lu(III) complexes $\tau_{rad,L}$ was the same (mean 5.77 ns), the difference between the largest (**YbL3a^{MOM}**)

and the smallest (**YbL0^{MOM}**) radiative ligand fluorescence lifetimes of Yb(III) species was 2.7 ns.

The antenna S_1 of **LnL^{MOM}** (≈ 28700 cm^{-1}) were estimated from the 0–0 phonon transitions in the 77 K steady-state emission spectra of Gd(III) complexes. These energy levels were 18400 cm^{-1} higher than the $^2F_{5/2}$ excited state of Yb(III). Hence, the ligand singlet is unlikely to be involved in direct resonance ET to the Yb(III) excited state. Therefore, we assumed that only PeT would contribute significantly to the non-radiative decay of S_1 in **YbL^{MOM}**, apart from other processes that depopulate the singlet excited states in Yb(III) and Lu(III) complexes equally. Thus, the differences between the radiationless rate constants of **YbL^{MOM}** and **LuL^{MOM}** would give k_{PeT}, calculated using Eq. (7). Neutral and +1 charged Yb(III) complexes had smaller rate constants of PeT quenching than the rest of the series. The most significant k_{PeT} was calculated for **YbL3b^{MOM}**, which was 2.8-fold larger than in **YbL0^{MOM}** (Table 22).

Table 22. Measured ligand fluorescence quantum yields, lifetimes, Yb(III) relative emission quantum yields and calculated PeT rate constants.

Complex	Φ_L (φ_{Ln}) [%] [a, b]	$\tau_{f,L}$ [ns] [b, c]	$\tau_{rad,L}$ [ns] [d]	k_{PeT} [ns^{-1}] [e]	φ_{Ln} [%] [f]
YbL0^{CF3}	4.77 (81)	-	-	-	77
YbL0^{Me}	4.20 (72)	-	-	-	82
YbL0^{MOM}	5.87 (100)	0.343	5.84	0.80	88
YbL1^{MOM}	5.43 (93)	0.340	6.26	0.86	81
YbL2^{MOM}	4.31 (73)	0.253	5.87	1.8	83
YbL3a^{MOM}	3.07 (52)	0.262	8.53	1.7	83
YbL3b^{MOM}	3.46 (59)	0.226	6.53	2.2	85
YbL3c^{MOM}	4.35 (74)	0.280	6.44	1.3	100
LuL0^{MOM}	8.30 (100)	0.468	5.64	/	/
LuL1^{MOM}	8.40 (101)	0.467	5.56	/	/
LuL2^{MOM}	7.97 (96)	0.459	5.76	/	/
LuL3a^{MOM}	7.69 (93)	0.447	5.81	/	/
LuL3b^{MOM}	7.63 (92)	0.447	5.86	/	/
LuL3c^{MOM}	7.15 (86)	0.430	6.01	/	/

The values carry relative experimental error of 10%. [a] Relative to quinine sulfate (Φ = 59% in 0.05 M H_2SO_4).[126] φ_L is relative to **LnL0^{MOM}**. [b] Mean of 2 or 3 independent measurements. [c] λ_{ex} = 341.5 nm. [d] Calculated using Eq. (6). [e] Calculated using Eq. (7). [f] Relative to **YbL3c^{MOM}**, the values are ±1–2%.

Dr. Julien Andres measured the photophysical properties of Yb(III) complexes in the NIR region. The NIR emission spectra of **YbL0** compounds showed three superimposable peaks of the $^2F_{5/2}\rightarrow{}^2F_{7/2}$ transition at 981, 996 and 1027 nm upon antenna excitation. The profiles of Yb(III) emissions were unchanged with the identical tricarboxylate binding site, supporting the hypothesis that the geometries around the central ion are the same. The NIR emission spectral shapes of **YbL^{MOM}** were more sensitive to carboxylates replaced by amide pendant arms than varied carbostyril substituents in **YbL0**.

The first band of the 4f-4f transition changed intensity, while the two longer wavelength components became more intense and lower in energy upon increasing the overall complex charge. The spectral patterns of Yb(III) emission were alike in all complexes, indicating similar coordination geometry of the emitting species (Figure 44).

Only relative Yb(III) emission quantum yields were determined due to the lack of appropriate reference compounds with NIR luminescence upon UV excitation. **YbL0^{CF3}** and **YbL0^{MOM}** were the least and the most NIR-emissive neutral complexes, respectively. **YbL0^{Me}** and **YbL1-3b^{MOM}** had the same φ_{Yb} = 83% within the experimental error. **YbL3c^{MOM}** had the most intense NIR luminescence in the entire series, and φ_{Ln} values of the other complexes were calculated relative to this emitter. The φ_{Ln} in **YbL0^{MOM}** was smaller by 12% than in **YbL3c^{MOM}** despite the same number of X-H oscillators in these molecules (Table 22).

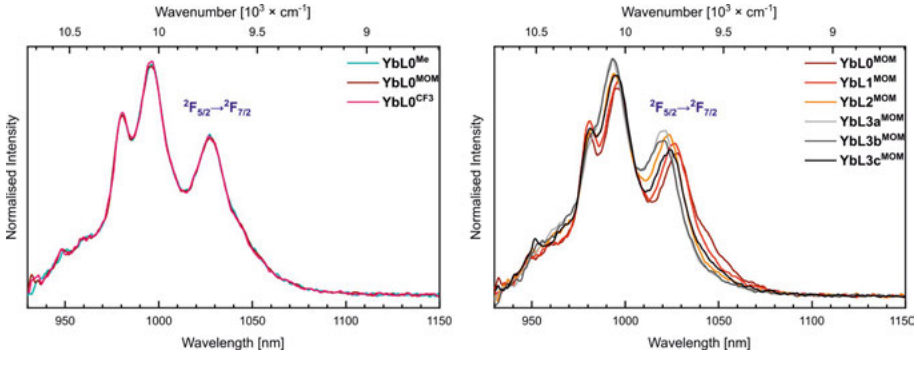

Figure 44. Normalised superimposed steady-state NIR emission spectra of **YbL0** (left) and **YbL^{MOM}** (right) complexes, λ_{ex} = 323 nm.[146]

Table 23. Measured ligand fluorescence and Yb(III) relative emission quantum yields, lifetimes and calculated PeT rate constants in D_2O (10 mM PIPES, pD 6.9).[131]

Complex	Φ_L (φ_{Ln}) [%] [a, b]	$\tau_{f,L}$ [ns] [b, c]	$\tau_{rad,L}$ [ns] [d]	k_{PeT} [ns^{-1}] [e]	φ_{Ln} [%] [f]
YbL0^{MOM}	5.90 (100)	0.313	5.30	1.0	89±6
YbL3a^{MOM}	3.34 (57)	0.218	6.52	2.4	100
LuL0^{MOM}	8.35 (100)	0.459	5.49	/	/
LuL3a^{MOM}	7.66 (92)	0.446	5.82	/	/

The values carry relative experimental error of 10%. [a] Relative to quinine sulfate (Φ = 59% in 0.05 M H_2SO_4).[126] φ_L is relative to **LnL0^{MOM}**. [b] Mean of 2 or 3 independent measurements. [c] λ_{ex} = 341.5 nm. [d] Calculated using Eq. (6). [e] Calculated using Eq. (7). [f] Relative to **YbL3a^{MOM}**.

We measured the photophysical properties of Ln(III) complexes in D_2O to eliminate the contribution of X-H quenching. The ligand-based photophysics was unchanged upon recording Φ_L and $\tau_{f,L}$ in D_2O, supporting the insensitivity of antenna S_1 to X-H oscillators (Table 23). The D_2O rate constants of PeT were also similar to the values obtained in H_2O. In +3 charged **YbL3a^{MOM}**, k_{PeT} was 2.4-fold larger than in neutral **YbL0^{MOM}**. Most importantly, the

relative Yb(III) emission intensity of the former complex was larger by 11% than that of the latter, meaning that the close φ_{Ln} values in H_2O were overshadowed by the deactivation from X-H bonds (Figure 45, left).

6.3 Sensitisation pathways in $\mathbf{YbL^R}$ complexes

As with antenna S_1, the Yb(III) excited state overlaps poorly with the ligand triplet energy level. The latter is located at 22600 cm^{-1}, making for a 12300 cm^{-1} difference. Hence, sensitisation pathways of Yb(III) luminescence, alternative to direct ET, were explored.

Antenna S_1 could participate in PeT, which might sensitise Yb(III) emission, as shown by the calculated PeT rate constants (Table 22, Table 23). In our systems, PeT is unfavourable from the ligand T_1.[21] The free energy change of PeT was calculated from antenna S_1 (Table 24). In neutral complexes, ΔG_{PeT} was thermodynamically uphill, and in positively charged $\mathbf{YbL1^{MOM}}$, the free energy change of PeT was nearly 0. For +2 and +3 charged species, PeT was calculated to be favourable based on the negative values of ΔG_{PeT}. However, the contribution of PeT to Yb(III) sensitisation was minor, as φ_{Ln} values of triamide compounds were only 1.13-fold larger than that of $\mathbf{YbL0^{MOM}}$.

Since PeT was not a plausible route to sensitise Yb(III) emission in the first half of the complex series ($\mathbf{YbL0^R}$ and $\mathbf{YbL1^{MOM}}$), we proposed that the $^2F_{5/2}$ excited state could be thermally populated via phonon-assisted energy transfer (PAET, Figure 45, right).[148–150] This process represents the radiationless decay of antenna T_1 to Yb(III) excited state. Then, the PAET rate constant is proportional to the Franck-Condon factor:

$$\mathrm{FC}_{(T=0)} = \left|\langle \chi_{a,p} | \chi_{b,0} \rangle\right|^2 = \frac{e^{-S} \times S^p}{p!} \tag{8}$$

$$S = \frac{Stokes\ shift}{2\hbar\omega_Q} \tag{9}$$

where S is the displacement of the higher $|b\rangle$ state relative to the lower $\langle a|$ state, also known as the Huang-Rhys factor, p is the reduced energy gap in $\hbar\omega_Q$ units between the $v = 0$ levels of $\langle a|$ and $|b\rangle$.[151,152]

In our complexes, two non-radiative deactivation pathways are possible from T_1: decay to $^2F_{5/2}$ or S_0. The former process can result in NIR emission from the Yb(III) excited state. The decay from the T_1 to S_0 state corresponds to the ligand phosphorescence, which is up to 6 times slower than the Yb(III) emission. Thus, we calculated the Franck-Condon factors for $T_1 \rightarrow {}^2F_{5/2}$ and $T_1 \rightarrow S_0$ pathways using Eq. (8) and (9), and the first pathway turned out to be 7–9 orders of magnitude larger than the second. This model also correlated the decreased φ_{Ln} of $\mathbf{YbL0^{CF3}}$ with the smallest quotient of the Franck-

Condon factors in the **YbL^{R}** series (Table 24). Thus, PAET is a viable sensitisation route even when the PeT process is unlikely. Moreover, PAET is the primary pathway yielding Yb(III) luminescence in tricarboxylate complexes. Since PeT was favourable to a certain extent in the positively charged Yb(III) compounds, the sum of combined sensitisation via PAET and PeT could increase NIR emission intensity, but only marginally.

Table 24. Calculated free energy change of PeT and the quotient of Franck-Condon factors.

Complex	E_{ox}^{Ant} [a]	E_{red}^{Yb} [a, b]	E_{S_1} [eV] [c]	ΔG_{PeT} [eV] [d]	$\frac{FC(T_1 \rightarrow {}^2F_{5/2})}{FC(T_1 \rightarrow S_0)}$ [e]
YbL0^{CF3}	>1.75 [f]	–2.42	3.42	>0.60	6.55×10^{7}
YbL0^{Me}	1.65 [f]	–2.42	3.58	0.34	1.76×10^{9}
YbL0^{MOM}	1.76 [g]	–2.42	3.56	0.47	1.19×10^{8}
YbL1^{MOM}	1.76 [g]	–1.92	3.57	–0.04	1.19×10^{8}
YbL2^{MOM}	1.76 [g]	–1.70	3.57	–0.26	1.19×10^{8}
YbL3a^{MOM}	1.76 [g]	–1.55	3.57	–0.41	1.19×10^{8}
YbL3b^{MOM}	1.76 [g]	–1.56	3.55	–0.38	1.19×10^{8}
YbL3c^{MOM}	1.76 [g]	–1.60	3.56	–0.35	2.08×10^{8}

[a] V vs NHE. [b] Measured in DMF (0.1 M *n*-Bu_4ClO_4, 0.10 V/s) with [**YbL^{MOM}**] = 0.5 mM.[146] The values for **YbL0^{CF3}** and **YbL0^{Me}** are approximated to be the same as for **YbL0^{MOM}**. [c] Estimated from the 0–0 phonon transitions in Gd(III) complexes steady-state emission spectra at 77 K.[146] [d] Calculated using Eq. (5), with ΔE_{Coul} = 0.15 eV.[80] [e] Calculated using Eq. (8) and (9). [f] Value from [21]. [g] Value from [130].

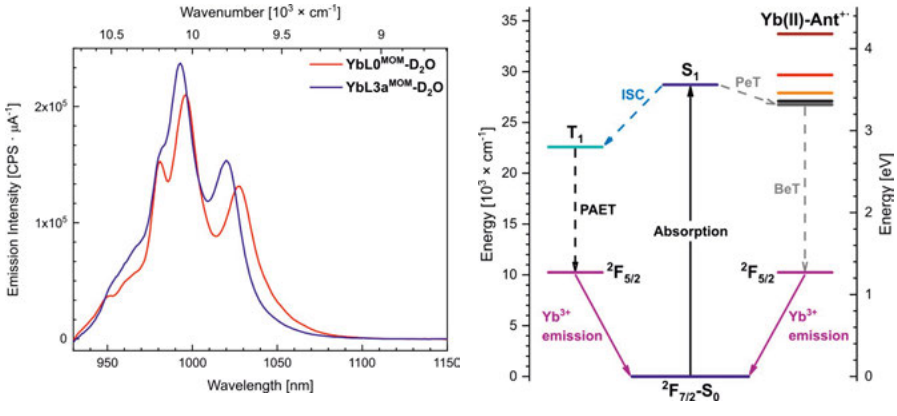

Figure 45. Steady-state NIR emission spectra of **YbL0,3a^{MOM}** in D_2O (left, 10 mM PIPES, pD 6.9),[131] λ_{ex} = 331 nm, front slit: 14 nm, exit slit: 5 nm and the sensitisation pathways of Yb(III) luminescence via PAET or PeT-BeT processes (right).[146]

6.4 Conclusions

We analysed the sensitisation pathways of NIR luminescence in the set of Yb(III) complexes with the varying electronic structure of the metal binding

site or the sensitising antenna. These compounds had one major diastereomer in solution as examined by ^{1}H NMR spectroscopy. The structural analogy of Yb(III) compounds was confirmed by the similar spectral shapes of the 4f-4f emissions. The ligand fluorescence intensities and lifetimes were affected by the increasing overall charge of the complex, consistent with facilitated PeT in positively charged Yb(III) compounds. The rate constants of PeT in +3 charged complexes were twice as large as in the neutral species.

All Yb(III) complexes were NIR-emissive, despite the positive free energy change of PeT in neutral compounds. In complexes with inefficient antenna-to-Ln PeT, phonon-assisted energy transfer was favourable to sensitise Yb(III) luminescence. The complexes with sensitisation from combined electron and energy transfer pathways were only 11–12% more emissive than their analogues, wherein PeT was thermodynamically uphill. Nevertheless, the effect from PeT sensitisation was similar in +3 charged complexes after removing the inner-sphere X-H oscillators.

This study shows that the literature-acclaimed sensitisation pathways need to be verified on every luminescent system to establish methods for improving NIR emission properties. This approach would facilitate understanding which processes should be accelerated due to the sensitising effects (PAET) and which pathways should be avoided for their detrimental impact (X-H quenching). The electron transfer processes contributed to sensitised Yb(III) luminescence only slightly in our systems (PeT).

7. Improved Yb(III) emission in tacn-based complexes compared to cyclen derivatives (Paper VI)

In the previous chapter, we showed that PAET was the main pathway leading to the sensitised Yb(III) luminescence for our complexes based on cyclen ligands. The NIR emission intensity was moderately increased through PeT compared to the systems where this process was unfavourable. Another way to control the Ln(III) luminescence quantum yield is to improve the intrinsic ability of the Ln(III) ion to emit.[24] Then, the NIR emission intensity could be increased by enhancing the intrinsic quantum yield of Yb(III) complexes, provided that the sensitisation efficiency of the Ln(III) remains unchanged.

Eu(III) complexes of tacn-dipicolinate ligands had larger Φ_{Ln}^{Ln} (mean 17.8% for **EuL^{X}**, Figure 46, left)[130] than those of the cyclen-based compounds (12% for **EuL0^{MOM}**).[128] The values of η_{sens} in **EuL^{X}** were diminished by intraligand PeT from the carbostyril antenna to the picolinate moiety (η_{sens} = 20% and 43%, Φ_{Ln} = 3.6% and 5.1% for **EuL^{OMe}** and **EuL0^{MOM}**, respectively).[128,130] As the rates of the sensitising and quenching processes are Ln(III) dependent, we decided to test the emissive properties of the analogous Yb(III) compounds (Figure 46, left).

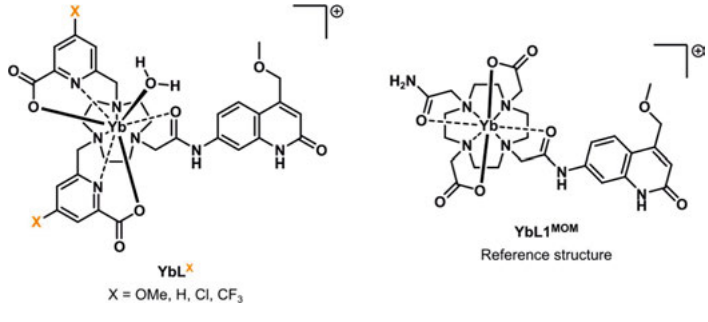

Figure 46. Yb(III) complexes based on tacn-dipicolinate ligands (left) and cyclen-based reference structure from Chapter 6 (right).[153]

YbL^{X} (X = OMe, H, Cl, CF_3) complexes were based on known ligands[130] consisting of tacn macrocyclic core, equipped with two methylenepicolinate donors and a secondary amide-linked 4-MOM-carbostyril antenna. The ligands contained either functionalised pyridylcarboxylates in the *para*-position

with OMe, Cl and CF_3 groups or unsubstituted picolinate pendant arms. Along with the structural and photoluminescent studies of the tacn-dipicolinate Yb(III) complexes, we intended to compare their NIR emission intensities with that of the cyclen-based reference structure (Figure 46, right). These ligands are octadentate but vary in their donor sites and can impose different geometries on the Ln(III) ion.

7.1 Structural studies of $\mathbf{YbL^X}$ complexes in solution and solid state

The new Yb(III) compounds were obtained by the complexation reaction between the tacn-based $\mathbf{L^X}$ ligands and $YbCl_3$ in an aqueous-ethanolic 1:1 mixture at 45 °C for 16 h. $\mathbf{YbL^X}$ complexes were purified by column chromatography on neutral alumina using CH_3CN:H_2O as the eluent mixture and were characterised by HPLC-MS and HRMS, confirming their molecular formulae.

The complete structural characterisation of $\mathbf{YbL^X}$ compounds via NMR spectroscopy was not possible due to their limited solubility. Nevertheless, in the ^{1}H NMR spectra of the Yb(III) compounds measured at r.t. in CD_3OD, 31–37 peaks were observed from 57 ppm to –35 ppm (Figure 47, left). Each magnetically non-equivalent proton in the Yb(III) complexes would give a separate signal[154] (28 resonances for $\mathbf{YbL^H}$ and 30 for $\mathbf{YbL^{OMe,Cl,CF3}}$). Thus, the number of the chemical shifts observed in the ^{1}H NMR spectra agrees with a single diastereomer present in solution or a mixture of $\mathbf{YbL^X}$ stereoisomers undergoing fast exchange on the NMR time scale. Due to the helical chirality of Yb(III) complexes, each diastereomer was expected to be a racemic mixture.

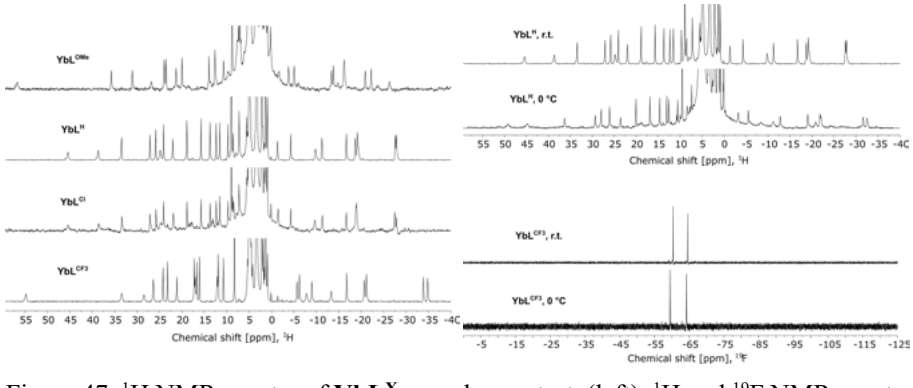

Figure 47. ^{1}H NMR spectra of $\mathbf{YbL^X}$ complexes at r.t. (left). ^{1}H and ^{19}F NMR spectra of $\mathbf{YbL^H}$ and $\mathbf{YbL^{CF3}}$, respectively, at r.t. and at 0 °C (right). All spectra were measured in CD_3OD at 400 MHz for ^{1}H NMR, and at 376 MHz for ^{19}F NMR.[153]

Cooling down the CD_3OD solution of **YbL^{H}** to 0 °C displaced the proton resonances up to 5 ppm relative to the r.t. spectra indicating the influence of the paramagnetic shifts induced by Yb^{3+}.[137] Similar effects with a smaller displacement factor (1 ppm) were observed in the ^{19}F NMR spectra of **YbL^{CF3}** at the same temperature (Figure 47, right). These observations correlated well with the results from the NMR spectra of the analogous Eu(III) complexes exhibiting either a single diastereomer or a fast equilibrium between several species.[130] Since all **YbL^{X}** complexes had a similar isomeric composition in solution, we assumed that the differences in photophysical properties would arise from the *para*-substituents on picolinate pendant arms instead of the structural varieties.

We successfully obtained **YbL^{CF3}-F** and **YbL^{H}** single crystals appropriate for X-ray crystallography. The single crystals of **YbL^{CF3}-F** were obtained after slow vapour diffusion of glyme into the concentrated aqueous solution of the complex containing an equiv. of KF. The single crystals of **YbL^{H}** formed without a fluoride source, using dioxane as the antisolvent. The coordination polyhedron around the central ion was a distorted tricapped trigonal prism in both complexes (CN = 9, Figure 48). F^- and H_2O ligands were capping one of the trigonal prismatic faces in **YbL^{CF3}-F** and **YbL^{H}** complexes, respectively.

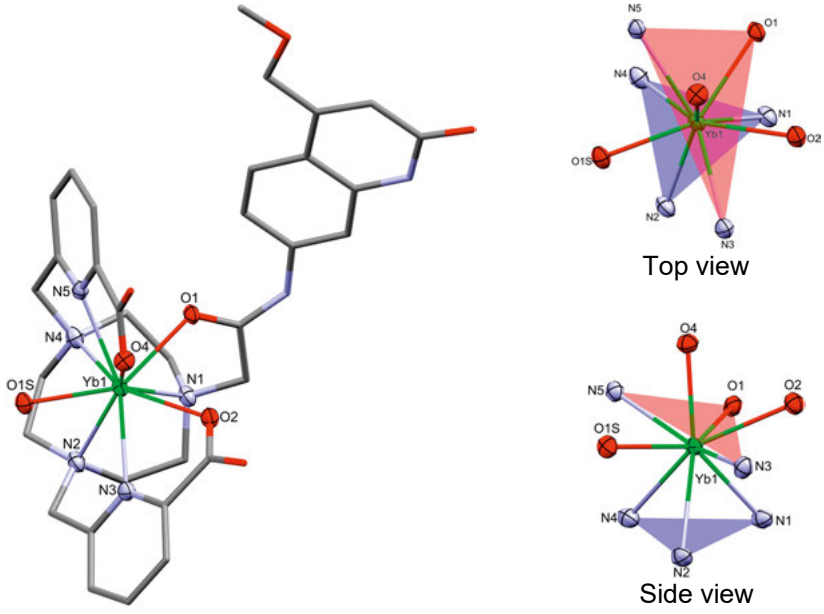

Figure 48. Solid-state structure of **YbL^{H}** (left, $\Lambda(\lambda\lambda\lambda)$ isomer) and coordination environment of Yb(III) in **YbL^{H}** from the top and side view (right). Protons, chloride counterions and water molecules were omitted for clarity. Yb(III) coordinating atoms were depicted as ellipsoids at 50% probability, the remaining structure is shown as capped sticks.[153]

We measured the ψ and ω torsion angles formed by NCCN of the tacn ring and the picolinate pendant arms or NCCO of the carbostyril linker amide. In both crystals of Yb(III) compounds, the sign combinations of the ψ and ω torsion angles were consistent with $\Delta(\lambda\lambda\lambda)$ and $\Lambda(\delta\delta\delta)$ isomers. The presence of two enantiomers of a single diastereomer in **YbL^{X}** was consistent with the previous results for Ln(III) complexes of tacn-trispicolinate ligands, which also had enantiomeric pairs.[155,156] The X-ray crystallography data corresponded with ^{1}H NMR spectroscopy results reaffirming the presence of a single diastereomer in both solid state and solution. The structural similarities of **YbL^{X}** complexes allowed the direct comparison of their photoluminescent properties.

7.2 Photophysical characterisation of **YbL^{X}** compounds in the UV-Vis and NIR regions

Absorption and steady-state luminescence spectroscopy measurements were performed in the aqueous 10 mM PIPES buffer solutions at pH 6.5. The introduction of picolinate groups in **YbL^{X}** contributed to a more intense absorbance at 263–306 nm compared to the same region in the absorption spectrum of **YbL1^{MOM}** (Figure 49, left). The combined picolinate π–π* and C=O n–π* transitions increased the absorbance of the higher energy band 1.5–2 fold in the following order: **YbL^{OMe}** < **YbL^{H}** ≈ **YbL^{Cl}** < **YbL^{CF3}**. However, **YbL^{X}** had the carbostyril-centred π–π* absorption at similar λ_{abs} as the related Yb(III) complexes carrying the same MOM-antenna. The carbostyril absorption region was superimposable in all Yb(III) compounds. The excitation wavelength used in the luminescence experiments was chosen to excite only the antenna.

Excitation of Yb(III) complexes at λ_{ex} = 329 nm resulted in ligand-based UV-visible and metal-based NIR emission. The residual antenna fluorescence was found at the same wavelengths with identical λ_{em} as for previously described cyclen-based complexes with 4-MOM-carbostyril (Figure 49, right). The fluorescence band intensity was dependent on the *para*-substituents of the picolinate pendant arms in **YbL^{X}**. The largest ligand fluorescence quantum yield was for the complex with electron-donating methoxy groups (Φ_L = 4.6%). **YbL^{H}** had 21% smaller Φ_L than its OMe-analogue. In the Yb(III) picolinates functionalised with electron-withdrawing Cl and CF_3 substituents, the antenna-based emission intensities decreased 2.3-fold and 4.7-fold, respectively, compared to that of **YbL^{OMe}**. Even in the latter complex, Φ_L was 15% smaller than in **YbL1^{MOM}** (Table 25). Ln(III) complexes of **L^{X}** ligands had a similar trend of decreasing Φ_L, which was caused by intraligand PeT from the carbostyril antenna to the picolinate pendant arms.[130] More

electron-withdrawing substituents rendered picolinate groups more reducible, promoting PeT from the carbostyril.[130]

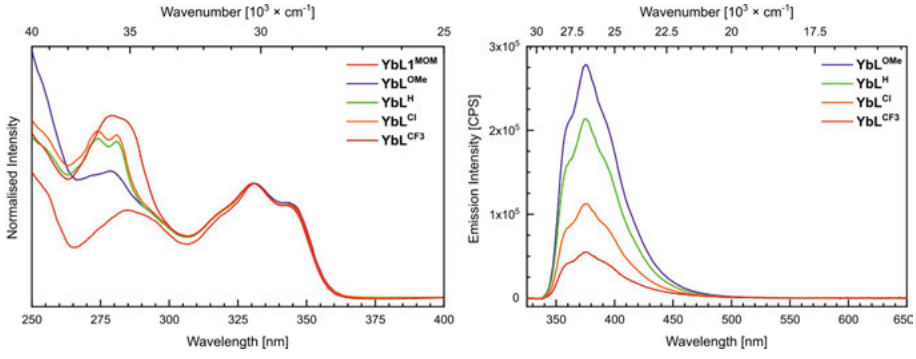

Figure 49. Normalised superimposed absorption spectra of **YbL1^{MOM}** and **YbL^{X}** (left), λ_{abs} = 330–331 nm and steady-state emission spectra of **YbL^{X}** complexes (right), λ_{ex} = 329 nm, front slit: 2 nm, exit slit: 1.5 nm.[153]

The quenching effect of intraligand PeT on the antenna S_1 was also noticed in the shorter ligand fluorescence lifetimes of **YbL^{X}** than that of **YbL1^{MOM}**. Among tacn-based Yb(III) complexes, $\tau_{f,L}$ could be determined only for *p*-methoxypicolinate (0.26 ns) and the unsubstituted derivative (0.20 ns). **YbL^{Cl,CF3}** antenna fluorescence lifetimes were shorter than the instrumentation limit (minimum 0.15 ns). **YbL^{X}** radiative ligand fluorescence lifetimes were also shorter than those of the cyclen-based complexes (mean 5.44 ns vs 6.26 ns for **YbL1^{MOM}**). To compare the extent of antenna S_1 quenching by intraligand PeT in **YbL^{X}**, we calculated the non-radiative ligand decay rate constants ($k_{nr,L}$) as the difference between the antenna fluorescence and radiative rate constants ($k_{f,L}$ and $k_{rad,L}$, Table 25). In **YbL1^{MOM}**, $k_{nr,L}$ was 1.3-fold and 1.7-fold smaller than in **YbL^{OMe}** and **YbL^{H}**, respectively, affirming the presence of intraligand PeT quenching of the ligand S_1 in the Yb(III) picolinates.

Table 25. Measured ligand fluorescence quantum yields, lifetimes, Yb(III) relative emission quantum yields and calculated non-radiative rate constants.

Complex	Φ_L (φ_{Ln}) [%] [a, b]	$\tau_{f,L}$ [ns] [c]	$\tau_{rad,L}$ [ns] [d]	$k_{nr,L}$ [ns^{-1}] [e]	φ_{Ln} [%] [f]
YbL^{OMe}	4.62 (100)	0.26	5.55	3.72	96
YbL^{H}	3.66 (79)	0.20	5.32	4.95	94
YbL^{Cl}	2.01 (44)	<0.15	-	-	100
YbL^{CF3}	0.977 (21)	<0.15	-	-	68
YbL1^{MOM}	5.43	0.34 [b]	6.26	2.78	72

The values carry relative experimental error of 10%. [a] Relative to quinine sulfate (Φ = 59% in 0.05 M H_2SO_4).[126] φ_L is relative to **YbL^{OMe}**. [b] Mean of 2 or 3 independent measurements. [c] λ_{ex} = 341.5 nm. [d] Calculated using Eq. (6). [e] Calculated as $1/\tau_{f,L} - 1/\tau_{rad,L}$. [f] Relative to **YbL^{Cl}**, the values are ±1–2%.

The NIR emission spectra of **YbL^{X}** were alike, indicating a similar coordination environment of Yb(III). Two peaks centred at 978 nm and 1006 nm of the $^{2}F_{5/2}\rightarrow{}^{2}F_{7/2}$ transition were observed instead of the three present in the NIR emission spectra of **YbL^{MOM}** complexes (Figure 50, left). These differences are concordant with the structural variations of **YbL^{X}** and **YbL^{MOM}** compounds, adopting different geometries.

Yb(III) complexes based on tacn-dipicolinates (except for **YbL^{CF3}**) were more emissive in the NIR region than their cyclen derivatives. The latter became apparent as the φ_{Yb} values of **YbL^{MOM}** had to be multiplied by 0.89 to convert them to the same reference as φ_{Yb} of **YbL^{X}**. Hence, the strongest cyclen-based NIR emitter was 11% less luminescent than **YbL^{Cl}**. Even the second and third-best relative Yb(III) luminescence quantum yields in the **YbL^{X}** series were 7% and 5% larger than that of **YbL3c^{MOM}**, respectively. The only Yb(III) picolinate complex having a lower φ_{Ln} than that in the set of **YbL^{MOM}** compounds was **YbL^{CF3}** (φ_{Yb} = 72%, Table 25).

The likely reason for the small relative Yb(III) emission quantum yield in the *p*-trifluoromethylpicolinate complex is efficient intraligand PeT. The free energy change of PeT from carbostyril antenna to picolinate was calculated for all **YbL^{X}** compounds (Table 26). The resulting ΔG_{PeT} values agreed with the antenna fluorescence quantum yields: the largest Φ_{L} was for the complex with the least negative free energy change of PeT. Thus, among Yb(III) tacn-dipicolinates, intraligand PeT was the most efficient in **YbL^{CF3}**, owing to the most negative ΔG_{PeT}. The latter also explained the smallest φ_{Yb} of the CF_3-substituted picolinate in the series of **YbL^{X}** complexes.

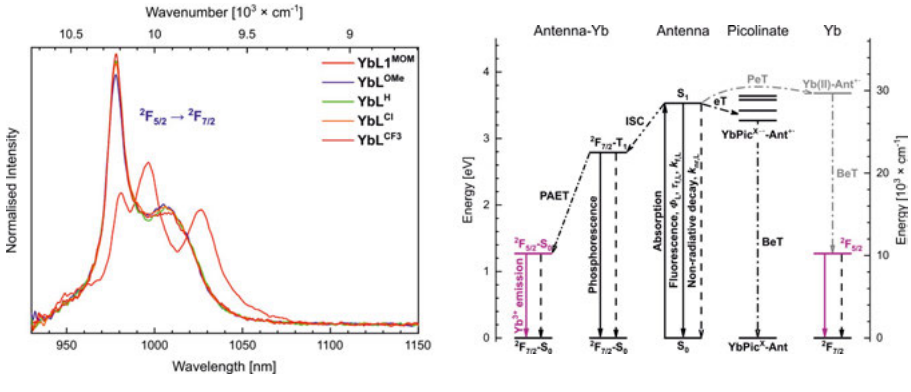

Figure 50. Normalised steady-state NIR emission spectra of **YbL^{X}**, λ_{ex} = 323 nm (left). Sensitisation and quenching pathways in **YbL^{X}** complexes (right).[153]

Along with the driving force for intraligand PeT, we estimated the thermodynamic feasibility of Yb(III) reduction by PeT from the photoexcited carbostyril. We assumed that Yb(III)/Yb(II) reduction potentials of positively charged **YbL^{X}** are similar to that of **YbL1^{MOM}**, as we could not determine the

E_{red}^{Yb} of the former complexes. With the Yb(III)/Yb(II) reduction potential of –1.92 V vs NHE, the free energy change of antenna-to-Yb PeT was thermodynamically neutral. Thus, the sensitisation of Yb(III) luminescence could happen via PAET. The Franck-Condon factors for the non-radiative decay of the antenna T_1 to the $^2F_{5/2}$ excited state were 8–9 times larger than the phosphorescence of the carbostyril in **YbL^X** compounds (Table 26). Notably, the quotient of Franck-Condon factors for **YbL3c^{MOM}** and **YbL^X** (X = H, Cl, CF_3) were identical, meaning that the improved φ_{Yb} values of Yb(III) picolinates were counterbalanced by intraligand PeT quenching in the CF_3-substituted complex (Figure 50, right).

Table 26. Calculated free energy change of PeT and the quotient of Franck-Condon factors.

Complex	E_{ox}^{Ant} [a, b]	E_{red}^{Py} [a, c]	E_{S_1} [eV] [d]	ΔG_{PeT} [eV] [e]	$\frac{FC(T_1 \rightarrow {}^2F_{5/2})}{FC(T_1 \rightarrow S_0)}$ [f]
YbL^{OMe}	1.76	–1.88	3.54	–0.05	4.05×10^9
YbL^{H}	1.76	–1.82	3.56	–0.13	2.08×10^8
YbL^{Cl}	1.76	–1.66	3.55	–0.28	2.08×10^8
YbL^{CF3}	1.76	–1.51	3.56	–0.44	2.08×10^8

[a] V vs NHE. [b] Value from [130]. [c] Measured in DMF (0.1 M *n*-Bu_4ClO_4, 0.10 V/s) with [**YbL^X**] = 0.5 mM.[153] [d] Estimated from the 0–0 phonon transitions in Gd(III) complexes steady-state emission spectra at 77 K.[146] [e] Calculated using Eq. (5), with ΔE_{Coul} = 0.15 eV.[80] [f] Calculated using Eq. (8) and (9).

Among Yb(III) tacn-dipicolinate complexes, **YbL^{Cl}** was the most NIR-emissive, despite having the second-most favourable intraligand PeT quenching. The overall NIR emission quantum yield in Yb(III) compounds is the product of the efficiency of all the sensitising processes (η_{sens}) and the intrinsic ability of the Ln(III) to luminesce [Φ_{Ln}^{Ln}, Eq. (2)]. We could not determine either of these parameters for **YbL^X**; however, in the analogous Eu(III) complexes, the Ln(III) intrinsic quantum yields were 1.5-fold larger than in cyclen-based compounds with the same carbostyril antenna.[130] Yb(III) may similarly have increased Φ_{Ln}^{Ln} in their tacn complexes compared to the cyclen-based ones, which would positively contribute to the NIR emission intensity. Due to the detrimental effect of carbostyril-to-picolinate PeT on the NIR luminescence of the CF_3-functionalised complex, the overall sensitisation efficiency in **YbL^X** was expected to be lower than in **YbL3c^{MOM}**. However, the negative consequences of intraligand PeT might have been compensated for by the altered Yb(III) intrinsic quantum yield.

7.3 Conclusions

We have prepared and structurally characterised the new series of tacn-based dipicolinate Yb(III) complexes appended with a 4-methoxymethylcarbostyril

antenna. The solution and solid state studies revealed the presence of single species with tricapped trigonal prismatic geometry for all Yb(III) compounds. The more electron-withdrawing substituents on picolinate pendant arms promoted intraligand photoinduced electron transfer from the excited carbostyril antenna to pyridines, as shown by the diminished ligand fluorescence quantum yields and lifetimes in the trifluoromethyl-substituted ligands.

Despite the intraligand PeT quenching, the Yb(III) tacn-dipicolinates were appreciably more emissive than the cyclen-based compounds. This result was intriguing, as the best NIR emitter of the new complex series had the second-largest driving force for PeT from the antenna to picolinates. As in the cyclen species, the sensitisation of tacn-based Yb(III) complexes was likely to proceed via PAET, as the metal-centred PeT from the carbostyril was not favourable.

The ligand design plays a decisive role in endowing complexes with the target photophysical properties. However, the nature of Ln(III) could make a difference in the sensitisation of 4f-4f emission. For example, the introduction of pyridylcarboxylate in a cyclen-based Eu(III) complex backfired with intraligand PeT from the carbostyril to the picolinate (see Chapter 2). While the same process was happening in Yb(III) tacn compounds, they turned out more emissive even with more reducible pyridines in the structures. Thus, the intrinsic properties of Ln(III) also play a significant role in the design of highly emissive complexes.

8. Concluding remarks and future outlook

This thesis investigated the structure-property relationships in a series of widely used macrocyclic Ln(III) compounds. Structural characterisation of these complexes coupled with quantitative analysis of their electrochemical and photophysical properties allowed the establishment of some guidelines for creating brighter Ln(III) emitters. Increasing Ln(III) emission intensity via reduced quenching could result in a smaller amount of luminophores needed for cellular visualisation or analyte detection. We have identified PeT as a major quenching pathway, the elimination of which could substantially increase Eu(III) luminescence in macrocyclic complexes. Poorly emissive Sm^{3+} and Dy^{3+} are also sensitive to photoredox quenching, and eliminating possible PeT pathways in these emitters could yield a larger library of useful luminescent probes.

By installing bioconjugable groups in the carbostyril part of the ligand, we made Ln(III) complexes applicable for targeted conjugation with biomolecules. Click reactions between the cyclooctyne and azide-functionalised Ln(III) luminophores were possible. Upon saturation of the Eu(III) coordination sphere with a bidentate picolinate, the effects of intraligand PeT quenching were observed, which offset the impact of the eliminated coordinated water molecule and resulted in similarly emissive complexes (Paper I).

The variation of the Ln(III) coordination sphere from –3 charged to a neutral environment destabilised the Eu +3 oxidation state. Such changes in the complex structures correlated with decreasing Eu(III) emission intensity, which was the lowest for the +3 charged species containing the most reducible Eu(III) centre. Thus, the Ln(III) emission intensity of the complex with more readily reducible Eu(III) was diminished due to PeT, as the vibrational quenching was of similar magnitude in all these species. Fluoride binding decreased PeT quenching through Eu^{3+} stabilisation, opening up an unstudied way of designing anion-responsive probes (Paper II).

We developed a set of Ln(III) compounds with altered antenna orientation by installing a tertiary amide linker. Such complexes with carbostyril antennae were appreciably more emissive than their secondary amide-linked analogues, and the increase in emissive properties was still maintained even with a more reducible Eu(III). Fluoride binding in +2 charged carbostyril-appended compounds improved metal emission quantum yields by preventing PeT, which was not the case for +3 charged coumarin-sensitised complexes. So,

ostensibly similar emitters might be susceptible to different pathways of luminescence quenching (Paper III).

By complexing Ln(III) with the macrocyclic ligands of lower denticity, we aimed to introduce more coordination sites for anion binding. Upon fluoride addition, the most significant increase in the Eu(III) emission intensity was for the complexes with the most efficient PeT quenching and the largest number of inner-sphere water molecules. Similar experiments with added cyanide revealed strong quenching of the Eu(III) luminescence by the anion. Thus, it was possible to use the same complexes to detect two anions with identical charges via the opposite changes they caused in the Ln(III) emission (Paper IV).

As Yb(III) emission can be sensitised by a process initiated by PeT, we made Yb(III) reduction more accessible by creating positively charged complexes and compared them to overall charge-neutral species. The more favourable PeT from the antenna to Yb(III) resulted in a moderate increase in the NIR luminescence intensity. The NIR emission of Yb(III) complexes that had inefficient PeT was sensitised via phonon-assisted energy transfer, which was likely the predominant sensitisation pathway for all our Yb(III) systems. Hence, Horrock's PeT process, often assumed to be the main pathway in the literature, had a minor contribution to the overall Yb(III) sensitisation efficiency (Paper V).

Changing the type of binding site from cyclen-based to the picolinate-containing ligand in Yb(III) compounds promoted intraligand PeT from the carbostyril antenna to the easily reducible pyridines. This process depopulated the ligand first excited states. However, the NIR emission intensity was larger than in the other complexes lacking picolinates but sensitised via the same antenna. This outcome was attributed to the altered geometry of the Yb(III) coordination environment, which could also change the intrinsic ability of the Ln(III) ion to emit light (Paper VI).

Future perspectives created for Ln(III) complexes by this work include the determination of binding constants via luminescence titrations, and the analysis of Eu(III) compounds cyclic voltammetry upon fluoride addition. We would also like to develop new techniques for following fluoride binding to Ln(III) ions. For NIR-emissive lanthanides, we would like to study the intrinsic quantum yields and sensitisation efficiencies of Yb(III) complexes to find ways to control the intensity of sensitised luminescence.

To conclude, the design of Ln(III) luminophores has to deal with balancing between their structures, photophysics of the sensitising and emitting components, and the redox properties of the Ln(III) ions. By establishing harmony between all these criteria, complexes with tuneable properties could be created for the required optical applications.

Popular Science Summary

A wide range of unsolved medical problems requires novel solutions. Challenges include (*i*) the development of new drugs for currently untreatable illnesses, (*ii*) the creation of early diagnosis tools, and (*iii*) the molecular-level understanding of the mechanisms underpinning health and disease. Resolving these challenges is some of the reasons why healthcare workers collaborate with biologists, physicists, and chemists to find preventive measures and avoid the late-stage development of diseases.

Luminescence imaging uses light to obtain information about the system of interest, and it is a tool that is increasingly utilised for the detection of biological processes in living organisms or cells. The fundamental base of this imaging method is luminescence, which is the light emission of a substance when it returns to its ground state from an excited state. The excited state can be reached in several ways, including light irradiation, chemical reaction, or energy transfer from different excited species. The substances emitting light are called luminophores, which are usually chemical compounds. Common luminophores consist of organic molecules mainly composed of carbon (plus mostly hydrogen, oxygen, and nitrogen). Other types of luminophores include metal complexes, macromolecules such as proteins, and even nanoparticles.

A group of metals that have unique luminescence properties are called lanthanides. Lanthanides can give a pure red or green colour of luminescence distinct from the blue emission of biomolecules (Figure 51). Furthermore, lanthanide emission spectra are characteristic of the metal as a fingerprint. The emission of the lanthanides can last up to six times longer than that of common organic luminophores, making them useful for time-delayed luminescence detection. This property can significantly improve the signal-to-noise ratio, and the reliability of the measurement. Lanthanides are photostable, non-toxic relative to other heavy metals and can be coupled to luminophores that were proven to be biocompatible. Many processes can quench the emission of the luminophores, which diminishes their brightness. In this thesis, the ways of decreasing the effects of luminescence quenching in lanthanide luminophores were investigated.

We equipped our lanthanide compounds with reactive handles that linked these luminophores with the biomolecules. These “click” handles enable attachment to structures carrying a complementary functionality with high precision. Such modification ensured that the luminophores could be used within

cells. We showed that installing these reactive handles and linking the lanthanide complexes through them did not diminish the lanthanide emission intensity.

In the following parts of the thesis, we studied different ways to increase the brightness of lanthanide luminophores via inhibiting processes responsible for the decrease in emission intensity. Lanthanide complexes are often excited by energy transfer from a nearby organic chromophore, the so-called "antenna". The antenna in its excited state is a strong reductant, which means it is prone to donate an electron, and in some cases, can reduce the lanthanide ion. For Europium (a red emitter), this decreases the emission intensity, while for Ytterbium (which emits in the near-infrared, a biologically attractive region), it has been assumed to increase the luminescence intensity.

We modified the chemical structures of lanthanide compounds to prevent lanthanide reduction. We could quantify the effect of this process, and we could identify structural features that could counteract the lanthanide reduction upon shining light. In Europium complexes where this process was strongly quenching the luminescence, we found that it could be suppressed by adding fluoride and, therefore, provide a method for fluoride detection. Fluoride detection is important due to the high toxicity of this anion in high concentrations and its being necessary for dental health in small amounts. We also noticed that the photoredox quenching of Europium luminescence depends on the type of antennae and their orientations relative to the metal centre. Not only the nature of lanthanide but also the chemical structure around the metal centre is principal in creating bright luminophores.

We showed that, at least in some cases, Ytterbium could be excited by another previously little studied processes. These pathways were relevant for most of the luminescence sensitisation of Ytterbium. At the same time, the promoted reduction of Ytterbium in these luminophores had a marginal effect on increasing their brightness. Understanding the mechanisms of Ytterbium sensitisation is crucial for developing near-infrared bright-emitting luminophores and using them in the biologically attractive region.

Figure 51. Visible emission of a common organic luminophore, and the corresponding lanthanide compounds with Terbium, Europium, Dysprosium and Samarium (from left to right). Reproduced from http://www.cchem.berkeley.edu/knrgrp/ln.html

Populärvetenskaplig Sammanfattning (Popular Science Summary in Swedish)

Ett stort antal svårlösta medicinska problem behöver nya lösningar. Utmaningarna inkluderar (*i*) utveckling av nya läkemedel för sjukdomar som idag är obotliga, (*ii*) framtagande av verktyg som möjliggör tidig diagnos, och (*iii*) förbättrad molekylär förståelse av de bakomliggande mekanismerna om vad som ligger till grund för hälsa och sjukdom. Att lösa dessa utmaningar är några av skälen till att anställda inom vården samarbetar med biologer, fysiker och kemister för att hitta förebyggande åtgärder och undvika att sjukdomarna når sena utvecklingstadier.

Luminescensavbildning använder ljus för att få information om biomolekylära system, och det är ett verktyg som i allt högre grad används för in vivo-detektion av biologiska processer. Den grundläggande basen för denna avbildningsmetod är luminescens, det vill säga emission av ljus från en kemisk förening när den återgår till sitt elektroniska grundtillstånd från ett exciterat tillstånd. Det exciterade tillståndet kan nås på flera sätt, inklusive ljusexcitation, en kemisk reaktion eller energiöverföring från en annan exciterad molekyl. De ämnen som avger ljus kallas luminoforer, och är vanligtvis kemiska föreningar. Vanliga luminoforer består av organiska molekyler med kol som huvudsaklig beståndsdel (mestadels tillsammans med kväve, syre och väte). Andra typer av luminoforer inkluderar metallkomplex, makromolekyler såsom proteiner, och till och med nanopartiklar.

En grupp metaller som har unika luminescensegenskaper kallas lantanider. Lantanider kan ge en ren röd eller grön färg av luminescens som är skild från den blå emissionen som kommer från biomolekyler. Därutöver är deras emissionsspektra karakteristiska för metallen, vilket fungerar som ett slags fingeravtryck. Tidsspannet för emissionen av lantaniderna kan vara upp till sex gånger längre än för vanliga organiska luminoforer. Detta gör dem användbara för tidsfördröjd luminescensdetektering, vilket kan förbättra signal-brusförhållandet avsevärt och därmed öka mätningens tillförlitlighet. Lantanider är fotostabila, icke-toxiska i förhållande till andra tungmetaller och kan kopplas till luminoforer som har visat sig vara biokompatibla. Flera olika processer kan försvaga emissionen från luminoforerna, vilket minskar deras ljusstyrka. I min avhandling undersöktes olika tillvägagångssätt för att reducera effekterna av luminescensförsvagning i lantanidluminoforer.

Vi utrustade våra lantanidföreningar med reaktiva ”handtag” som möjliggjorde att vi kunde koppla samman luminoforerna med biomolekylerna. Dessa "klick"-handtag gör det möjligt att med hög precision fästa lantanidkomplexen på strukturer som har en kompletterande funktionalitet. Modifieringen säkerställde att luminoforerna kunde användas i celler. Vi visade att inkorporering av de reaktiva handtagen, och att länkning av lantanidkomplexen via handtagen, inte minskade intensiteten hos lantanidemissionen.

I de efterföljande delarna av avhandlingen undersökte vi olika sätt att öka ljusstyrkan hos lantanidluminoforerna genom att inhibera processer som leder till minskad emissionsintensitet. Lantanidkomplex exciteras ofta genom energiöverföring från en närliggande organisk kromofor, den så kallade "antennen". Antennen i sitt exciterade tillstånd är starkt reducerande, vilket innebär att den är benägen att donera en elektron, och i vissa fall kan den reducera lantanidjonen. För europium (en röd sändare) minskar detta emissionsintensiteten, medan för ytterbium (som sänder ut i det nära-infraröda, ett biologiskt attraktivt område) har man antagit att det ökar luminescensintensiteten.

Vi modifierade de kemiska strukturerna hos lantanidföreningar för att förhindra reduktion av lantaniden. Vi kunde kvantifiera effekten av processen i fråga och kunde identifiera strukturella egenskaper som sannolikt kan motverka reduktionsprocessen vid belysning med ljus. I komplex med europium där processen kraftigt försvagade luminescensen fann vi att effekten kunde vändas till det motsatta genom tillsats av fluoridjoner, vilket resulterade i en metod för fluoriddetektion. Detektion av fluoridjoner är viktigt på grund av den höga toxiciteten hos dessa när de förekommer i höga koncentrationer, samtidigt som fluoridjoner är nödvändiga i små mängder för tandhälsan. Vi märkte också att europiumreduktionen och försvagning av lantanidluminescensen beror på vilken typ av antenner som används och deras orientering i förhållande till metallcentret. Inte enbart lantanidenatomens egenskaper utan även den kemiska strukturen runt metallcentret är viktiga för att skapa ljusstarka luminoforer.

Vi visade att ytterbium kunde exciteras av andra processer som sällan studerats tidigare. Dessa relaxationsprocesser var relevanta för det mesta av luminescensintensiteten hos ytterbium. Samtidigt hade den förbättrade reduktionen av ytterbium i dessa luminoforer en marginell effekt på att öka dess ljusstyrka. Att förstå dessa mekanismer är avgörande för att utveckla ljusemitterande luminoforer som emitterar i nära-infrarödområdet och använda dem i den biologiskt attraktiva regionen.

Научно-популярное краткое изложение (Popular Science Summary in Russian)

Широкому диапазону неразрешенных медицинских проблем необходимы новые решения. В частности, среди таких проблем разработка новых лекарств от пока что неизлечимых болезней, создание устройств для ранней диагностики, а также понимание механизмов развития заболеваний на молекулярном уровне. Преодоление этих препятствий является одной из нескольких причин сотрудничества работников здравоохранения с биологами, физиками и химиками, необходимого, чтобы найти профилактические меры и выигрывать время на поздних стадиях заболеваний.

Люминесцентная визуализация использует свет для получения информации об интересующих системах, и она является инструметом, который все чаще используется для наблюдения за биологическими процессами в живых организмах или клетках. Фундаментальной основой этого метода визуализации является люминесценция, то есть излучение света веществом при его возвращении из возбужденного состояния в основное. Возбужденное состояние может достигаться несколькими путями, в том числе при облучении светом, в ходе химических реакций или в результате переноса энергии от других возбужденных частиц. Химические соединения, которые излучают свет, называются люминофорами и обычно представляют собой сложные вещества. Чаще всего люминофоры это органические молекулы, то есть построеные из углерода (чаще всего в сочетании с водородом, кислородом и азотом). Люминофорами также могут быть координационные соединения металлов, макромолекулы, такие как белки, и даже наночастицы.

Группа металлов с уникальными люминесцентными свойствами называется лантанидами. Лантаниды обладают люминесценцией чистого красного или зеленого цвета, отличимой от синей эмиссии биомолекул. Более того, их спектр испускания индивидуален для каждого металла, как отпечаток пальца. Излучение лантанидов длится до шести раз дольше по сравнению с обычными органическими люминофорами, что делает их удобными для наблюдения за люминесценцией с временным разрешением, существенно улучшая отношение сигнал/шум, и, следственно, достоверность измерений. Лантаниды фотостабильны, нетоксичны по сравнению с другими тяжелыми металлами и могут быть совмещены с другими люминофорами с доказанной биосовместимостью. Многие процессы могут приводить к гашению люминесценции, что снижает яркость люминофоров. В настоящей работе были

изучены способы подавления гашения люминесценции в лантанидных люминофорах.

Мы снабдили наши лантанидные комплексы реакционноспособными якорями, которые связали эти люминофоры с биомолекулами. Эти «клик»-якоря позволяли присоединять комплексы к структурам, содержащим комплементарные функции, с высокой точностью. Такие модификации обеспечили применимость люминофоров внутри клеток. Мы показали, что установка этих реакционноспособных якорей и связывание с их помощью лантанидных комплексов не приводит к снижению интенсивности излучения лантанидов.

В последующих частях этой работы мы изучили разные способы повышения яркости лантанидных люминофоров с помощью подавления процессов, ответственных за снижение интенсивности излучения. Лантанидные комплексы часто возбуждаются путем переноса энергии от близлежащих органических хромофоров, так называемых «антенн». Антенна в своем возбужденном состоянии является сильным восстановителем, то есть способна отдавать электрон, и в некоторых случаях может восстанавливать ион лантанида. Для европия (с красным излучением) этот процесс снижает интенсивность излучения, в то время как для иттербия (который излучает в ближней инфракрасной области, что привлекательно для применения в биологии) этот способ предположительно повышает интенсивность люминесценции.

Мы модифицировали химические структуры лантанидных соединений таким образом, чтобы предотватить в них восстановление лантанида. Мы смогли количественно определить эффект от этого процесса и найти структурные закономерности, которые смогли бы ему противодействовать. Для комплексов европия, в которых этот процесс эффективно гасил люминесценцию, мы обнаружили возможность подавлять этот процесс с помощью добавления фторида, что можно использовать как метод определения этого иона. Количественное опредение фторида важно ввиду его высокой токсичности при больших концентрациях вкупе с важной ролью для здоровья зубов в небольших количествах. Мы также обнаружили, что восстановление европия и гашение люминесценции лантанидов зависит от типа антенны и ее ориентации относительно центрального иона металла. Не только природа лантанида, но и химическая структура окружения иона металла важна для создания ярких люминофоров.

Мы показали, что по крайней мере в нескольких случаях иттербий возбуждается другими, ранее малоизученными путями. Эти механизми были ответственны за большую часть интенсивности люминесценции иттербия. В то же время усиленное восстановление иттербия в этих люминофорах лишь незначительно увиличивало их яркость. Понимание этих механизмов очень важно для создания ярких в ближней инфракрасной области люминофоров и для их использования в биологически привлекательной области спектра.

Acknowledgments

EN: My work at Uppsala University would not be as productive and fruitful without the following persons.

I am very grateful to my supervisor, Eszter Borbas, for recruiting me and allowing me to continue the research in lanthanide chemistry from solution point of view. I thank the trust, encouragement and support that you gave me throughout this time. I will always remember your constant supply of honey when I was lacking the one from Bashkortostan. And I think we had a lot in common, if not in character but at least in the ideas we shared both scientifically and on many other topics. I will be eternally grateful for everything I learnt from you and from the people in your group! Nagyon köszönöm!

I am thankful to my co-supervisor, Andreas Orthaber, for the collaborative initiative in terms of crystallography. I also thank you for conducting the course on basics in single crystal X-ray crystallography as well. I wish you the best of luck for future and more enthusiastic people to your group!

I express my acknowledgements to Sascha Ott for making me a part of the SMC programme, helping me with educational affairs and your Christmas gatherings that cheered up during the darkest Swedish winters, to Anders Thapper for making the labs safe place to work (even with the cyanide in my fumehood), to Henrik Ottoson for proofreading my Swenglish popular science summary and to ever-smiling Stefano Crespi that became such a nice enlargement of the department and who also kindly proofread my thesis after his own (!) offering of help.

I convey my gratitude to Daniel Kovacs for the numerous experimental techniques you taught me and being a colleague that I wish I could have for much longer than I did. I was pleased to finish the numerous projects you left for me and made me a part of and I think I did a pretty good job in making sure that none of them were left behind. However, the legacy that you have left in the Borbas group is recalled up to date and will be remembered and acknowledged for even longer than that! I wish you all the best in your future and hope that we could keep in touch! Köszönöm!

I was delighted to work with Emilie Mathieu, and I thank you for your energy, joy and words of support in the most needed times. I am also grateful to you for teaching me electrochemical measurements and being a nice company at the conference in Villard-de-Lans. Thanks to your family for inviting me over for a dinner!

I would like to thank Julien Andres for valuable thoughts and suggestions in the Yb projects we worked on together. You were always referenced by Eszter as a very good spectroscopist and I was glad to experience it by myself.

I was happy to collaborate with Jordann Wells. Thank you for measuring my crystals even when their quality could have been better. I enjoyed our discussions on crystal structures, and thanks for sharing them with me. I hope you enjoy working back in Edinburgh and I wish you all the best!

I am grateful to Fiona Siemens for sharing a short-term project which resulted in a publication. I wish you a bright future and decisive choices on your way that will allow you to do what you like. Thanks for keeping in touch and meeting me for fika when you had your travel around Scandinavia!

I thank Brian D. McCarthy for proofreading my licentiate thesis and the research feedback you provided me since I started my PhD studies. I was glad to meet you here and enjoyed your company. SMC surely misses you and so do I!

I am thankful to Dulcie Phipps, Ellen Demeyere and Agnès Sipos for the possibility to finish your projects even if I have never met you in person.

I was glad to work with the current members of Borbas group who are Daniel Kocsi, Monika Tomar and Rohan Bhimpuria. I thank you for providing a good atmosphere in the laboratory and making a creative mood for research. You were great colleagues to work with! Daniel, it was fun to have Swedish classes alongside you and Monika, it was a pleasure to travel with you to Aussois and I hope I was nice guide in Paris! Rohan, thank you for proofreading my thesis and for taking care of LCMS when I was writing it!

I would also like to mention some of the previous members of Borbas group, who are Kiran Reddy Baddigam and Eirini Serveta. Both of you were smiling, optimistic and so honest. It was nice working with you!

The ever-changing composition of groups in the SMC division made me forgetful of many names. However, I would still like to mention that it was nice to share some time in the labs with Tomáš Slanina, Wangchuk Rabten, Julien Lyonnet, Edgar Anies, Hemlata Agarwala, Ben Johnson, Timofey Liseev, Anup Rana, Muhammad Anwar Shameem, Holly Redman, Michele Bedin, Rebekka Meyer and probably many more!

Those of SMC members that are still making a great company nowadays for which I am thankful are Leandro Cid Gomes, Anna Arkhypchuk, Nina F. Suremann, Thi Thuan Tran, Roman Peshkov, Nathalie Proos Vedin, Rajesh Deka and everyone else!

Thank you Leif Hammarström for your research feedback during my licentiate thesis presentation practices, you have given valuable thoughts, which I appreciated! The same goes to Jacinto Sá and Reiner Lomoth. Also, I acknowledge Katarina Edwards, Lars Gedda and Victor Agmo Hernandez for access to your fluorometer and help with my initial TCSPC measurements.

As I shared the office with PhysChem programme, some people from there became dear to me and helped with discussions from mechanistic point of

view, questions with scientific dilemma or just with their hugs, smiles and positive attitude. Of course, I am talking about Mariia Pavliuk, Nidhi Kaul, Andrew J. Bagnall, Andrea Rosichini, Nora Eliasson, Andjela Brnovic, Julian Schindler, Samir Chattopadhyay and Alenka Križan. You have been kind to me and I hope it was reciprocal from my side too!

Dear João Rodrigues and Kateryna Kukil, it was nice to do my PhD alongside yours and I wish you all the best for your future wherever you continue your career!

Sergii Shylin, I enjoyed our conversations whenever we met and your erudition was always leaving me speechless! Alina Sekretareva, I was delighted when you finally started your group and I hope you will continue working with your favourite research!

I would like to acknowledge the ERASMUS+ staff training programme for giving me an opportunity to do a research exchange in Brest, France.

I am grateful to Rik Van Deun and Anna M. Kaczmarek and people from your groups for helping me with NIR measurements at Ghent University.

I would like to thank Peter Nockemann and Igor V. Svitan'ko for being my referees when I applied for the PhD position with Eszter. Without your help, I might not end up where I am now!

For all my Ukrainian colleagues, I am deeply sorry about the invasion of your country by the Russian state. I will never forgive what my country did to yours, and I stand by you in protecting the sovereignty of the whole of Ukraine. **Слава Україні!**

FR: Je remercie Raphaël Tripier, Véronique Patinec et toute l'équipe de la chimie macrocyclique pour le temps partagé pendant mon stage à l'UBO. C'était très bien à faire mon stage avec vous et j'ai beaucoup apprécié toutes les journées grâce à vous. Merci beaucoup pour tous!

Je remercie la famille Laurans pour être ma famille en France et pour toujours m'aider quand j'avais besoin quelque chose. C'était chouette d'avoir deux mois avec vous pendant mon stage à Brest et toutes les autres fois quand je suis venu en Bretagne. Cher Maxime, sans toi je ne pourrais jamais terminer mon doctorat en Suède même quand j'étais loin de toi. Min hine yaratam, minen maturim!

DE: Vielen Dank Familie Schmidt, dass Sie mich in Deuz willkommen geheißen und in Ihrer Familie aufgenommen haben

BA: Йомғаҡлап, рәхмәт һүҙҙәремде апайыма һәм әсәйемә бағышлайым. Рәхмәт һеҙгә һәр ваҡыт миңә ярҙам иткәнегеҙ өсөн, һеҙ минең иң изге, иң яҡын, иң ышаныслы һәм иң тоғро кешеләрем. Мин һеҙҙе һәр ваҡыт иҫкә алдым, пандемия йәки һуғыш булғас һәм күрешмәгәс, мин һеҙҙе нығ ҡ нағындым. Оҙаҡламай осраша алырбыҙ тип өмөтләнәм һәм уйланам. Мин һеҙҙе бик нығ ҡ яратам, һәм тиҙҙән осрашыуыбыҙҙы өмөт итеп ҡалам!

References

[1] Huang, C.; Bian, Z. Chapter 1 Introduction. In *Rare Earth Coordination Chemistry: Fundamentals and Applications*; John Wiley & Sons (Asia), 2010; pp 1–40.

[2] Szabadvary, F. Chapter 73 The History of the Discovery and Separation of the Rare Earths. In *Handbook on the Physics and Chemistry of Rare Earths*; 1988; Vol. 11, pp 33–80.

[3] Gadolin, J. . Undersökning Af En Svart Tung Stenart Ifrån Ytterby Stenbrott i Roslagen. *Kongl. Vetenskaps Acad. Nya Handl.* **1794**, *15*, 137–155.

[4] Anthony, John W.; Bideaux, Richard A.; Bladh, Kenneth W.; Nichols, M. C. . *Handbook of Mineralogy*; Mineralogical Society of America, Chantilly, VA 20151-1110, USA, 2001.

[5] Greenwood, N. N.; Earnshaw, A. . Chapter 30 The Lanthanide Elements (Z = 58–71). In *Chemistry of the Elements*; Butterworth-Heinemann, 1997; pp 1227–1249.

[6] Friedman, H. G.; Choppin, G. R.; Feuerbacher, D. G. The Shapes of the f Orbitals. *J. Chem. Educ.* **1964**, *41* (7), 354–358.

[7] De Bettencourt-Dias, A. Introduction to Lanthanide Ion Luminescence. In *Luminescence of Lanthanide Ions in Coordination Compounds and Nanomaterials*; John Wiley & Sons, Ltd, 2014; pp 1–48.

[8] Cotton, S. *Lanthanide and Actinide Chemistry*; 2006.

[9] Brik, M. G.; Srivastava, A. M. . Chapter 1.8 Electronic Properties of the Lanthanide Ions. In *Rare Earth Chemistry*; De Gruyter, 2020; pp 83–96.

[10] Bünzli, J.-C. G. Lanthanide Luminescence: From a Mystery to Rationalization, Understanding, and Applications. In *Handbook on the Physics and Chemistry of Rare Earths*; Elsevier B.V., 2016; Vol. 50, pp 141–176.

[11] Carnall, W. T. The Absorption and Fluorescence Spectra of Rare Earth Ions in Solution. *Handb. Phys. Chem. Rare Earths* **1979**, 38.

[12] Cotton, S. Electronic and Magnetic Properties of the Lanthanides. In *Lanthanide and Actinide Chemistry*; John Wiley & Sons, Ltd: Chichester, UK, 2006; pp 61–87.

[13] C. Gorller-Walrand, K. B. Chapter 167 Spectral Intensities of F-f Transitions. In *Handbook on the Physics and Chemistry of Rare Earths*; Elsevier Science B.V., 1998; Vol. 25, pp 101–264.

[14] Weissman, S. I. Intramolecular Energy Transfer The Fluorescence of Complexes of Europium. *J. Chem. Phys.* **1942**, *10* (4), 214–217.

[15] Carnall, W.T.; Crosswhite, H.; Crosswhite, H. M. . *Energy Level Structure and Transition Probabilities in the Spectra of the Trivalent Lanthanides in LaF_3*; 1978.

[16] Carnall, W. T.; Goodman, G. L.; Rajnak, K.; Rana, R. S. A Systematic Analysis of the Spectra of the Lanthanides Doped into Single Crystal LaF_3. *J. Chem. Phys.* **1989**, *90* (7), 3443–3457.

[17] Carnall, W. T.; Goodman, G. L.; Rajnak, K.; Rana, R. S. *A Systematic Analysis of the Spectra of the Lanthanides Doped into Single Crystal LaF_3*; 1988.
[18] Van Vleck, J. H. The Puzzle of Rare-Earth Spectra in Solids. *J. Phys. Chem.* **1937**, *41* (1), 67–80.
[19] Comby, S.; Bünzli, J. C. G. Chapter 235 Lanthanide Near-Infrared Luminescence in Molecular Probes and Devices. In *Handbook on the Physics and Chemistry of Rare Earths*; 2007; Vol. 37, pp 217–470.
[20] Yuster, P.; Weissman, S. I. Effects of Perturbations on Phosphorescence: Luminescence of Metal Organic Complexes. *J. Chem. Phys.* **1949**, *17* (12), 1182–1188.
[21] Kovacs, D.; Lu, X.; Mészáros, L. S.; Ott, M.; Andres, J.; Borbas, K. E. Photophysics of Coumarin and Carbostyril-Sensitized Luminescent Lanthanide Complexes: Implications for Complex Design in Multiplex Detection. *J. Am. Chem. Soc.* **2017**, *139* (16), 5756–5767.
[22] Bünzli, J.-C. G.; Eliseeva, S. V. Basics of Lanthanide Photophysics. In *Lanthanide Luminescence: Photophysical, Analytical and Biological Aspects*; Springer-Verlag Berlin Heidelberg, 2010; pp 1–45.
[23] Werts, M. H. V.; Jukes, R. T. F.; Verhoeven, J. W. The Emission Spectrum and the Radiative Lifetime of Eu^{3+} in Luminescent Lanthanide Complexes. *Phys. Chem. Chem. Phys.* **2002**, *4* (9), 1542–1548.
[24] Binnemans, K. Interpretation of Europium(III) Spectra. *Coord. Chem. Rev.* **2015**, *295*, 1–45.
[25] Bünzli, J. C. G.; Piguet, C. Lanthanide-Containing Molecular and Supramolecular Polymetallic Functional Assemblies. *Chem. Rev.* **2002**, *102* (6), 1897–1928.
[26] Tripier, R.; Tircsó, G.; Platas-Iglesias, C.; Harriswangler, C. Importance of Ligand Design in Lanthanide Azamacrocyclic Complexes Relevant to Biomedical Applications. *Handb. Phys. Chem. Rare Earths* **2022**, *61*, 129–220.
[27] Parker, D. Rare Earth Coordination Chemistry in Action: Exploring the Optical and Magnetic Properties of the Lanthanides in Bioscience While Challenging Current Theories. In *Handbook on the Physics and Chemistry of Rare Earths*; Elsevier B.V., 2016; Vol. 50, pp 269–299.
[28] Cox, J. P. L.; Jankowski, K. J.; Kataky, R.; Parker, D.; Beeley, N. R. A.; Boyce, B. A.; Eaton, M. A. W.; Millar, K.; Millican, A. T.; Harrison, A.; Walker, C. Synthesis of a Kinetically Stable Yttrium-90 Labelled Macrocycle-Antibody Conjugate. *J. Chem. Soc. Chem. Commun.* **1989**, No. 12, 797–798.
[29] Borbas, K. E.; Bruce, J. I. Synthesis of Asymmetrically Substituted Cyclen-Based Ligands for the Controlled Sensitisation of Lanthanides. *Org. Biomol. Chem.* **2007**, *5* (14), 2274–2282.
[30] Kleinerman, M. Energy Migration in Lanthanide Chelates. *J. Chem. Phys.* **1969**, *51* (6), 2370–2381.
[31] Latva, M.; Takalo, H.; Mukkala, V.-M.; Matachescu, C.; Rodríguez-Ubis, J. C.; Kankare, J. Correlation between the Lowest Triplet State Energy Level of the Ligand and Lanthanide(III) Luminescence Quantum Yield. *J. Lumin.* **1997**, *75* (2), 149–169.
[32] Andres, J.; Chauvin, A.-S. Energy Transfer in Coumarin-Sensitised Lanthanide Luminescence: Investigation of the Nature of the Sensitiser and Its Distance to the Lanthanide Ion. *Phys. Chem. Chem. Phys.* **2013**, *15* (38), 15981.
[33] Samuel, A. P. S.; Xu, J.; Raymond, K. N. Predicting Efficient Antenna Ligands for Tb(III) Emission. *Inorg. Chem.* **2009**, *48* (2), 687–698.

[34] Beeby, A.; Clarkson, I. M.; Dickins, R. S.; Faulkner, S.; Parker, D.; Royle, L.; De Sousa, A. S.; Williams, J. A. G.; Woods, M. Non-Radiative Deactivation of the Excited States of Europium, Terbium and Ytterbium Complexes by Proximate Energy-Matched OH, NH and CH Oscillators: An Improved Luminescence Method for Establishing Solution Hydration States. *J. Chem. Soc. Perkin Trans. 2* **1999**, *2* (3), 493–503.

[35] Stein, G.; Würzberg, E. Energy Gap Law in the Solvent Isotope Effect on Radiationless Transitions of Rare Earth Ions. *J. Chem. Phys.* **1975**, *62* (1), 208–213.

[36] Dickins, R. S.; Parker, D.; De Sousa, A. S.; Williams, J. A. G. Closely Diffusing O-H, Amide N-H and Methylene C-H Oscillators Quench the Excited State of Europium Complexes in Solution. *Chem. Commun.* **1996**, No. 6, 697–698.

[37] Keopp, J. L.; Windsor, M. W. Luminescence and Energy Transfer in Solutions of Rare-Earth Complexes. I. Enhancement of Fluorescence by Deuterium Substitution. *J. Chem. Phys.* **1965**, *42* (5), 1599–1608.

[38] Parker, D.; Williams, J. A. G. Getting Excited about Lanthanide Complexation Chemistry. *J. Chem. Soc. Dalt. Trans.* **1996**, No. 18, 3613.

[39] Parker, D.; Gareth Williams, J. A. Luminescence Behaviour of Cadmium, Lead, Zinc, Copper, Nickel and Lanthanide Complexes of Octadentate Macrocyclic Ligands Bearing Naphthyl Chromophores. *J. Chem. Soc. Perkin Trans. 2* **1995**, No. 7, 1305–1314.

[40] Oude Wolbers, M. P.; Van Veggel, F. C. J. M.; Snellink-Ruël, B. H. M.; Hofstraat, J. W.; Geurts, F. A. J.; Reinhoudt, D. N. Photophysical Studies of M-Terphenyl-Sensitized Visible and near-Infrared Emission from Organic 1:1 Lanthanide Ion Complexes in Methanol Solutions. *J. Chem. Soc. Perkin Trans. 2* **1998**, No. 10, 2141–2150.

[41] Wahsner, J.; Seitz, M. Perdeuterated 2,2′-Bipyridine-6,6′-Dicarboxylate: An Extremely Efficient Sensitizer for Thulium Luminescence in Solution. *Inorg. Chem.* **2013**, *52* (23), 13301–13303.

[42] Bischof, C.; Wahsner, J.; Scholten, J.; Trosien, S.; Seitz, M. Quantification of C−H Quenching in Near-IR Luminescent Ytterbium and Neodymium Cryptates. *J. Am. Chem. Soc.* **2010**, *132* (41), 14334–14335.

[43] Doffek, C.; Alzakhem, N.; Molon, M.; Seitz, M. Rigid, Perdeuterated Lanthanoid Cryptates: Extraordinarily Bright near-IR Luminophores. *Inorg. Chem.* **2012**, *51* (8), 4539–4545.

[44] Doffek, C.; Wahsner, J.; Kreidt, E.; Seitz, M. Breakdown of the Energy Gap Law in Molecular Lanthanoid Luminescence: The Smallest Energy Gap Is Not Universally Relevant for Nonradiative Deactivation. *Inorg. Chem.* **2014**, *53* (7), 3263–3265.

[45] Winkless, L.; Tan, R. H. C.; Zheng, Y.; Motevalli, M.; Wyatt, P. B.; Gillin, W. P. Quenching of Er(III) Luminescence by Ligand C-H Vibrations: Implications for the Use of Erbium Complexes in Telecommunications. *Appl. Phys. Lett.* **2006**, *89* (11), 1–4.

[46] Iwamuro, M.; Adachi, T.; Wada, Y.; Kitamura, T.; Nakashima, N.; Yanagida, S. Photosensitized Luminescence of Neodymium(III) Coordinated with 8-Quinolinolates in DMSO-D6. *Bulletin of the Chemical Society of Japan*. 2000, pp 1359–1363.

[47] Tsvirko, M. P.; Meshkova, S. B.; Venchikov, V. Y.; Topilova, Z. M.; Bol'shoĭ, D. V. Determination of Contributions of Various Molecular Groups to Nonradiative Deactivation of Electronic Excitation Energy in β-Diketonate

Complexes of Ytterbium(III). *Opt. Spectrosc. (English Transl. Opt. i Spektrosk.* **2001**, *90* (5), 669–673.
[48] Scholten, J.; Rosser, G. A.; Wahsner, J.; Alzakhem, N.; Bischof, C.; Stog, F.; Beeby, A.; Seitz, M. Anomalous Reversal of C-H and C-D Quenching Efficiencies in Luminescent Praseodymium Cryptates. *J. Am. Chem. Soc.* **2012**, *134* (34), 13915–13917.
[49] Kovacs, D.; Phipps, D.; Orthaber, A.; Borbas, K. E. Highly Luminescent Lanthanide Complexes Sensitised by Tertiary Amide-Linked Carbostyril Antennae. *Dalt. Trans.* **2018**, *47* (31), 10702–10714.
[50] Güden-Silber, T.; Klein, K.; Seitz, M. 4,4′-Bis(Trifluoromethyl)-2,2′-Bipyridine-a Multipurpose Ligand Scaffold for Lanthanoid-Based Luminescence/19F NMR Probes. *Dalt. Trans.* **2013**, *42* (38), 13882–13888.
[51] Glover, P. B.; Bassett, A. P.; Nockemann, P.; Kariuki, B. M.; Van Deun, R.; Pikramenou, Z. Fully Fluorinated Imidodiphosphinate Shells for Visible- and NIR-Emitting Lanthanides: Hitherto Unexpected Effects of Sensitizer Fluorination on Lanthanide Emission Properties. *Chem. - A Eur. J.* **2007**, *13* (22), 6308–6320.
[52] Iman, K.; Shahid, M. Life Sensors: Current Advances in Oxygen Sensing by Lanthanide Complexes. *New J. Chem.* **2019**, *43* (3), 1094–1116.
[53] Beeby, A.; Parker, D.; Williams, J. A. G. Photochemical Investigations of Functionalised 1,4,7,10-Tetraazacyclododecane Ligands Incorporating Naphthyl Chromophores. *J. Chem. Soc. Perkin Trans. 2* **1996**, *8* (8), 1565–1579.
[54] Parker, D. Luminescent Lanthanide Sensors for pH, pO_2 and Selected Anions. *Coord. Chem. Rev.* **2000**, *205* (1), 109–130.
[55] Bobba, G.; Bretonnière, Y.; Frias, J. C.; Parker, D. Enantiopure Lanthanide Complexes Incorporating a Tetraazatriphenylene Sensitiser and Three Naphthyl Groups: Exciton Coupling, Intramolecular Energy Transfer, Efficient Singlet Oxygen Formation and Perturbation by DNA Binding. *Org. Biomol. Chem.* **2003**, *1* (11), 1870–1872.
[56] Law, G. L.; Pal, R.; Palsson, L. O.; Parker, D.; Wong, K. L. Responsive and Reactive Terbium Complexes with an Azaxanthone Sensitiser and One Naphthyl Group: Applications in Ratiometric Oxygen Sensing in Vitro and in Regioselective Cell Killing. *Chem. Commun.* **2009**, No. 47, 7321–7323.
[57] Main, M.; Snaith, J. S.; Meloni, M. M.; Jauregui, M.; Sykes, D.; Faulkner, S.; Kenwright, A. M. Using the Ugi Multicomponent Condensation Reaction to Prepare Families of Chromophore Appended Azamacrocycles and Their Complexes. *Chem. Commun.* **2008**, No. 41, 5212–5214.
[58] Schweitzer, C.; Schmidt, R. Physical Mechanisms of Generation and Deactivation of Singlet Oxygen. *Chem. Rev.* **2003**, *103* (5), 1685–1757.
[59] Quici, S.; Cavazzini, M.; Marzanni, G.; Accorsi, G.; Armaroli, N.; Ventura, B.; Barigelletti, F. Visible and Near-Infrared Intense Luminescence from Water-Soluble Lanthanide [Tb(III), Eu(III), Sm(III), Dy(III), Pr(III), Ho(III), Yb(III), Nd(III), Er(III)] Complexes. *Inorg. Chem.* **2005**, *44* (3), 529–537.
[60] Hueting, R.; Tropiano, M.; Faulkner, S. Exploring Energy Transfer between Pyrene Complexes and Europium Ions-Potential Routes to Oxygen Sensors. *RSC Adv.* **2014**, *4* (83), 44162–44165.
[61] Watkis, A.; Hueting, R.; Sørensen, T. J.; Tropiano, M.; Faulkner, S. Controlling Energy Transfer in Ytterbium Complexes: Oxygen Dependent Lanthanide Luminescence and Singlet Oxygen Formation. *Chem. Commun.* **2015**, *51* (86), 15633–15636.

[62] Beeby, A.; Dickins, R. S.; FitzGerald, S.; Govenlock, L. J.; Maupin, C. L.; Parker, D.; Riehl, J. P.; Siligardi, G.; Williams, J. A. G. Porphyrin Sensitization of Circularly Polarised Near-IR Lanthanide Luminescence: Enhanced Emission with Nucleic Acid Binding. *Chem. Commun.* **2000**, *1* (13), 1183–1184.

[63] Klink, S. I.; Hebbink, G. A.; Grave, L.; Van Veggel, F. C. J. M.; Reinhoudt, D. N.; Slooff, L. H.; Polman, A.; Hofstraat, J. W. Sensitized Near-Infrared Luminescence from Polydentate Triphenylene-Functionalized Nd3+, Yb3+, and Er3+ Complexes. *J. Appl. Phys.* **1999**, *86* (3), 1181–1185.

[64] Sørensen, T. J.; Kenwright, A. M.; Faulkner, S. Bimetallic Lanthanide Complexes That Display a Ratiometric Response to Oxygen Concentrations. *Chem. Sci.* **2015**, *6* (3), 2054–2059.

[65] Parker, D.; Fradgley, J. D.; Wong, K. L. The Design of Responsive Luminescent Lanthanide Probes and Sensors. *Chem. Soc. Rev.* **2021**, *50* (14), 8193–8213.

[66] Kovacs, D.; Borbas, K. E. The Role of Photoinduced Electron Transfer in the Quenching of Sensitized Europium Emission. *Coord. Chem. Rev.* **2018**, *364*, 1–9.

[67] Lakowicz, J. R. . Mechanisms and Dynamics of Fluorescence Quenching. In *Principles of Fluorescence Spectroscopy*; Springer US, 2006; pp 331–351.

[68] Breen, P. J.; Hild, E. K.; Horrocks, W. D. W. Spectroscopic Studies of Metal Ion Binding to a Tryptophan-Containing Parvalbumin. *Biochemistry* **1985**, *24* (19), 4991–4997.

[69] Horrocks, W. D.; Bolender, J. P.; Smith, W. D.; Supkowski, R. M. Photosensitized Near Infrared Luminescence of Ytterbium(III) in Proteins and Complexes Occurs via an Internal Redox Process. *J. Am. Chem. Soc.* **1997**, *119* (25), 5972–5973.

[70] Morss, L. R. Thermochemical Properties of Yttrium, Lanthanum, and the Lanthanide Elements and Ions. *Chem. Rev.* **1976**, *76* (6), 827–841.

[71] Parker, D.; Williams, J. A. G. Modest Effectiveness of Carbostyril 124 as a Sensitising Chromophore in Europium and Terbium Amide Complexes Based on 1, 4, 7, 10-Tetraazacyclododecane. *J. Chem. Soc. Perkin Trans. 2* **1996**, *8* (8), 1581–1586.

[72] Aime, S.; Batsanov, A. S.; Botta, M.; Dickins, R. S.; Faulkner, S.; Foster, C. E.; Harrison, A.; Howard, J. A. K.; Moloney, J. M.; Norman, T. J.; Parker, D.; Royle, L.; Williams, J. A. G. Nuclear Magnetic Resonance, Luminescence and Structural Studies of Lanthanide Complexes with Octadentate Macrocyclic Ligands Bearing Benzylphosphinate Groups. *J. Chem. Soc., Dalt. Trans.* **1997**, 3623–3636.

[73] Xiao, M.; Selvin, P. R. Quantum Yields of Luminescent Lanthanide Chelates and Far-Red Dyes Measured by Resonance Energy Transfer. *J. Am. Chem. Soc.* **2001**, *123* (29), 7067–7073.

[74] Ge, P.; Selvin, P. R. Carbostyril Derivatives as Antenna Molecules for Luminescent Lanthanide Chelates. *Bioconjug. Chem.* **2004**, *15* (5), 1088–1094.

[75] Abusaleh, A.; Meares, C. F. Excitation and De-excitation Processes in Lanthanide Chelates Bearing Aromatic Sidechains. *Photochem. Photobiol.* **1984**, *39* (s1), 763–769.

[76] Dickins, R. S.; Howard, J. A. K.; Maupin, C. L.; Moloney, J. M.; Parker, D.; Riehl, J. P.; Siligardi, G.; Williams, J. A. G. Synthesis, Time-Resolved Luminescence, NMR Spectroscopy, Circular Dichroism and Circularly

Polarised Luminescence Studies of Enantiopure Macrocyclic Lanthanide Tetraamide Complexes. *Chem. - A Eur. J.* **1999**, *5* (3), 1095–1105.
[77] Kirk, W. R.; Wessels, W. S.; Prendergast, F. G. Lanthanide-Dependent Perturbations of Luminescence in Indolylethylenediaminetetraacetic Acid-Lanthanide Chelate. *J. Phys. Chem.* **1993**, *97* (40), 10326–10340.
[78] Faulkner, S.; Burton-Pye, B. P.; Khan, T.; Martin, L. R.; Wray, S. D.; Skabara, P. J. Interaction between Tetrathiafulvalene Carboxylic Acid and Ytterbium DO3A: Solution State Self-Assembly of a Ternary Complex Which Is Luminescent in the near IR. *Chem. Commun.* **2002**, *2* (16), 1668–1669.
[79] Pope, S. J. A.; Burton-Pye, B. P.; Berridge, R.; Khan, T.; Skabara, P. J.; Faulkner, S. Self-Assembly of Luminescent Ternary Complexes between Seven-Coordinate Lanthanide(III) Complexes and Chromophore Bearing Carboxylates and Phosphonates. *Dalt. Trans.* **2006**, No. 23, 2907–2912.
[80] Beeby, A.; Faulkner, S.; Williams, J. A. G. pH Dependence of the Energy Transfer Mechanism in a Phenanthridine-Appended Ytterbium ComplexNear-IR Luminescence and Energy Transfer in Lanthanide Complexes. Part 2.1. *J. Chem. Soc. Dalt. Trans.* **2002**, No. 9, 1918–1922.
[81] Weller, A. Electron-Transfer and Complex Formation in the Excited State. *Pure Appl. Chem.* **1968**, *16* (1), 115–124.
[82] Weller, A. Photoinduced Electron Transfer in Solution: Exciplex and Radical Ion Pair Formation Free Enthalpies and Their Solvent Dependence. *Zeitschrift fur Phys. Chemie* **1982**, *133* (1), 93–98.
[83] Fu, L. M.; Ai, X. C.; Li, M. Y.; Wen, X. F.; Hao, R.; Wu, Y. S.; Wang, Y.; Zhang, J. P. Role of Ligand-to-Metal Charge Transfer State in Nontriplet Photosensitization of Luminescent Europium Complex. *J. Phys. Chem. A* **2010**, *114* (13), 4494–4500.
[84] Junker, A. K. R.; Sørensen, T. J. Illuminating the Intermolecular vs. Intramolecular Excited State Energy Transfer Quenching by Europium(III) Ions. *Eur. J. Inorg. Chem.* **2019**, *2019* (9), 1201–1206.
[85] Nielsen, L. G.; Sørensen, T. J. Including and Declaring Structural Fluctuations in the Study of Lanthanide(III) Coordination Chemistry in Solution. *Inorg. Chem.* **2020**, *59* (1), 94–105.
[86] Spirlet, M. R.; Jean Rebizant, J.; Desreux, J. F.; Loncin, M. F. Crystal and Molecular Structure of Sodium Aquo(1,4,7,10-Tetraazacyclododecane-1,4,7,10-Tetraacetato)Europate(III) Tetrahydrate, $Na^{+}(EuDOTA{\cdot}H_2O)^{-}{\cdot}4H_2O$, and Its Relevance to NMR Studies of the Conformational Behavior of the Lanthanide Complexes Formed by Th. *Inorg. Chem.* **1984**, *23* (3), 359–363.
[87] Aime, S.; Barge, A.; Benetollo, F.; Bombieri, G.; Botta, M.; Uggeri, F. A Novel Compound in the Lanthanide(III) DOTA Series. X-Ray Crystal and Molecular Structure of the Complex Na[La(DOTA)La(HDOTA)]·10H2O. *Inorg. Chem.* **1997**, *36* (19), 4287–4289.
[88] Desreux, J. F. Nuclear Magnetic Resonance Spectroscopy of Lanthanide Complexes with a Tetraacetic Tetraaza Macrocycle. Unusual Conformation Properties. *Inorg. Chem.* **1980**, *19* (5), 1319–1324.
[89] Aime, S.; Botta, M.; Ermondi, G. NMR Study of Solution Structures and Dynamics of Lanthanide(III) Complexes of Dota. *Inorg. Chem.* **1992**, *31* (21), 4291–4299.
[90] Hoeft, S.; Roth, K. Struktur Und Dynamik von Lanthanoid-Tetraazacyclododecantetraacetat-(DOTA-)Komplexen in Lösung. *Chem. Ber.* **1993**, *126* (4), 869–873.
[91] Jacques, V.; Desreux, J. F. Quantitative Two-Dimensional EXSY Spectroscopy and Dynamic Behavior of a Paramagnetic Lanthanide

Macrocyclic Chelate: YbDOTA(DOTA = 1,4,7,10-Tetraazacyclododecane-N,N′,N″,N‴-Tetraacetic Acid). *Inorg. Chem.* **1994**, *33* (18), 4048–4053.
[92] Aime, S.; Botta, M.; Fasano, M.; Marques, M. P. M.; Geraldes, C. F. G. C.; Pubanz, D.; Merbach, A. E. Conformational and Coordination Equilibria on DOTA Complexes of Lanthanide Metal Ions in Aqueous Solution Studied by ^{1}H-NMR Spectroscopy. *Inorg. Chem.* **1997**, *36* (10), 2059–2068.
[93] Brittain, H. G.; Desreux, J. F. Luminescence and NMR Studies of the Conformational Isomers of Lanthanide Complexes with an Optically Active Polyaza Polycarboxylic Macrocycle. *Inorg. Chem.* **1984**, *23* (26), 4459–4466.
[94] Batsanov, A. S.; Beeby, A.; Bruce, J. I.; Howard, J. A. K.; Kenwright, A. M.; Parker, D. Direct NMR and Luminescence Observation of Water Exchange at Cationic Ytterbium and Europium Centres. *Chem. Commun.* **1999**, No. 11, 1011–1012.
[95] Benetollo, F.; Bombieri, G.; Calabi, L.; Aime, S.; Botta, M. Structural Variations across the Lanthanide Series of Macrocyclic DOTA Complexes: Insights into the Design of Contrast Agents for Magnetic Resonance Imaging. *Inorg. Chem.* **2003**, *42* (1), 148–157.
[96] Howard, J. A. K.; Kenwright, A. M.; Moloney, J. M.; Parker, D.; Port, M.; Navet, M.; Rousseau, O.; Woods, M. Structure and Dynamics of All of the Stereoisomers of Europium Complexes of Tetra(Carboxyethyl) Derivatives of Dota: Ring Inversion Is Decoupled from Cooperative Arm Rotation in the RRRR and RRRS Isomers. *Chem. Commun.* **1998**, No. 13, 1381–1382.
[97] Parker, D.; Dickins, R. S.; Puschmann, H.; Crossland, C.; Howard, J. A. K. Being Excited by Lanthanide Coordination Complexes: Aqua Species, Chirality, Excited-State Chemistry, and Exchange Dynamics. *Chem. Rev.* **2002**, *102* (6), 1977–2010.
[98] Andres, J.; Hersch, R. D.; Moser, J. E.; Chauvin, A. S. A New Anti-Counterfeiting Feature Relying on Invisible Luminescent Full Color Images Printed with Lanthanide-Based Inks. *Adv. Funct. Mater.* **2014**, *24* (32), 5029–5036.
[99] Bodman, S. E.; Butler, S. J. Advances in Anion Binding and Sensing Using Luminescent Lanthanide Complexes. *Chem. Sci.* **2021**, *12* (8).
[100] Bünzli, J. C. G. Lanthanide Luminescence for Biomedical Analyses and Imaging. *Chem. Rev.* **2010**, *110* (5), 2729–2755.
[101] Hermanson, G. T. Fluorescent Probes. In *Bioconjugate Techniques*; Elsevier Science & Technology, 2013; pp 395–463.
[102] Singh, K.; Singh, S.; Srivastava, P.; Sivakumar, S.; Patra, A. K. Lanthanoplatins: Emissive Eu(III) and Tb(III) Complexes Staining Nucleoli Targeted through Pt-DNA Crosslinking. *Chem. Commun.* **2017**, *53* (45), 6144–6147.
[103] Pal, R.; Parker, D. A Ratiometric Optical Imaging Probe for Intracellular PH Based on Modulation of Europium Emission. *Org. Biomol. Chem.* **2008**, *6* (6), 1020–1033.
[104] Montgomery, C. P.; Murray, B. S.; New, E. J.; Pal, R.; Parker, D. Cell-Penetrating Metal Complex Optical Probes: Targeted and Responsive Systems Based on Lanthanide Luminescence. *Acc. Chem. Res.* **2009**, *42* (7), 925–937.
[105] Pershagen, E.; Nordholm, J.; Borbas, K. E. Luminescent Lanthanide Complexes with Analyte-Triggered Antenna Formation. *J. Am. Chem. Soc.* **2012**, *134* (24), 9832–9835.
[106] Pershagen, E.; Borbas, K. E. Multiplex Detection of Enzymatic Activity with Responsive Lanthanide-Based Luminescent Probes. *Angew. Chemie - Int. Ed.* **2015**, *54* (6), 1787–1790.

[107] Pandya, S.; Yu, J.; Parker, D. Engineering Emissive Europium and Terbium Complexes for Molecular Imaging and Sensing. *Dalt. Trans.* **2006**, No. 23, 2757–2766.
[108] Montgomery, C. P.; New, E. J.; Palsson, L. O.; Parker, D.; Batsanov, A. S.; Lamarque, L. Emissive and Cell-Permeable 3-Pyridyl- and 3-Pyrazolyl-4-Azaxanthone Lanthanide Complexes and Their Behaviour in Cellulo. *Helv. Chim. Acta* **2009**, *92* (11), 2186–2213.
[109] Bünzli, J.-C. G. Luminescence Bioimaging with Lanthanide Complexes. In *Luminescence of Lanthanide Ions in Coordination Compounds and Nanomaterials*; John Wiley & Sons Ltd: Chichester, United Kingdom, 2014; pp 125–196.
[110] Mathieu, E.; Sipos, A.; Demeyere, E.; Phipps, D.; Sakaveli, D.; Borbas, K. E. Lanthanide-Based Tools for the Investigation of Cellular Environments. *Chem. Commun.* **2018**, *54* (72), 10021–10035.
[111] Pershagen, E.; Borbas, K. E. Designing Reactivity-Based Responsive Lanthanide Probes for Multicolor Detection in Biological Systems. *Coord. Chem. Rev.* **2014**, *273–274*, 30–46.
[112] Butler, S. J. Quantitative Determination of Fluoride in Pure Water Using Luminescent Europium Complexes. *Chem. Commun.* **2015**, *51* (54), 10879–10882.
[113] Szíjjártõ, C.; Pershagen, E.; Ilchenko, N. O.; Borbas, K. E. A Versatile Long-Wavelength-Absorbing Scaffold for Eu-Based Responsive Probes. *Chem. - A Eur. J.* **2013**, *19* (9), 3099–3109.
[114] Ung, P.; Clerc, M.; Huang, H.; Qiu, K.; Chao, H.; Seitz, M.; Boyd, B.; Graham, B.; Gasser, G. Extending the Excitation Wavelength of Potential Photosensitizers via Appendage of a Kinetically Stable Terbium(III) Macrocyclic Complex for Applications in Photodynamic Therapy. *Inorg. Chem.* **2017**, *56* (14), 7960–7974.
[115] Zeng, Z.; Zhou, J.; Zhang, Y.; Qiao, R.; Xia, S.; Chen, J.; Wang, X.; Zhang, B. Photodynamic Properties of Hypocrellin A, Complexes with Rare Earth Trivalent Ions: Role of the Excited State Energies of the Metal Ions. *J. Phys. Chem. B* **2007**, *111* (10), 2688–2696.
[116] Walton, J. W.; Bourdolle, A.; Butler, S. J.; Soulie, M.; Delbianco, M.; Mc Mahon, B. K.; Pal, R.; Puschmann, H.; Zwier, J. M.; Lamarque, L.; Maury, O.; Andraud, C.; Parker, D. Very Bright Europium Complexes That Stain Cellular Mitochondria. *Chem. Commun.* **2013**, *49* (16), 1600–1602.
[117] D'Aléo, A.; Bourdolle, A.; Brustlein, S.; Fauquier, T.; Grichine, A.; Duperray, A.; Baldeck, P. L.; Andraud, C.; Brasselet, S.; Maury, O. Ytterbium-Based Bioprobes for near-Infrared Two-Photon Scanning Laser Microscopy Imaging. *Angew. Chemie - Int. Ed.* **2012**, *51* (27), 6622–6625.
[118] Mc Mahon, B. K.; Pal, R.; Parker, D. A Bright and Responsive Europium Probe for Determination of PH Change within the Endoplasmic Reticulum of Living Cells. *Chem. Commun.* **2013**, *49* (47), 5363–5365.
[119] Fradgley, J. D.; Starck, M.; Laget, M.; Bourrier, E.; Dupuis, E.; Lamarque, L.; Trinquet, E.; Zwier, J. M.; Parker, D. Targeted pH Switched Europium Complexes Monitoring Receptor Internalisation in Living Cells. *Chem. Commun.* **2021**, *57* (47), 5814–5817.
[120] Galland, M.; Le Bahers, T.; Banyasz, A.; Lascoux, N.; Duperray, A.; Grichine, A.; Tripier, R.; Guyot, Y.; Maynadier, M.; Nguyen, C.; Gary-Bobo, M.; Andraud, C.; Monnereau, C.; Maury, O. A "Multi-Heavy-Atom" Approach toward Biphotonic Photosensitizers with Improved Singlet-Oxygen Generation Properties. *Chem. - A Eur. J.* **2019**, *25* (38), 9026–9034.

[121] Mohamadi, A.; Miller, L. W. Brightly Luminescent and Kinetically Inert Lanthanide Bioprobes Based on Linear and Preorganized Chelators. *Bioconjug. Chem.* **2016**, *27* (10), 2540–2548.
[122] de Sousa, A. S. .; Croft, G. J. B. .; Wagner, C. A. .; Michael, J. P. .; Hancock, R. D. . Effect of Cyclohexylene Bridges on the Metal Ion Size Based Selectivity of Ligands in Aqueous Solution. *Inorg. Chem.* **1991**, *30* (18), 3525–3529.
[123] Reddy, D. R.; Pedró Rosa, L. E.; Miller, L. W. Luminescent Trimethoprim - Polyaminocarboxylate Lanthanide Complex Conjugates for Selective Protein Labeling and Time-Resolved Bioassays. *Bioconjug. Chem.* **2011**, *22* (7), 1402–1409.
[124] Kovacs, D.; Kiraev, S. R.; Phipps, D.; Orthaber, A.; Eszter Borbas, K. Eu(III) and Tb(III) Complexes of Octa- A Nd Nonadentate Macrocyclic Ligands Carrying Azide, Alkyne, and Ester Reactive Groups. *Inorg. Chem.* **2020**, *59* (1), 106–117.
[125] Gordon, C. G.; MacKey, J. L.; Jewett, J. C.; Sletten, E. M.; Houk, K. N.; Bertozzi, C. R. Reactivity of Biarylazacyclooctynones in Copper-Free Click Chemistry. *J. Am. Chem. Soc.* **2012**, *134* (22), 9199–9208.
[126] Suzuki, K.; Kobayashi, A.; Kaneko, S.; Takehira, K.; Yoshihara, T.; Ishida, H.; Shiina, Y.; Oishi, S.; Tobita, S. Reevaluation of Absolute Luminescence Quantum Yields of Standard Solutions Using a Spectrometer with an Integrating Sphere and a Back-Thinned CCD Detector. *Phys. Chem. Chem. Phys.* **2009**, *11* (42), 9850–9860.
[127] Vrachnou-Astra, E.; Katakis, D. A Study on the Interaction of Eu2+(Aq) with Pyridinecarboxylic Acids. *J. Am. Chem. Soc.* **1975**, *97* (19), 5357–5363.
[128] Kovacs, D.; Mathieu, E.; Kiraev, S. R.; Wells, J. A. L.; Demeyere, E.; Sipos, A.; Borbas, K. E. Coordination Environment-Controlled Photoinduced Electron Transfer Quenching in Luminescent Europium Complexes. *J. Am. Chem. Soc.* **2020**, *142* (30), 13190–13200.
[129] Kovacs, D. Photoinduced Electron Transfer in Luminescent Lanthanide Complexes, Uppsala University, 2019.
[130] Kovacs, D.; Kocsi, D.; Wells, J. A. L.; Kiraev, S. R.; Borbas, K. E. Electron Transfer Pathways in Photoexcited Lanthanide(Iii) Complexes of Picolinate Ligands. *Dalt. Trans.* **2021**, *50* (12), 4244–4254.
[131] Kiraev, S. R.; Mathieu, E.; Siemens, F.; Kovacs, D.; Demeyere, E.; Borbas, K. E. Lanthanide(III) Complexes of Cyclen Triacetates and Triamides Bearing Tertiary Amide-Linked Antennae. *Molecules* **2020**, *25* (22).
[132] Mani, T.; Tircsó, G.; Zhao, P.; Sherry, A. D.; Woods, M. Effect of the Regiochemistry of Butyl Amide Substituents on the Solution-State Structures of Lanthanide(III) DOTA-Tetraamide Complexes. *Inorg. Chem.* **2009**, *48* (21), 10338–10345.
[133] Alpoim, M. C.; Urbano, A. M.; Geraldes, C. F. G. C.; Peters, J. A. Determination of the Number of Inner-Sphere Water Molecules in Lanthanide(III) Polyaminocarboxylate Complexes. *J. Chem. Soc. Dalt. Trans.* **1992**, No. 3, 463.
[134] Kiraev, S. R.; Weber, R. R.; Wells, J. A. L.; Orthaber, A.; Kovacs, D.; Borbas, K. E. Analysis of Anion Binding Effects on the Sensitized Luminescence of Macrocyclic Europium(III) Complexes. *Anal. Sens.* **2022**, *2* (6).
[135] Kocsi, D.; Kovacs, D.; Wells, J. A. L.; Borbas, K. E. Reduced Quenching Effect of Pyridine Ligands in Highly Luminescent Ln(III) Complexes: The Role of Tertiary Amide Linkers. *Dalt. Trans.* **2021**, *50* (45), 16670–16677.

[136] Aime, S.; Barge, A.; Bruce, J. I.; Botta, M.; Howard, J. A. K.; Moloney, J. M.; Parker, D.; de Sousa, A. S.; Woods, M. NMR, Relaxometric, and Structural Studies of the Hydration and Exchange Dynamics of Cationic Lanthanide Complexes of Macrocyclic Tetraamide Ligands. *J. Am. Chem. Soc.* **1999**, *121* (24), 5762–5771.
[137] Harnden, A. C.; Parker, D.; Rogers, N. J. Employing Paramagnetic Shift for Responsive MRI Probes. *Coord. Chem. Rev.* **2019**, *383*, 30–42.
[138] Dickins, R. S.; Parker, D.; Bruce, J. I.; Tozer, D. J. Correlation of Optical and NMR Spectral Information with Coordination Variation for Axially Symmetric Macrocyclic Eu(III) and Yb(III) Complexes: Axial Donor Polarisability Determines Iigand Field and Cation Donor Preference. *Dalt. Trans.* **2003**, No. 7, 1264–1271.
[139] de Silva, A. P.; Gunaratne, H. Q. N.; Lynch, P. L. M.; Patty, A. J.; Spence, G. L. Luminescence and Charge Transfer. Part 3. The Use of Chromophores with ICT (Internal Charge Transfer) Excited States in the Construction of Fluorescent PET (Photoinduced Electron Transfer) pH Sensors and Related Absorption pH Sensors with Aminoalkyl Side . *J. Chem. Soc. Perkin Trans. 2* **1993**, No. 9, 1611.
[140] Saroja, G.; Sankaran, N. B.; Samanta, A. Photophysical Study of Two Carbostyril Dyes: Investigation of the Possible Role of a Rotary Decay Mechanism. *Chem. Phys. Lett.* **1996**, *249* (5–6), 392–398.
[141] Colas, K.; Doloczki, S.; Kesidou, A.; Sainero-Alcolado, L.; Rodriguez-Garcia, A.; Arsenian-Henriksson, M.; Dyrager, C. Photophysical Characteristics of Polarity-Sensitive and Lipid Droplet-Specific Phenylbenzothiadiazoles. *ChemPhotoChem* **2021**, *5* (7), 632–643.
[142] Gunnlaugsson, T.; Parker, D. Luminescent Europium Tetraazamacrocyclic Complexes with Wide Range pH Sensitivity. *Chem. Commun.* **1998**, No. 4, 511–512.
[143] Huang, S.-Y.; Pierre, V. C. A Turn-on Luminescent Europium Probe for Cyanide Detection in Water. *Chem. Commun.* **2018**, *54* (66), 9210–9213.
[144] Routledge, J. D.; Zhang, X.; Connolly, M.; Tropiano, M.; Blackburn, O. A.; Kenwright, A. M.; Beer, P. D.; Aldridge, S.; Faulkner, S. Lanthanide Complexes That Respond to Changes in Cyanide Concentration in Water. *Angew. Chemie Int. Ed.* **2017**, *56* (27), 7783–7786.
[145] Eliseeva, S. V.; Nguyen, T. N.; Kampf, J. W.; Trivedi, E. R.; Pecoraro, V. L.; Petoud, S. Tuning the Photophysical Properties of Lanthanide(III)/Zinc(II) "encapsulated Sandwich" Metallacrowns Emitting in the near-Infrared Range. *Chem. Sci.* **2022**, *13* (10), 2919–2931.
[146] Mathieu, E.; Kiraev, S. R.; Kovacs, D.; Wells, J. A. L.; Tomar, M.; Andres, J.; Borbas, K. E. Sensitization Pathways in NIR-Emitting Yb(III) Complexes Bearing 0, +1, +2, or +3 Charges. *J. Am. Chem. Soc.* **2022**, *144* (46), 21056–21067.
[147] Hartman, P.; Chan, H. K. Application of the Periodic Bond Chain (PBC) Theory and Attachment Energy Consideration to Derive the Crystal Morphology of Hexamethylmelamine. *Pharm. Res. An Off. J. Am. Assoc. Pharm. Sci.* **1993**, *10* (7), 1052–1058.
[148] Crosby, G.A., Kasha, M. Intramolecular Energy Transfer in Ytterbium Organic Chelates. *Spectrochim. Acta* **1958**, *10*, 377–382.
[149] Reinhard, C.; Güdel, H. U. High-Resolution Optical Spectroscopy of $Na_3[Ln(Dpa)_3]\cdot 13H_2O$ with Ln = Er^{3+}, Tm^{3+}, Yb^{3+}. *Inorg. Chem.* **2002**, *41* (5), 1048–1055.

[150] Van Dijk, J. M. F.; Schuurmans, M. F. H. On the Nonradiative and Radiative Decay Rates and a Modified Exponential Energy Gap Law for 4f-4f Transitions in Rare-Earth Ions. *J. Chem. Phys.* **1983**, *78* (9), 5317–5323.
[151] Jortner, J.; Bixon, M. Radiationless Transitions in Polyatomic Molecules. *Isr. J. Chem.* **1969**, *7* (2), 189–220.
[152] Solomon, E. I.; Lever, Alfred B. P. Inorganic Electronic Structure and Spectroscopy. **1999**.
[153] Kiraev, S. R.; Mathieu, E.; Kovacs, D.; Wells, J. A. L.; Tomar, M.; Andres, J.; Borbas, K. E. Improved Emission of Yb(III) Ions in Triazacyclononane-Based Macrocyclic Ligands Compared to Cyclen-Based Ones. *Dalt. Trans.* **2022**, *51* (43), 16596–16604.
[154] Walton, J. W.; Carr, R.; Evans, N. H.; Funk, A. M.; Kenwright, A. M.; Parker, D.; Yufit, D. S.; Botta, M.; De Pinto, S.; Wong, K. L. Isostructural Series of Nine-Coordinate Chiral Lanthanide Complexes Based on Triazacyclononane. *Inorg. Chem.* **2012**, *51* (15), 8042–8056.
[155] Carr, R.; Evans, N. H.; Parker, D. Lanthanide Complexes as Chiral Probes Exploiting Circularly Polarized Luminescence. *Chem. Soc. Rev.* **2012**, *41* (23), 7673–7686.
[156] Gateau, C.; Mazzanti, M.; Pécaut, J.; Dunand, F. A.; Helm, L. Solid-State and Solution Properties of the Lanthanide Complexes of a New Nonadentate Tripodal Ligand Derived from 1,4,7-Triazacyclononane. *Dalt. Trans.* **2003**, No. 12, 2428–2433.

Acta Universitatis Upsaliensis

Digital Comprehensive Summaries of Uppsala Dissertations from the Faculty of Science and Technology 2220

Editor: The Dean of the Faculty of Science and Technology

A doctoral dissertation from the Faculty of Science and Technology, Uppsala University, is usually a summary of a number of papers. A few copies of the complete dissertation are kept at major Swedish research libraries, while the summary alone is distributed internationally through the series Digital Comprehensive Summaries of Uppsala Dissertations from the Faculty of Science and Technology. (Prior to January, 2005, the series was published under the title "Comprehensive Summaries of Uppsala Dissertations from the Faculty of Science and Technology".)

Distribution: publications.uu.se
urn:nbn:se:uu:diva-489083

ACTA
UNIVERSITATIS
UPSALIENSIS
UPPSALA
2022